FORCED CONVECTION CONDENSATION FROM A VAPOR NONCONDENSABLE GAS MIXTURE

BY

MICHAEL K. WEST

A DISSERTATION PRESENTED TO THE GRADUATE SCHOOL
OF THE UNIVERSITY OF FLORIDA IN PARTIAL FULFILLMENT
OF THE REQUIREMENTS FOR THE DEGREE OF
DOCTOR OF PHILOSOPHY

UNIVERSITY OF FLORIDA
1992

UNIVERSITY OF FLORIDA LIBRARIES

Copyright 1992

by

Michael K. West

ACKNOWLEDGEMENTS

The support of Dr. Elmer Hansen has benefitted every aspect of this work. I am especially thankful for Dr. Hansen's elegant contributions to the experimental design and analysis. His suggestions led to practical solutions to some complex problems.

I thank Dr. Bruce Edwards and Dr. U. Kurzweg for their help with the analytic solution to the concentration equation.

I gratefully acknowledge Dr. C. K. Hsieh's enthusiastic desire to make this work a more rigorous and lasting contribution to the advancement of condensation research. His concern and encouragement have been continually inspiring.

The guidance of Dr. H. Ingley, Dr. Paul Oppenheim and Dr. R. Gaither is greatly appreciated. Their pragmatic engineering philosophies have sustained the application-oriented hypothesis of this basic research.

Sincere thanks go to Dr. Jim Klausner for his invaluable advice and guidance.

I thank Robert Harker and Jeff Studstill for their generous assistance in assembling the experimental apparatus.

TABLE OF CONTENTS

ACKNOWLEDGEMENTS iii

LIST OF TABLES vii

LIST OF FIGURES viii

KEY TO SYMBOLS xi

ABSTRACT xiv

CHAPTERS

1 INTRODUCTION 1

Problem Summary 2
Method of Attack 5
Impact of this Research 6

2 PROJECT OVERVIEW 8

Objectives 8
Project Structure 9
Finite Element Model Tasks 10
Experimental Model Tasks 10
Mathematical Model Tasks 10

3 LITERATURE REVIEW 12

Overview of Condensation Research 12
Methodologies for a Concentration Solution 14
Concentration Measurement Techniques 22
Interferometers 23
Probes 25
Experimental Investigations 28
Pertinence of the most Parallel Works 30

4 ANALYTIC METHODOLOGY 34

Presentation of the Governing Equations 34
Solution of the Concentration Equation 37
Solutions giving the Velocity Profile 40
Determination of the Characteristic Constants 41
Calculation of Heat and Mass Transfer 42
Mathematical Model 43
Finite Element Model 48

5 EXPERIMENTAL METHODOLOGY 51

Cooled-Wall Channel Subsystem 53
    Air-Side Channel 55
    Coolant-Side Channel 58
    Coolant Delivery Equipment 59
Concentration Probe Subsystem 61
    Concentration Probe 61
    Positioning Equipment 64
    Signal Conditioning Equipment 64
Data Analysis 65
System Qualification 69
    Cooled-Wall Channel Subsystem 70
    Concentration Probe Subsystem 71
    Standard Instrumentation 72
    Dry Heat Transfer Trials 73

6 RESULTS 77

Finite Element Analysis 77
    Velocity Vectors 77
    Buoyancy 78
Experimental Investigation 81
    Buoyancy 81
    Concentration and Temperature Profiles 82
    Heat and Mass Transfer Rates 89
Mathematical Model 91
    Concentration Solution 92
    Concentration Profiles 95
    Relative Humidity Profiles 100
    Heat and Mass Transfer Rates 105

7 CONCLUSIONS 112

Principal Conclusions 112
Relation to the Literature 114
Recommendations for Future Work 115
Recommendations for Improved Results 117

APPENDICES

A FINITE ELEMENT MODEL 119

B FORTRAN MODEL 125

C PROBE ANALYSIS 135

Adiabatic Saturation Analysis 136
Heat and Mass Transfer Analysis 138
Transient Response 140

D RADIATION EFFECTS 142

E PROBE-FIELD POTENTIAL 144

F INSTRUMENTATION AND PROCEDURE 147

Instrumentation Subsystem 147
Data Collection Procedure 149

REFERENCE LIST 152

BIOGRAPHICAL SKETCH 161

LIST OF TABLES

Table 2-1. List of objectives proposed at the commencement of this work. . . . 8

Table 3-1. Comparison of the most pertinent works found in the literature. . 14

Table 3-2. Comparison of concentration measurement methods reported in the literature. 23

Table 3-3. Boundary conditions and primary results of pertinent experimental work. 29

Table 3-4. Characteristic elements of the present research. 31

Table 5-1. Capabilities of the cooled-wall channel subsystem. 53

Table 5-2. Specifications of flow straighteners used at channel inlet. 57

Table 6-1. Comparison of predicted non-condensable gas film thickness with experimental data. 96

Table C-1. Results of example perturbation calculation. 138

Table F-1. Primary instrumentation used in the experimental system. 148

Table F-2. List of data taken for each trial. 150

Table F-3. List of data taken during each probe traverse. 151

LIST OF FIGURES

Figure 1-1. Typical temperature, concentration, and pressure profiles from the wall to the bulk vapor-gas mixture. 4

Figure 2-1. Organizational chart showing the principal relationships among activities of this project. 9

Figure 4-1. Results of model validation: concentration profiles of humid air, inlet air conditions are 78 F (26 C) 70% rh 45

Figure 4-2. Effect of specified velocity distribution, w, on concentration distribution, Φ. 46

Figure 4-3. Plot of FEA predicted velocity and temperature in the xz-plane 50

Figure 4-4. Plot of FEA predicted velocity in the yz-plane 50

Figure 5-1. Schematic diagram of the experimental system 52

Figure 5-2. Photograph of the cooled-wall channel and associated equipment. 54

Figure 5-3. Photograph of the laboratory installation. 54

Figure 5-4. Cross section drawing of the channel assembly. 56

Figure 5-5. Drawing of concentration probe tip detail and shank cross section. 62

Figure 5-6. Measured adiabatic-plate and cooled-plate specific humidity profiles 74

Figure 5-7. Heated-plate temperature profiles at $Re_L = 10^5$. 76

Figure 6-1. Plot of FEA predicted velocity vectors at center of channel. . . . 79

Figure 6-2. Plot of FEA predicted velocity vectors near the plate surface. . . 79

Figure 6-3. Measured concentration and temperature profiles at $Re_L = 3x10^4$ 83

Figure 6-4. Measured concentration and temperature profiles at $Re_L = 10^5$ . . 84

Figure 6-5. Correlation of measured difference between concentration and temperature boundary layer thicknesses. 86

Figure 6-6. Comparison of measured Nusselt number and Sherwood number with published empirical correlations. 90

Figure 6-7. Solution to the concentration equation plotted for $Re_x < 7x10^5$. . 93

Figure 6-8. Solution to the concentration equation plotted for $7x10^5 < Re_x \leq 2.42x10^6$. 94

Figure 6-9. Family of concentration profiles for $3x10^4 \leq Re_L \leq 9x10^5$ 97

Figure 6-10. Family of concentration profiles for $0.05 \leq C_D \leq 10$ 98

Figure 6-11. Family of relative humidity profiles for changing T_w 101

Figure 6-12. Family of relative humidity profiles for changing ϕ_i 103

Figure 6-13. Family of relative humidity profiles for $0.05 \leq C_D \leq 10$ 104

Figure 6-14. Sensible heat ratio versus Reynolds number with constant diffusion factor. 106

Figure 6-15. Sensible heat ratio versus isothermal wall temperature. 107

Figure 6-16. Sensible heat ratio versus diffusion factor C_D. 109

Figure 6-17. Sensible heat ratio versus Reynolds number with variable diffusion factor. 110

KEY TO SYMBOLS

Symbol	Name	Explanation
A_k	constant	coefficient in series solution
A_{xy}	channel area	normal to mixture flow
A_{xz}	wall area	for heat and mass transfer coefficient
c_p	nondimensional specific heat at constant pressure	
$c_{p,i}$	dimensional c_p	of species i
$c_{p,j}$	dimensional c_p	of species j
$c_{p,i+j}$	dimensional c_p	of the mixture of species i and j
C	concentration	mass of vapor per unit mass of mixture
C_i		at channel inlet
C_w		at liquid / gas-vapor mixture interface
C_D	diffusion factor	introduced in Chapter 6
D_{ij}	mass diffusivity	Fick's Law coefficient for species i and j
$f(\ )$	some function of	denotes independent variables
$f(\eta)$	stream function	dimensionless, used in Blasius's equation
Gr	Grashof number	ratio of buoyancy to viscous forces
Gr_L		based on gravity direction length
g	acceleration	due to gravity
h	convection heat transfer coefficient	
h_Z	average convection heat transfer coefficient	
h_{fg}	latent heat of vaporization	
h_m	convection mass transfer coefficient	
$h_{m,Z}$	average convection mass transfer coefficient	
K	permeability of porous medium	
k	thermal conductivity	
L	length	distance from leading to trailing edge
Le	Lewis number	ratio of thermal and mass diffusivities
Nu	Nusselt number	ratio of convection to conduction
P	nondimensional pressure	
P^*	pressure	
P_r	reference pressure	
Pr	Prandtl number	momentum:thermal diffusivities
p	artificial velocity	
$\bar{p}$	squared transformed artificial velocity	
Q_{cond}	total heat transfer due to latent heat of condensation	

Symbol	Name	Explanation
Q_{sens}	total heat transfer resulting in a temperature change	
R	gas constant	
R_o	channel half-width	distance from wall to centerline
R_w	resistance	of probe wire
Re	Reynolds number	ratio of inertia to viscous forces
Re_L		based on L
Re_x		based on a flow-direction distance
r	artificial distance	
$\bar{r}$	transformed artificial distance	
Sc	Schmidt number	ratio of momentum and mass diffusivities
Sh	Sherwood number	ratio of convection to diffusion
SHR	sensible heat ratio	ratio of sensible to total heat transfer
T	temperature	
T_i		vapor-gas mixture at channel inlet
T_w		vapor-gas mixture at wall
U_∞	velocity	outside the boundary layer
u	velocity[1]	in the flow-direction
V	characteristic velocity or voltage; context defined	
y	direction[2]	normal to wall
W_{sp}	specific humidity	mass H_2O per unit mass dry air
$W_{sp,i}$		at inlet
$W_{sp,m}$		mean outlet
$W_{sp,s}$		at saturation concentration

Greek Letters

α	artificial velocity or thermal diffusivity; context defined
β	volumetric thermal expansion coefficient
β_n	artificial acceleration
Γ	squared concentration excess
Δ	denotes a difference or change
δ	dimensionless momentum boundary layer thickness
$\delta_{t'}$	turbulent momentum boundary layer thickness
δ_c	dimensionless concentration boundary layer thickness
δ_t	dimensionless thermal boundary layer thickness
δ_L	free convection boundary layer thickness
ϵ	transformed distance into channel

---

[1] See Chapter 4 for additional velocity definitions.

[2] See Chapter 4 for additional length and direction definitions.

ζ	transformed axial coordinate
η	similarity variable
Θ	concentration in excess of inlet condition
θ	temperature in excess of wall condition
Λ	volumetric flow rate, volume per unit time
λ_k	eigenvalue
μ	dynamic viscosity
ν	kinematic viscosity
ξ	transformed normal coordinate
P	reference density
ρ	nondimensional density
ρ^*	density
τ	time constant
Φ	concentration in excess of wall condition
ϕ	relative humidity
Ψ	stream function

Subscripts

c	concentration
t	thermal
t'	turbulent
i	at inlet to channel or species "i"; context defined
j	species "j"
L	based on length
m	mean value across boundary layer
o	center or midchannel conditions
w	at channel wall
x	local conditions
s	saturation condition
Z	average over entire length in z-direction
∞	free stream conditions

Superscripts

$*$	dimensional quantity

Abstract of Dissertation Presented to the Graduate School
of the University of Florida in Partial Fulfillment of the
Requirements for the Degree of Doctor of Philosophy

FORCED CONVECTION CONDENSATION FROM A VAPOR NONCONDENSABLE GAS MIXTURE

By

Michael K. West

May 1992

Chairperson: Elmer C. Hansen
Major Department: Mechanical Engineering

A fundamental understanding of the relevant heat and mass transfer processes is necessary to further improve, from a theoretical basis, the design of condensing heat exchangers. The objective was to develop an experimentally supported mathematical model of vapor condensation from a mixture of noncondensable gas and vapor. The model was obtained from an analytically derived, exact, explicit, two-dimensional solution to the concentration boundary-layer equation. Both boundary-layer and fully developed flow in a channel were considered. Included in the model was an experimentally obtained diffusion inhibition correlation.

Water vapor concentration and temperature profiles of humid air were measured over a cooled fin model at velocities typical of a dehumidifying heat exchanger. A wet-bulb concentration probe was developed to make these measurements. A three dimensional finite element analysis of velocity and temperature further reconciled experimental measurements and model predictions. The experimental data supports an inhibited diffusion hypothesis. The hypothesis defines a relationship between the degree of diffusion inhibition and Reynolds number. Explanations of this relationship, based on boundary-layer gradients, are postulated.

Exchanger sensible heat ratio was found to increase with increasing inlet velocity, mainly due to increasing inhibition of diffusion. Using the finite element model and smoke visualization, it was confirmed that buoyancy induced convection currents disturb the laminar boundary layer, increasing heat and mass transfer. A noncondensable gas film was detected which decreases in thickness with increasing inlet velocity or diffusion resistance.

It was concluded that condensation rate is related to the gradient across the noncondensable film and the effective mass diffusivity of the vapor-gas mixture. It appears that the concentration gradient near the interface may be a strong function of gas film thickness. Condensation rate may be significantly increased by increasing the diffusion rate through the boundary layer or decreasing the gas film thickness.

CHAPTER 1
INTRODUCTION

A fundamental understanding of the relevant heat and mass transfer processes is necessary to further improve from a theoretical basis the design of condensing heat exchangers. Although the bulk performance of condensing heat exchangers has been widely studied, there has been little study of heat-exchanger condensation processes at the boundary-layer and molecular levels. The principal transfer process resistances involve the boundary layer. It follows that the most promising design tools would follow studies and models of the boundary layer. Furthermore, most works consider low noncondensable concentrations or use approximate analogies with dry heat transfer. Typically, condensing heat exchanger design is based on empirical test data, useful mainly to determine which heat exchanger is required for a specified application. Using this empirical method for design optimization results in a continuous test-revise loop.

A theoretical model of the exchanger boundary layer could facilitate predictions of the effects of new design features on performance at all operating conditions, preluding empirical tests. Additionally, an analytic model can implicitly suggest design goals based on explicit relationships between geometric and operating condition variables, and overall performance.

The heat exchanger type to be considered here involves condensation from a mixture of vapor and noncondensable gas. When the mixture is cooled to a temperature below the saturation temperature of the vapor, the vapor condenses to liquid. The saturation temperature of the noncondensable gas component of the mixture is much lower than that of the vapor.

There has been limited theoretical and experimental work reported on the condensing boundary layer and still less attention paid to condensation enhancement. Yet, the importance of understanding condensation heat and mass transfer mechanisms is reflected in numerous papers.

Problem Summary

The hypothesis is advanced by developing a boundary-layer model of condensation from a mixture of vapor and noncondensable gas. Development and use of the model will support the argument that a theoretically based boundary-layer analysis of mass transfer would be valuable for condensing heat exchanger optimization. The ultimate application of such a model would be to suggest and examine methods to increase condensation performance.

One useful performance gain is an increase in the ratio of mass to heat transfer rate. Enhancing mass transfer in condensing heat exchangers would allow them to operate at temperatures nearer the saturation point. Applications of this technology include heat exchangers used for air-conditioning and condensers used in electric power generation, petroleum refining, and food processing.

Condensation of vapor from noncondensable gas occurs when the vapor concentration exceeds saturation. This usually occurs at the cooled heat-exchanger surface rather than in the free stream. (Cooling the free stream to saturation would require a much colder fin surface, limiting the thermodynamic efficiency of the overall process.) Thus, the boundary layer very near the mixture-condensate interface is examined.

A diagram of the pertinent profiles is shown in Figure 1-1. The upper branch of the vapor concentration profile is similar to the temperature profile. The reduction in vapor concentration gradient at the interface, shown by the lower branch, is caused by a gas film. The presence of the gas film is not predicted by approximate solutions to the concentration equation.

The main condensation resistance types are believed to be conduction resistance through the condensate film, mass transfer resistance at the interface, and diffusion resistance through the mixture. The condensate film is usually very thin and its temperature profile is almost linear so that conduction resistance is negligible.[3]

Mass transfer resistance at the interface is essentially phase change resistance. Phase change, for a finite heat transfer rate, is relatively instantaneous. The time for molecular agglomeration from the vapor to the liquid phase to occur is insignificant compared to the time for removal of the latent heat to occur. Thus, phase change resistance is also negligible.

Diffusion resistance results in the formation of a condensation-inhibiting

---

[3] This is easily verified using Fourier's conduction rate equation.

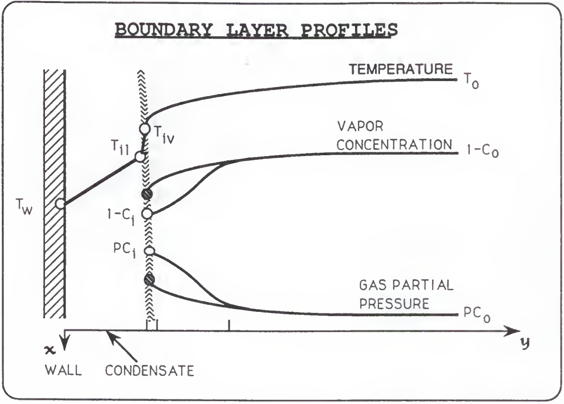

Figure 1-1. Typical temperature, concentration, and pressure profiles from the wall to the bulk vapor-gas mixture.

gas film at the interface. As the vapor condenses from the mixture it leaves behind a film of noncondensable gas at the condensate-mixture interface. The gas film can be equated to a high gas concentration and thus a lower vapor partial pressure at the interface. In turn, this reduces the vapor concentration gradient and slows the rate of mass transfer.

This resistance can also be qualitatively examined at the molecular level. Diffusion is hindered by collision with the noncondensable molecules and limited by the strength of the gradient. The gradient is weakened by the gas film at the interface. This is where the condensation rate would gain most from a strong concentration gradient. The gas molecules at the interface diffuse towards the free stream further hindering the flow of vapor to the interface.

Method of Attack

Techniques for an experimental and analytical examination of the condensing boundary layer over a heat-exchanger fin were developed. Two heat-exchanger fins form a cooled-wall channel. Methodologies for examination of the gas film over one wall followed a three-pronged attack: (i) a concentration probe capable of detecting the gas film was used to measure boundary-layer profiles; (ii) an exact, explicit, two-dimensional solution to the concentration equation was found, and a mathematical boundary-layer model was developed based on this solution and an experimentally derived diffusion correlation; and (iii) a three dimensional finite element analysis of velocity and temperature was used to further reconcile experimental measurements and model predictions.

Finite element analysis affords the ability to model three-dimensional flow in a channel. This allows an analysis of temperature and concentration induced buoyancy effects. Heat and mass transfer rates may be increased by buoyancy induced convection currents that disturb an otherwise laminar boundary layer.

Experimentally measured concentration profiles are lacking in the literature. The experimental portion of this work provided measured profiles, as well as condensing and dry heat transfer coefficients. The heat-exchanger fin was modeled as an isothermal flat plate to establish a boundary condition and yield a more useful interpretation of the results. Dimensioning of the channel was based on 25× dynamic similitude to expand the boundary layer. A miniature dry bulb--wet bulb thermocouple probe was used to measure concentration and temperature profiles over the vertically mounted plate. Smoke visualization was employed to study buoyancy effects.

An exact explicit solution to the concentration equation, unavailable in the literature, readily provides the concentration of vapor at any point in the channel. It is also easily extended to a computer model of the boundary layer that can calculate profiles and heat and mass transfer rates. Unlike a polynomial approximation of the concentration boundary-layer profile, the exact solution renders the noncondensable film. The resulting model predicts the effect of boundary condition and fluid property changes on velocity, temperature, and concentration profiles, and on sensible and latent heat transfer rate.

Impact of this Research

The experimental examination of the condensing boundary layer contributes significantly to current knowledge about condensation. Few studies have been reported which explore this area. The mathematical model of forced convection condensation advances our understanding of the concentration boundary layer and could lead to further optimization of condensing heat-exchanger designs. An expansion of current understanding of the heat and mass transfer processes occurring at and near the condensate-mixture interface allowed identification of a significant resistance to condensation heat transfer, namely diffusion resistance. Development of the experimental method tests a new means of measuring the concentration gradient.

This work expands current knowledge of condensation heat transfer as applied to condensing heat exchangers and the boundary layer adjacent to the condensation surface. It may suggest techniques to increase the latent heat transfer coefficient. Additionally, it may lead to a technology for increasing the condensation rate in condensing heat exchangers without a decrease in coolant temperature or change in surface area.

Calibration and use of the concentration probe, developed for this work, validated it as an economical instrument for the measurement of weak concentration gradients over distances as small as 0.05 mm (0.002 in). Such an instrument would be useful to the heat and mass transfer research community.

By approaching the challenge of increasing latent heat transfer armed with results from this research effort, the likelihood of success is improved.

CHAPTER 2
PROJECT OVERVIEW

The goal of this work is to develop an experimentally supported model of vapor condensation from a mixture of noncondensable gas and vapor. This was accomplished using an exact explicit solution to the concentration equation.

Objectives

The purpose was advanced by satisfying the objectives listed in Table 2-1.

Table 2-1. List of objectives proposed at the commencement of this work.

Objectives

1. Complete a closed form solution of vapor concentration throughout flow over a cooled plate.
2. Use the solution to develop a model of the concentration boundary layer giving profiles and heat and mass transfer rates.
3. Experimentally measure concentration and temperature profiles.
4. Improve the model based on experimental results.
5. Use the results to examine the dominating contributions to the resistance in condensation mass transfer.
6. (Optional) Experimentally measure wet and dry heat and mass transfer coefficients.

Project Structure

Three activities were completed to satisfy the project objectives. Each activity, as diagrammed in Figure 2-1, proceeds from the objectives.

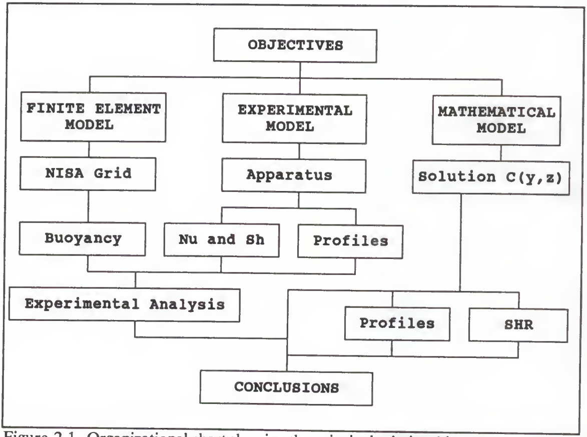

Figure 2-1. Organizational chart showing the principal relationships among activities of this project.

The primary function of the finite element model was to determine the severity of buoyancy effects on the flow. The experimental model provided temperature and concentration profiles, heat and mass transfer coefficients, and a qualitative examination of vorticity. The mathematical model was refined using results of the experimental work. Conclusions were based on the experimental analysis together with the profiles and mass transfer predicted by the refined mathematical model.

Finite Element Model Tasks

1. Develop a three dimensional finite element grid capable of predicting the effects of buoyancy on a velocity vector representation of the flow in a narrow channel.
2. Compare the results of two finite element analyses, one considering and the other neglecting buoyancy, and establish the qualitative effect of buoyancy on the velocity vectors.

Experimental Model Tasks

1. Design and construct an experimental apparatus capable of modeling the flow of moist air in a channel with wall condensation, of measuring condensing and dry heat transfer coefficients, and of visualizing buoyancy-induced vorticity.
2. Design and construct a miniature dry--wet bulb thermocouple probe capable of measuring the temperature and concentration profiles over one wall of the channel.
3. Compile concentration and temperature profile data at a series of velocities representative of a dehumidifying heat exchanger. Also collect heat and mass transfer data.
4. Perform analyses of the data to: (i) determine the effect of inlet air velocity on concentration profile characteristics, (ii) suggest the dominating resistances to mass transfer, and (iii) facilitate refinement of the mathematical model.

Mathematical Model Tasks

1. Complete an exact explicit two-dimensional solution to the concentration equation.
2. Extend the solution to produce a computer model of the condensing

boundary layer in a channel giving velocity, temperature, and concentration profiles, and sensible and latent heat transfer rates. Use experimental results to refine the model.

3. Use the model to postulate the dominating condensation resistances and predict the effect of these resistances on the sensible heat ratio of a typical dehumidifying heat exchanger.

CHAPTER 3
LITERATURE REVIEW

A thorough review of the literature applicable to condensation of a vapor from a noncondensable gas was accomplished. A total of 76 research investigations, performed between 1908 and 1990 (most after 1960), were reviewed by the author.[4] The studies reviewed were grouped into four categories: bulk condensing heat exchanger behavior, theoretical analyses of boundary-layer dynamics, concentration measurement methodologies, and experimental investigations.

Overview of Condensation Research

Beginning with the work of Nusselt (1916), condensation of pure saturated vapors in free convection has been extensively studied. Several years earlier, the work of Prandtl (1904) opened the way for theoretical forced convection condensation studies. Several years later, investigations considering noncondensable gas were performed. They were initiated to determine the effect of air on condensation rate in steam condensers, to explain striking reductions in heat transfer rate. With the advent of digital computers in the late 1960s, boundary-layer concentration profiles were found by numerical solution of the boundary-layer equations.

---

[4] Sources included the Engineering Index; and Compendex database searches of dissertation, engineering, and chemical abstracts.

Most investigations of forced convection condensation from a mixture of vapor and noncondensable gas have considered steam-air mixtures having 100 or more times the concentration of water vapor in humid air. The present work focuses on humid air. Furthermore, most performance models of dehumidifying heat exchangers have treated the exchanger in bulk (McQuiston, 1981; Turaga et al., 1988). Only a few works have presented calculated or measured concentration boundary-layer profiles. The papers most pertinent to this investigation are listed in Table 3-1.

One exception, which does not consider the exchanger in bulk, is an investigation performed by Eckels and Rabas (1987). They considered the boundary layer over the surfaces of a finned-tube dehumidifying heat exchanger. Specifically, the work implemented boundary-layer suction theory to analyze the effect of transverse velocity on momentum, heat and mass transfer. Overall air and water side enthalpy changes were measured. It was found that sensible heat transfer coefficient is elevated up to 50% when condensation occurs. The Chilton-Colburn heat and mass transfer analogy was found to hold well at velocities less than about 3 m/s (600 FPM), but the analogy prediction was lower than the experimental data at high velocities. They concluded that transverse velocity effects were significant.

Table 3-1. Comparison of the most pertinent works found in the literature.

PI-AUTHOR year	GEOM	ANALYSIS	EXP	C(i,j)
Koh 1962	xy	simil-integr-numer	num	not solved
Sparrow 1967	xy	simil-integr-numer	num	not solved
Taitel 1969	xy	simil-integr-numer	num	not solved
Lebedev 1969	xy	similarity	YES	not measured
Minkowycz 1969	xy	similarity-integral	num	derivative
Denny 1971	xy	CFD	num	YES
Denny 1972	xy	CFD	num	implicit
Kotake 1978	rx	integral	num	axial only
Kotake 1980	xy	dimensional	-	implicit
Raffellini 1980	xy	fin equation	YES	not measured
Rose 1980	xy	approximate	num	not solved
Schröppel 1981	xy	Hermetian-numer	num	not solved
Kotake 1985	xy	perturbation	-	not solved
Legay- 1986	xy	CFD	YES	not measured
Nolte 1988	rθz	energy balance	YES	YES
Coney 1989	xyz	Newton iteration	num	not solved
Coney 1989a	xyz	data only	YES	not measured
Huhtiniemi 1989	xy	data only	YES	not measured
Siddique 1989	xy	ener balance-num	num	not solved
Chaoyang 1989	xy	similarity	num	not solved
THIS WORK	xy	exact explicit	YES	YES

Methodologies for a Concentration Solution

Nusselt (1916) formulated the classical theory of film condensation. His work considered smooth laminar film condensation of a pure saturated vapor condensing on an isothermal wall. Refinements include the presence of noncondensable gas (Othmer, 1929). Moy (1969) provides a thorough account of the developments of free convection condensation in his dissertation.

The study of forced convection flow over a flat plate begins with Prandtls boundary-layer conservation equations of 1904, given by Schlichting (1955), which can be reduced to the following system

$$\frac{\partial u}{\partial x} + \frac{\partial v}{\partial y} = 0$$

$$u\frac{\partial u}{\partial x} + v\frac{\partial u}{\partial y} = \nu\frac{\partial^2 u}{\partial y^2} \tag{3-1}$$

$$u(y=0) = v(y=0) = 0 \qquad u(y=\infty) = U_\infty$$

since the flow is steady and there is no pressure gradient in the flow direction. The classic solution to the boundary-layer equations was found by Von H. Blasius (1908). The continuity equation is satisfied using the stream function Ψ(x,y),

$$\frac{\partial \psi}{\partial x} = -u \qquad \frac{\partial \psi}{\partial y} = v \tag{3-2}$$

which is introduced into the momentum equation. By transforming variables from Ψ(x,y) to f(η) where

$$\eta = y\sqrt{\frac{U_\infty}{\nu x}} \tag{3-3}$$

the set of boundary-layer equations, (3-1), is reduced to the single nonlinear ordinary differential equation referred to as the Blasius equation,

$$\begin{gathered} 2f''' + f''f = 0 \\ f(\eta=0) = 0 = f'(\eta=0) \qquad f'(\eta=\infty) = 1 \end{gathered} \tag{3-4}$$

to which Blasius (1908) found a solution. Blasius substituted series expansions for f and its derivatives of the form

$$\begin{aligned} f(\eta) &= A_0 + A_1\eta + \frac{A}{2!}\eta^2 + \frac{A_2}{3!}\eta^3 + \frac{A_3}{4!}\eta^4 + \frac{B}{5!}\eta^5 + \ldots \\ f''(\eta) &= A + A_2\eta + \frac{A_3}{2!}\eta^2 + \frac{B}{3!}\eta^3 + \frac{B_1}{4!}\eta^4 + \frac{B_2}{5!}\eta^5 + \ldots \end{aligned} \tag{3-5}$$

into the differential equation (3-4) to determine the first eight coefficients of the series. Howarth (1938) calculated the next four terms in the series, providing acceptable accuracy for $\eta > 3.5$, $f'(\eta = 3.5) \approx 0.91$. The series solution, as given by Tietjens (1970), is

$$\begin{aligned} f'(\eta) = \frac{u}{U_\infty} = 0.332\eta \; - \; 2.296{\cdot}10^{-3}\eta^4 \; + \; 1.9967{\cdot}10^{-5}\eta^7 \; - \\ 1.5694{\cdot}10^{-7}\eta^{10} \; + \; 1.1294{\cdot}10^{-9}\eta^{13} \; - \\ 7.6348{\cdot}10^{-12}\eta^{16} \; + \; 4.9468{\cdot}10^{-14}\eta^{19} \; - \\ 3.0579{\cdot}10^{-16}\eta^{22} \; + \; 1.799{\cdot}10^{-18}\eta^{25} \; - \\ 1.0104{\cdot}10^{-20}\eta^{28} \; + \; 5.456{\cdot}10^{-23}\eta^{31} \; - \\ 2.839{\cdot}10^{-25}\eta^{34} \; + \; - \; \ldots, \end{aligned} \tag{3-6}$$

The well-known energy and species equations which apply to the steady boundary layer over a flat plate are

$$\begin{aligned} u\frac{\partial T}{\partial x} + v\frac{\partial T}{\partial y} &= \alpha\frac{\partial^2 T}{\partial y^2} \\ u\frac{\partial C}{\partial x} + v\frac{\partial C}{\partial y} &= D_{ij}\frac{\partial^2 C}{\partial y^2} \end{aligned} \tag{3-7}$$

The similarity of form between the equations of (3-7) and the momentum equation of (3-1) suggest that Blasius' solution may also satisfy the energy and concentration equations. It does, but only if the following conditions are satisfied:

1. The coefficient of the second order terms in equation (3-7), α and D_{ij}, must be equal to ν (giving $Pr = Sc = 1$); recall that η is defined using ν in equation (3-3).
2. The variables T and C must be defined such that the specified velocity, temperature, and concentration boundary conditions are analogous.
3. The rate of mass entering or leaving the surface is so small that it does not effect the velocity profile.
4. The specific heats of the two species are equal; the mixture remains homogeneous with respect to specific heat.
5. Heat and mass are transferred to or from the fluid at the surface only. This precludes the generation of heat due to viscous dissipation and homogeneous condensation.
6. The physical properties of the fluids are constant with time, position, velocity, and temperature.

Pohlhausen[5] showed that the relationship between the thermal and hydrodynamic boundary layers is approximately given by

$$\frac{\delta}{\delta_t} \approx Pr^{\frac{1}{3}} \tag{3-8}$$

Extending the mass transfer analogy suggests a similar relation between the concentration and hydrodynamic boundary layers, given by equation (3-9).

Subsequent work has furthered this result. Koh (1962) used an iterative

---

[5] See Welty et al. (1976).

$$\frac{\delta}{\delta_c} \approx Sc^{\frac{1}{3}} \tag{3-9}$$

procedure to find boundary conditions at the liquid-vapor interface which satisfy Blasius' equation (3-4) for the liquid film. (The work considers only pure vapor.) Having the solution to the liquid and vapor momentum equations, the liquid energy equation was directly integrated to yield the temperature profile in the liquid film.

The first to propose a theory, based on the conservation laws, alone, that considers the presence of noncondensables was Sparrow and Lin (1964). The work was spurred by growing evidence that even a small amount of noncondensable gas causes a marked reduction in heat transfer in steam condensers. Hampson (1951) performed one of the first experimental investigations of this effect. He found a 33% reduction in heat transfer rate. Up until then, the main concern of most investigations was the condensation of pure saturated vapor. The presence of noncondensables had not been considered.

Lebedev et al. (1969) experimentally studied heat and mass transfer from humid air on a flat plate. (The work of Lebedev et al., (1969), was submitted before that of Sparrow et al., (1967).) They employed the classic similarity solution to the boundary-layer equations.

Sparrow et al. (1967) also considered the presence of noncondensable gas. They solved the similarity form of the boundary-layer equations both numerically and using a Kármán-Pohlhausen type integral solution. Continuing this work, Minkowycz and Sparrow (1969) focused on the effect of superheating; thus the work applies to pure vapor as well as to mixtures of vapor and gas.

An important conclusion of the work of Sparrow et al. (1967) is that interfacial resistance has a negligible effect on forced convection condensation of steam. This refutes the work of Baer and McKelvey (1958) which was based on kinetic theory. Harriot (1960) had also disagreed with Baer and McKelvey, declaring that diffusion effects are entirely responsible for the loss of heat transfer. Sparrow and Eckert (1961) had previously investigated the diffusional theory and provided a qualitative conclusion only.

The concentration distribution in direct contact condensation was obtained by Taitel and Tamir (1969) using a numerical solution to the similarity form of the momentum equation and the integral form of the concentration equation. They also employed an integral method based on second order polynomial approximations to the temperature and concentration profiles.

The first published set of concentration profiles for forced convection was produced by Denny et al. (1971).[6] They employed an implicit finite difference method with forward marching to solve the conservation equations. The conditions they considered are the following: velocity from 0.03 to 3 m/s (6 to 600 FPM), steam mass fraction from 0.900 to 0.999, free stream temperature from 38 to 100 C (100 to 212 F), and temperature difference from 2.7° to 22.2°C (5° to

---

[6] For the case of free convection, Moy (1969) plotted velocity, temperature and concentration distributions in the liquid and vapor boundary layers using a numerical method.

40°F). Denny and Jusionis (1972) continued this work by considering binary mixture condensation with methanol, propanol, acetone, and CCl_4. They also used variable fluid properties.

Supersaturation and homogeneous condensation were studied by HijiKata and Mori (1973). The researchers used the boundary-layer integral method to solve the conservation equations. Second order polynomial profiles were assumed, except for the temperature profile for which a polynomial of order n was employed. Their work demonstrated that $n \geq 2$.

The first investigation to focus on condensation with noncondensables in channel geometry was performed by Kotake (1978). He used the integral method to study condensation rate. In a subsequent work, Kotake (1980) presented a complete set of governing equations for the mixture and liquid film, and formulated the characteristic quantities that describe the flow. Kotake (1985) then extended this work for multicomponent mixtures, and determined the effect of a small amount of noncondensable gas by using a perturbation solution to the governing equations.

Flow through a porous medium was considered by Chaoyang and Chuanjing (1989). They employed a linear velocity profile, expressing the governing equations as given in equation (3-10). Using a similarity procedure analogous to that of Blasius' solution where momentum diffusivity is replaced with mass diffusivity in the similarity variables η and Ψ, the governing equations are reduced to the form given in equation (3-11).

$$\frac{\partial u}{\partial x}+\frac{\partial v}{\partial y}=0$$

$$u=-\frac{K}{\mu}\frac{\partial P}{\partial x}=U_{\infty} \qquad (3\text{-}10)$$

$$u\frac{\partial C}{\partial x}+v\frac{\partial C}{\partial y}=D_{ij}\frac{\partial^2 C}{\partial y^2}$$

$$f'=1$$

$$2\Phi''+f\Phi'=0 \qquad (3\text{-}11)$$

$$\Phi(\eta=0)=1 \qquad \Phi(\eta=\infty)=1$$

where Φ is the nondimensional gas concentration. The researchers present an analytic solution to this system:

$$\Phi = 1-\frac{erf[(\eta+f(0))/2]-erf[f(0)/2]}{1-erf[f(0)/2]} \qquad (3\text{-}12)$$

A closed form series solution to the Graetz problem[7] in mass transfer was given by Mansour (1989). The problem is described by the equations given in equation (3-13) employing the boundary conditions of (3-14). A product solution of equation (3-13) produces a Sturm-Liouville system which is, in turn, transformed into a form of the Schrödinger differential equation.

$$(1-\xi^2)\frac{\delta\Theta}{\delta\zeta} = \frac{\delta^2\Theta}{\partial\xi}$$

$$\Theta=\frac{(C-C_i)}{(C_s-C_i)} \qquad \xi=\frac{y^*}{R_0} \qquad \zeta=\frac{x^*D_{ij}}{\frac{3}{2}R_0^2u} \qquad (3\text{-}13)$$

---

[7] This problem considers a channel with a velocity profile that is fully developed before the onset of mass transfer (Eckert and Drake, 1972).

$$\xi=-1 : \Theta=1 \qquad \xi= 1 : \Theta=0 \qquad \zeta= 0 : \Theta=0 \tag{3-14}$$

Proceeding from a confluent hypergeometric function, the solution given is

$$\Theta(\xi,\zeta)=\sum_{k=0}^{\infty} A_k e^{-\lambda_k \zeta^2}\cdot\frac{\xi^{-\frac{1}{2}}}{\Gamma(1+\frac{1}{2})} \mathrm{M}_{\lambda_{\frac{k}{4}\pm\frac{1}{4}}}(\lambda_k \xi^2) \tag{3-15}$$

where $\mathrm{M}_{m,k}$ is known as Whittacker's function (Slater, 1960).

Other developments in the solution of the governing equations are limited with respect to the concentration equation. An approximate solution was employed by Rose (1980) to find heat transfer. Schröppel (1981) numerically integrated the system of governing equations using a finite difference method of Hermitian type. Coney et al. (1989b) considered a copper fin. Fin temperature distribution, liquid film thickness, and heat conduction through the fin were obtained using a Newtonian iteration procedure. Siddique et al. (1989) combined an energy balance at the interface with a similarity solution and numerically solved the system to predict the effect of hydrogen on steam condensation.

Concentration Measurement Techniques

Five methods for determining the concentration of vapor in a gas have been used for investigations reported in the literature. They are listed in Table 3-2. The laser holographic interferometer and the two-wave polarization schlieren interferometer are similar visualization devices. The fundamental difference between the two is their light source. Accuracy is limited since the fringe values represent integrated changes over the thickness of the flow field test

Table 3-2. Comparison of concentration measurement methods reported in the literature.

METHOD	REPORTED BY	ADVANTAGE	DRAWBACK
laser holographic interferometer	Kobayashi and Matsumoto, 1987	sharp fringes accuracy	complexity expense
schlieren interferometer	Usmanov et al., 1988	visual result	complexity
miniature wet-bulb probe	Peterson and Tien, 1987	small tip size	intrusive
hot-wire probe	Brown and Rebollo, 1972	fast response	empirical solution
dew-point probe	Nolte and Mayinger, 1988	accuracy	complexity

section. Determination of concentration from density requires assumptions or additional measurements. The miniature wet-bulb probe and the hot-wire probe are simple and precise instruments, but they are intrusive. The dew-point probe, a complex device, has the simplest analytical procedure. The five works employing these methods have established their value for differing applications.

Interferometers

The two optical interferometers appraised here enable precise flow visualization. Optical methods offer quick response, no disturbance of the flow field, and the opportunity to observe boundary-layer dynamics. Changes in the refractive properties of the fluid, due to a density change, cause phase interferences between two light beams. The resulting interference fringes are mathematically related to density change in the flow field using relationships between optical path length, refractive indices, and wavelength. Measurement of the fringe locations on the interferograms, along with some assumptions, yields concentration as a function of position.

Using this method and an He-Ne laser source, the concentration profiles in a thermosyphon were measured by Kobayashi and Matsumoto (1987). They used a variety of vapors (water, benzene, and acetone) and noncondensable gases (air and helium). Concentration measurement resolution was from 1.6% to 4.0%, and temperature errors were about 2° to 3°C. To obtain concentration from density, the researchers assumed that the vapor was in a saturated state corresponding to its temperature.

In a similar investigation, concentration profiles in a horizontal cylinder under natural convection were measured by Usmanov et al. (1988). The working fluids were H_2O-He and H_2O-CO_2. Although not explicitly expressed, their reported concentration measurements have a resolution of about 2 percent. They do not discuss the method used to determine concentration from density measurements. Light diffraction prevented them from making measurements closer than 0.2 to 0.3 mm (0.008 to 0.010 in) to the surface.

After review of the above works, it is evident that the main disadvantages of optical methods are a result of the difficulties in obtaining quantitative concentration profiles from the interferograms. In addition, the apparatus is complex and expensive. Density changes, which interferograms show as discrete fringes over a finite distance, are caused by temperature and pressure changes as well as concentration changes. The fringes indicate only density *difference*, thus the density at some point in the field must be known. Furthermore, only approximate determination of the reference refractive index is possible without knowing the concentration beforehand. Finally, diffraction near the surface, as reported by Usmanov et al. (1988), may preclude measurement of the very thin noncondensable film.

Probes

The probes appraised here are a hot-wire probe, a dew point probe, and a wet-bulb probe. All have the potential to precisely measure the concentration profile, including the noncondensable gas film. The probes provide an output voltage related to some thermodynamic process from which concentration can be obtained. Typically, an accurate traversing mechanism is used to move the probe tip through the boundary layer.

Linear traverses of 3.8 cm (1.5 in) across an 8.2 ℓ (500 in^3) volume of unspecified shape were made by Brown and Rebollo (1972) using a hot-wire probe. The diameter of their probe was 2 mm (0.08 in). The probe consisted of a hollow glass tube with a platinum wire spanned across an orifice at the working tip of the tube. A vacuum pump drew the mixture sample through the 0.028 mm (0.0011 in) orifice at the probe tip and across the 0.013 mm (0.0005 in) platinum wire. The power required to maintain the wire at a fixed temperature was found using a dimensional analysis of the form given in equation (3-16).

$$\frac{(V^2-V_0^2)}{R_w} = f(p_o,\rho_o,T_o,R,C_p,\mu_o,k_o,d,T_w,p_d) \tag{3-16}$$

The probe was then calibrated using varying isothermal concentrations of Krypton, Argon, or Helium in Nitrogen at constant temperature; condensation was not considered. Through dimensional analysis, together with the assumption that the voltage is not sensitive to flow velocity (which was shown to hold), a semi-empirical relationship between voltage and concentration was obtained. Resolution is claimed to be 0.5% of reading. An excellent characteristic of the hot-wire probe is its very small time constant of 2 ms. Using a smaller orifice, 0.0025 mm (0.0001 in), the investigators were able to obtain a time response of 0.2 ms.

Traverses of 8 mm (0.3 in) across a 40.5 mm (1.6 in) diameter annular tube were made by Nolte and Mayinger (1988) using a dew-point probe. Steam and air were the working fluids. Condensation was on the inner wall of the annulus. The probe determined dew point temperature by measuring the temperature of the thin 0.1 mm (0.004 in) copper foil probe tip with a miniature thermocouple. Probe diameter was 2.5 mm (0.1 in). The probe body consisted of three concentric capillary tubes. Cool air, supplied via the center tube, caused the temperature of the foil to drop. A sudden change in thermocouple output occurred when the foil reached the dew point temperature due to a change in heat transfer coefficient. The air leaves through the second tube, and the third provides insulation. Uncertainty was reported as ±1% for a 95% H_2O mixture, and ±2% for a 10% H_2O mixture. The time constant was shown to be about 2 s.

In a third experiment, traverses across a 41.3 mm (1.6 in) diameter thermosyphon were made by Peterson and Tien (1987) using a miniature wet-bulb probe. The working fluids were H_2O and He. The probe tip diameter was 1.5 mm (0.06 in), and the body was 6.4 mm (0.25 in) in diameter. The tip consisted of a fine-gauge thermocouple embedded in a liquid-soaked porous sphere, and a dry thermocouple radially offset 2.0 mm (0.08 in) from the sphere. The thermocouples provided wet-bulb and dry-bulb readings, respectively. From these readings the thermodynamic wet-bulb temperature, which is defined by the adiabatic saturation process, can be determined using the Lewis relation. (Fortunately, for H_2O-air the wet-bulb reading and the adiabatic saturation temperature are very close.) Accuracy was found to be better than 1%. The time constant is long, it was reported to be about 20 s.

Following review of the above work, the advantages and drawbacks of each probe are apparent. All have the disadvantage of physically disturbing the flow, and conversely, they provide high accuracy. The researchers reduced the intrusiveness effect by minimizing the probe size and using nonporous materials with low thermal conductivity. All have a finite response time that differs by an order of magnitude or more among the three probes. The hot-wire probe is by far the quickest ($\tau = 0.002$ s) but the non-rigorous calculation of concentration from the voltage output of the probe necessitates many assumptions and boundary conditions. Concentration is more readily obtained using the dew-point probe.

However, it is much slower to respond ($\tau = 2$ s) and the design is the most complex of the three. The wet-bulb probe also readily yields concentration, but with additional analysis due to the instrument dependence of wet-bulb *readings* (in contrast to *thermodynamic* wet-bulb *temperature* which is a property). Nevertheless, the wet-bulb probe's accuracy is better than 1%, as reported by Peterson and Tien (1987). The wet-bulb design is the simplest of the three and it is the slowest to respond ($\tau = 20$ s).

Experimental Investigations

Literature addressing condensation via experimental methods are considerably scarcer than papers based on analytic work. As a whole, experimental work has focused more on condensation heat transfer rate and less on boundary-layer dynamics. However, there are a few exceptions. The most pertinent experimental investigations are outlined in Table 3-3.

Condensation from humid air was studied by Lebedev et al. (1969), Raffellini and Tarabusi (1980), and Coney et al. (1989b). Lebedev et al. (1969) measured heat and mass transfer coefficients of condensation on a flat plate in a duct. They observed that mass transfer accounted for an increasing proportion of the total heat transfer as the inlet moisture content was increased. Additionally, they concluded that mass transfer increases with increasing velocity and temperature difference. The researchers suggested that heat and mass transfer predictions can be summed to yield total heat transfer. The work of Raffellini

Table 3-3. Boundary conditions and primary results of pertinent experimental work.

P-AUTHOR/yr	U_∞ [m/s]	C_{vap} [kg/kg]	FOCUS
Lebedev 1966	0.5 - 4.0	0.005 - 0.17	Nu,Sh
Asano 1979	0.3 - 2.3	0.213 - 0.97	T,q,Nu,Sh
Raffelli- 1979	1.5 - 5	0.006 - 0.02	T(fin),η,h
Legay- 1985	3 - 6	saturated	u,v,T,q,Nu
Nolte 1988	1.5 - 12	0.59 - 0.95	u,C,q,Nu,Sh
Coney 1989a	2 - 10	0.005 - 0.02	T(fin),Nu,η
Huhtin- 1989	1 - 3	0.3 - 0.7	h
THIS WORK	0.3 - 12	0.004 - 0.02	T,C,Nu,SHR

and Tarabusi (1980), and of Coney et al. (1989b), focused on fin temperature distribution and fin efficiency of copper fins in a duct. They showed that fin surface temperature increases with velocity, temperature, and concentration. Raffellini and Tarabusi (1980) showed that mass transfer decreased fin efficiency and increased heat transfer coefficient, and that end fins had a different temperature distribution than central fins. Coney at al. (1989b) observed that flow disturbances increased heat transfer.

Nolte and Mayinger (1988) measured axial velocity and concentration profiles. They also measured heat transfer coefficients as a function of inlet concentration for condensation of steam-air in an annular channel. The results show a decrease in heat transfer near the inlet only (x/L<.25, L=2 m=78.7 in) with increasing air concentration.

The remainder of the investigators considered much higher condensable concentrations. Asano et al. (1979) measured vapor-phase heat and mass fluxes in their study of condensation on a vertical flat plate. In addition to steam, the condensables were methanol, benzene, and carbon tetrachloride. Air was the noncondensable gas. Legay-Desesquelles and Prunet-Foch (1985, 1986) used only saturated mixtures of 40 to 60 C (104 to 140 F) air and steam. Both longitudinal and transverse velocity profiles, boundary-layer thickness, and temperature profiles are provided in these two related papers.

Pertinence of the most Parallel Works

Many experimental and numerical studies of condensation have been reported since the 1950s, yet most of these studies have focused on steam condensers. Several works show that much of the disparity in heat transfer coefficients measured among tests can be attributed to unconsidered noncondensable gas. Because of the lack of reliable experimental data and a validated model, the development of improved condensing heat exchangers is hampered by the non-rigorous nature of many empirical correlations and analogies, and by cumbersome implicit solution methods.

Most studies have not considered the elements of one promising application of condensation enhancement, commercial and residential air-conditioning. In this case, the noncondensable (air) concentration is very high; and the effect of temperature and face velocity on sensible heat ratio are theoretically unexplained in a rigorous manner. The studies which explore forced convection condensation of a vapor from a noncondensable gas over a flat plate do not completely and conclusively address the topic. There is little experimental data, and no exact explicit solution to or measurements of the concentration profile for this fundamental heat and mass transfer problem, in the literature reviewed. Methods for measuring the concentration profile are not fully developed.

The elements of the present work are aimed at contributing to these areas. They are given below in Table 3-4.

Table 3-4. Characteristic elements of the present research.

1. FORCED CONVECTION
2. NONCONDENSABLE GAS
3. CARTESIAN GEOMETRY
4. SUPERHEATED VAPOR
5. EXPERIMENTAL CONCENTRATION MEASUREMENT
6. EXPLICIT ANALYSIS
7. LAMINAR FLOW
8. HIGH NONCONDENSABLE CONCENTRATION
9. CONCENTRATION PROFILES
10. HEAT-MASS TRANSFER RATIO

Although valuable, many pertinent works are peripheral to the proposed work. Twenty-six of the reviewed works are parallel to the proposed activity. They will be discussed further in light of the characteristic criteria of this work.

Six of the 26 parallel works are fundamentally separate from the proposed activity since they address less than six of the elements in Table 3-4. Peterson and Tien (1987) presented and verified their mini-wet bulb measurements of helium/water gas concentration profiles in a gas-loaded two-phase thermosyphon.

Tu and Wang (1988) performed an analytical study of a two-phase thermosyphon. The effects of noncondensable gas on wall temperature profile and condensation heat transfer are given. Concentration profiles were not considered. Usmanov et al. (1988) used an interferometric procedure to obtain concentration fields of six water vapor - air mixtures in natural convection only. Tanner et al. (1965) experimentally determined the effect of low concentrations (2 to 500 ppm) of noncondensable gas on the condensation heat transfer rate of steam in a condenser. Wang and Tu (1988) considered only small amounts of noncondensable gas in a tube. Brouwers (1989) presented an analytical study of condensation of a pure vapor on a plate.

The remaining 20 studies, which address six or more of the elements listed above, are characterized in Table 3-1. Of these, seven of the reviewed papers were particularly relevant to this work. Experiments were described in six of these seven papers. Denny et al. (1971) provided concentration profiles but did not perform an experiment.

Lebedev et al. (1969) studied vapor condensation from humid air on a liquid-cooled flat plate in a controlled closed-loop duct. The analysis focused on measuring the onset and effects of turbulence, and on determining local heat- and mass-transfer coefficient changes due to condensation. Concentration profiles were not considered.

Nolte and Mayinger (1988) investigated condensation from a mixture of steam and air in a horizontal annular flow channel[8]. Concentration profiles in the radial, circumferential, and longitudinal direction were measured with their newly developed dew-point probe. Also, temperature profiles and total heat flux were determined. Reynolds numbers varied from 1500 to 13,000.

Legay-Desesquelles and Prunet-Foch (1985 and 1986) measured temperature profiles and sensible heat ratio, but only for saturated steam-air mixtures.

Coney et al. (1989b), and also Kazeminejad (1987) and Raffellini and Tarbusi (1980), studied dehumidification of moist air over a fin. They measured fin surface temperature profiles, took photographs for condensate visualization, developed heat-transfer correlations, and determined fin efficiencies. Measurements of mixture temperature and concentration distribution were not taken. The apparatus used by Raffellini and Tarbusi (1980) models, in geometric and dynamic similitude, a dehumidifying heat-exchanger fin.

Concentration profiles were calculated in an analysis by Denny et al. (1971); no experiment was performed. They solved the mass, momentum, energy, and concentration equations (viscous dissipation was neglected) using implicit finite difference equations (in Fortran IV on an IBM 360/91). Profiles for local condensation heat transfer, velocity, temperature, and concentration are plotted in their paper. Only high vapor mass fractions, from 0.9 to 0.999, were considered.

---

[8] Future work planned by Nolte and Mayinger is to develop correlations for heat and mass transfer coefficients (Nusselt and Sherwood numbers) for different steam concentrations and Reynolds numbers.

CHAPTER 4
ANALYTIC METHODOLOGY

The physical case modeled is heat and mass transfer to the isothermal flat surfaces of a channel under forced convection. The temperature and concentration gradient can be induced either by both surfaces, or by one surface if the opposite surface is adiabatic and impermeable. The surface could also be the simpler case of a flat plate in external flow. A mixture of vapor and noncondensable gas is introduced at the entrance to the channel, or to the leading edge of the flat plate, and flows parallel to it. The inlet velocity, temperature, and concentration are uniform and the flow condition is laminar. Development of velocity, temperature, and concentration boundary layers occur downstream from the leading edge of the walls or plate. Boundary conditions are such that condensation begins at the upstream edge of the surface. The two velocity boundary layers over the opposite walls of the channel cause an increase in core, or centerline, velocity. Parallel flow develops after the boundary layers meet. In the case of the flat plate, the conditions outside the boundary layer are constant.

Presentation of the Governing Equations

The cartesian orientation chosen for this analysis is consistent with condensation literature: x is the condensate flow direction, y is the direction normal to the surface, and z is the mixture flow direction (Kotake, 1980). The variables (x,y,z) are nondimensional according to

$$x = \frac{x^*}{X} \qquad y = \frac{y^*}{Y} \qquad z = \frac{z^*}{Z} \tag{4-1}$$

where (X,Y,Z) are characteristic lengths of the geometry and (x^*,y^*,z^*) are lengths in meters (feet). Similarly, the corresponding velocity variables (u,v,w) are nondimensional according to equation (4-2).

$$u = \frac{u^*}{U} \qquad v = \frac{v^*}{V} \qquad w = \frac{w^*}{W} \tag{4-2}$$

The quantities ρ, P, and c_p are nondimensional according to

$$\rho = \frac{\rho^*}{\mathrm{P}} \qquad P = \frac{P^*}{P_r} \qquad c_p = \frac{(c_{p,i} - c_{p,j})}{c_{p,i+j}} \tag{4-3}$$

where P is the reference density, P_r is the reference pressure, and c_p is the difference between the specific heats of each of the components i and j divided by that of the bulk mixture $i+j$. The nondimensional temperature θ and concentrations Γ and Φ are in excess of wall conditions (subscript w), and the concentration C is intrinsically nondimensional as described by the relations

$$\theta = \frac{T - T_w}{T_i - T_w} \qquad \Gamma = \Phi^2 = \left(\frac{C - C_w}{C_i - C_w}\right)^2 \qquad C = \frac{m_{vapor}}{m_{mixture}} \left[\frac{kg}{kg}\right] \tag{4-4}$$

where (in these relations) subscript *i* refers to the inlet condition.

The ensuing analysis is simplified by applying the following assumptions:

1. Effects of kinetic energy, viscous work and diffusion work, and compressible heating are negligible.
2. Buoyancy forces are negligible.
3. Mixture conditions at the leading edge are uniform and constant.
4. The mixture velocity in the *x* direction, perpendicular to the bulk flow, is negligible.
5. The surface is isothermal.
6. The mixture flow is laminar.
7. The condensate temperature profile is linear, and the temperature gradient is small.
8. The interfacial resistance is negligible, as justified by Sparrow et al. (1967).
9. Phase change occurs at the interface only.

The nondimensionalized conservation equations which describe the flow of a vapor-gas mixture with heat and mass transfer at the surface are then

$$\begin{gathered}
\frac{\partial}{\partial y}(\rho v)+\frac{YW}{ZV}\frac{\partial}{\partial z}(\rho w)=0 \\
\frac{\partial}{\partial z}(\rho w^2)+\frac{ZV}{YW}\frac{\partial}{\partial z}(\rho v w)=\frac{-Pr}{\rho_r W^2}\frac{\partial P}{\partial z}+\frac{ZV}{YW}\frac{\nu}{VY}\frac{\partial^2 w}{\partial y^2} \\
\frac{\partial}{\partial y}(\rho v\theta)+\frac{YW}{ZV}\frac{\partial}{\partial z}(\rho w\theta)=\frac{\nu}{VY}\frac{1}{Pr}\frac{\partial^2\theta}{\partial y^2}+\frac{YW}{ZV}\frac{c_p}{Sc}\frac{\partial C}{\partial y}\frac{\partial\theta}{\partial y} \\
\frac{\partial}{\partial y}(\rho v C)+\frac{YW}{ZV}\frac{\partial}{\partial z}(\rho w C)=\frac{\nu}{VY}\frac{\rho}{Sc}\frac{\partial^2 C}{\partial y^2}
\end{gathered} \qquad (4\text{-}5)$$

Solution of the Concentration Equation

For simplicity, the continuity equation of (4-5) can be reduced to

$$\frac{\partial v}{\partial y}+\frac{\partial w}{\partial z}=0 \quad if \quad \frac{YW}{ZV}=1 \tag{4-6}$$

and by assuming that the mixture is incompressible. This will ease the determination of the characteristic constants *Z* and *V*, performed in a subsequent section of this chapter, on page 41.

Solution of the concentration equation of (4-5) with the boundary conditions

$$C(y=0)=C_w \quad C(y=1-\frac{2R_0}{Y})=C_w \qquad C(z=0)=C_i \quad C(z=\infty)=C_w \tag{4-7}$$

begins by application of the assumption of incompressibility and substitution of equation (4-6). This procedure yields

$$(VY\frac{Sc}{\nu})v\frac{\partial C}{\partial y}+(\frac{WY^2}{Z}\frac{Sc}{\nu})w\frac{\partial C}{\partial z}=\frac{\partial^2 C}{\partial y^2} \tag{4-8}$$

which can be recast as

$$C_{yy}+pC_y=rC_z \tag{4-9}$$

by employing the relations

$$p\doteq-(VY\frac{Sc}{\nu})v \qquad r\doteq(\frac{WY^2}{Z}\cdot\frac{Sc}{\nu})w \tag{4-10}$$

It is convenient to replace the concentration C with the concentration excess Φ, defined in equation (4-4), which produces a system with simple boundary conditions:

$$\Phi_{yy} + p\Phi_y = r\Phi_z$$
$$y=0,\ y=1,\ z=\infty : \Phi=0 \qquad z=0 : \Phi=1 \tag{4-11}$$

The system is converted to normal form with the transformation

$$\Phi = \mathrm{M}e^{-\frac{1}{2}\int p dy} \tag{4-12}$$

where **M** is a function of (y,z). The resulting system is

$$\mathrm{M}_{yy} - \frac{p^2}{4}\mathrm{M} = r\mathrm{M}_z$$
$$y=0,\ y=1,\ z=\infty : \mathrm{M}=0 \qquad z=0 : \mathrm{M}=e^{\frac{p}{2}y} \tag{4-13}$$

The independent variable y is then transformed according to

$$\eta = \frac{\pi Y}{2R_0}y \tag{4-14}$$

and the coefficients are grouped using the relations

$$\alpha \doteq \frac{pR_o}{\pi Y} \qquad \bar{p} \doteq (\frac{pR_o}{\pi Y})^2 \qquad \bar{r} \doteq r(\frac{2R_o}{\pi Y})^2 \tag{4-15}$$

A new system where M is now a function of (η,z) is produced:

$$\mathrm{M}_{\eta\eta} - \bar{p}\mathrm{M} = \bar{r}\mathrm{M}_z$$
$$\eta=0,\ \eta=\pi,\ z=\infty : \mathrm{M}=0 \qquad z=0 : \mathrm{M}=e^{\alpha\eta} \tag{4-16}$$

Application of the finite Fourier sine transform,

$$S[M_{\eta\eta}(\eta,z)] = \int_0^\pi M_{\eta\eta}\sin(n\eta)d\eta = -n^2N(n,z) \tag{4-17}$$

using integration by parts, yields the governing equation

$$N_z + \beta_n N = 0 \qquad \text{where} \quad \beta_n = \frac{n^2+\bar{p}}{\bar{r}} \tag{4-18}$$

that implicitly satisfies the η boundary conditions. Solution of equation (4-18) is trivial. Using the transformed z boundary condition

$$N(z=0) = S[M(z=0)] = S[e^{\alpha\eta}] = \frac{n}{n^2+\alpha^2}[1-(-1)^n e^{\alpha\pi}] \tag{4-19}$$

the solution is

$$N = N(z=0)\,e^{-\beta_n z} \tag{4-20}$$

Subsequent to inverting the finite Fourier sine, η, exponential, and superposition transforms the final solution to the system of (4-11) is found to be

$$\Phi = \frac{2}{\pi}e^{-\frac{py}{2}}\sum_n^\infty \frac{n}{n^2+\alpha^2}[1-(-1)^n e^{\alpha\pi}]\,e^{-\beta_n z}\sin(\frac{n\pi Y}{2R_o}y) \tag{4-21}$$

The concentration distribution solution given in equation (4-21) was validated by substituting it into the differential equation of (4-11), using a symbolic manipulator[9]. The first term of the solution does indeed satisfy the differential equation, thus the series is a correct solution.

Solutions giving the Velocity Profile

The above solution to the concentration equation applies to flows with a known velocity distribution such as potential, external, entry region, or parallel flow. So, an appropriate velocity distribution must be specified to model these cases. The velocity profiles types employed here are constant, laminar, and turbulent.

Potential flow along a flat surface is described with a constant velocity distribution. External flow is described using the series solution to the Blasius equation described in Chapter 3. Fully developed parallel flow between two flat walls results in a parabolic velocity distribution of the form

$$w = 1 - (2y-1)^2 \qquad (4\text{-}22)$$

Flow in the inlet length of a channel results in development of a boundary layer under the influence of an accelerated external stream (Schlichting, 1955). The centerline velocity is approximated by the equation

$$w\Big|_{y=\frac{1}{2}} \approx [\, 1 + 1.7208\,\varepsilon \,] \qquad \varepsilon = \sqrt{\frac{\nu Z}{R_o^2\, W}\, z} \qquad (4\text{-}23)$$

---

[9] With considerable assistance from B. Edwards, Ph.D.of the Department of Mathematics at the University of Florida. The package used was *Mathematica* by Wolfram Research, Inc. of Champaign, Illinois.

The transverse velocity due to boundary-layer growth and vapor migration is also calculated.[10]

For the purposes of study only, a turbulent velocity profile of the form given in equation (4-24) is also considered (Schlichting, 1955).

$$w = \left(\frac{Y}{\delta_{t'}}y\right)^{\frac{1}{7}} \qquad \delta_{t'} = 0.37(Z\cdot z)\left[\frac{ZW}{\nu}z\right]^{-\frac{1}{5}} \tag{4-24}$$

Two velocity distributions are employed to model the flow between closely spaced fins. The inlet distribution is used from the leading edge downstream until ϵ attains a value of 0.4, then a switch to the parallel flow distribution is made. This procedure results in a discontinuity because the real boundary-layer distribution asymptotically transforms into the parabolic profile after the boundary layers meet. The discontinuity is negligible for the conditions considered here.

Determination of the Characteristic Constants

The characteristic constants that nondimensionalize the position and velocity variables, defined in equations (4-1) and (4-2), are determined by inspection of the continuity and momentum conservation equations. For simplicity the continuity equation of (4-6) yields, by choice

$$\frac{ZV}{YW} = 1 \tag{4-25}$$

---

[10] See Appendix B for the equations used in this calculation.

Consequently, the momentum equation of (4-5) requires that

$$\frac{\nu}{VY} = 1 \qquad (4\text{-}26)$$

if the convective terms and friction term are to be of the same order of magnitude (Kotake, 1980). If W is arbitrarily defined as the channel inlet velocity, and Y as the distance between the two surfaces, Z and V are found using the relations

$$Z = \frac{Y^2 W}{\nu} \qquad V = \frac{\nu}{Y} \qquad (4\text{-}27)$$

Calculation of Heat and Mass Transfer

Determination of sensible and latent heat transfer to the surface is based on these well known relations:

$$Q_{sens} = (\rho_{gas} W A_{xy}) c_{p,i+j} \Delta T \qquad Q_{cond} = (\rho_{gas} W A_{xy}) h_{fg} \Delta\left(\frac{C}{1-C}\right) \qquad (4\text{-}28)$$

Heat transfer is found from the temperature distribution by integration. Assuming that T is not a function of x, the proper relation is

$$Q_{sens} = \rho_{gas} X c_{p,i+j} \int [(wT)_z - (wT)_{z+dz}] dy \qquad (4\text{-}29)$$

The temperature distribution can be related to the velocity distribution or to the concentration distribution using the equations

$$\delta_t \sim \delta \mathrm{Pr}^{-\frac{1}{3}} \qquad \vee \qquad \delta_t \sim \delta_c \mathrm{Pr}^{-\frac{1}{3}} \mathrm{Sc}^{\frac{1}{3}} \qquad (4\text{-}30)$$

In a similar manner, the heat transfer due to condensation is given by

$$Q_{cond} = \rho_{gas} X h_{fg} \int [(\frac{C}{1-C} w)_z - (\frac{C}{1-C} w)_{z+dz}] dy \tag{4-31}$$

Mathematical Model

The velocity, temperature, and concentration equations previously described along with the above derived relations for heat and mass transfer form the basis of the model. The equations were translated into the Fortran code which is described in Appendix B. The model is configured to provide dimensional and nondimensional profiles, and local and overall heat and mass transfer rates. Properties and boundary conditions can be varied to predict their effect on profiles and transfer rates.

The Fortran model was qualified by running a series of limiting cases having known trivial solutions. The first case specified inlet concentration equal to wall concentration, the second predicted profiles at the leading edge, and the third specified infinite diffusion resistance. In every case the model delivered the expected result. Concentration profiles were linear for the first case, the predicted leading edge concentration profiles matched the specified leading edge boundary conditions of the second case, and zero mass transfer was predicted for the third case.

Next, a few dimensional concentration profiles were plotted by varying the wall temperature, as shown in Figure 4-1. The figure shows the concentration profile across the boundary layer with $y=0$ corresponding to the wall. Mean concentration increases with increase in wall temperature, as expected. Noncondensable film thickness is unaffected by wall temperature since the curves are similar and collapse when plotted as concentration excess. Finally, the effect of velocity distribution on concentration distribution was examined. Constant, laminar, and turbulent velocity profiles were successively specified under the same boundary conditions. The results indicate that concentration distribution is only a weak function of velocity distribution. Both the nondimensional concentration and the matching nondimensional velocity profiles are shown in Figure 4-2, as is some experimental concentration data. The matching profiles in the figure are plotted using the same style of line. As expected, the centerline velocity is greater than the inlet velocity (w exceeds 1 at $y=1$) for the two viscid flow cases specified. For the potential flow case, w is constant and equal to 1, and the corresponding concentration profile is slightly steeper than the other concentration profiles predicted using a laminar or turbulent velocity distribution. The noncondensable film ($\Phi < 0.01$) is thickest ($\delta_{c,n}=0.018$) using the laminar profile, thinner using the turbulent profile ($\delta_{c,n}=0.0018$), and almost nonexistent using the linear profile.

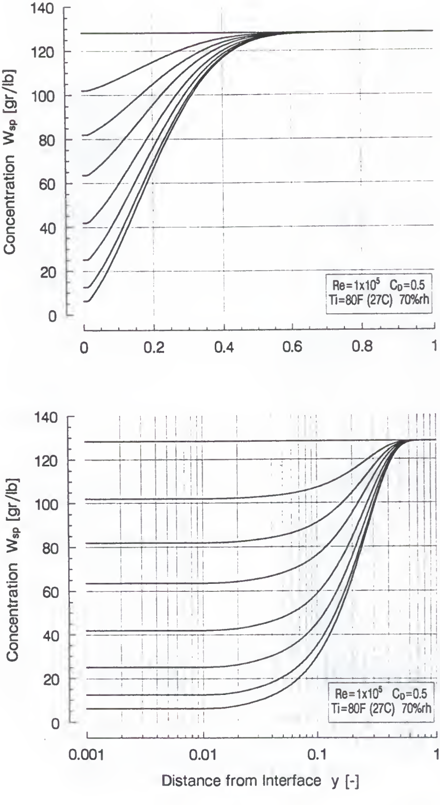

Figure 4-1. Results of model validation: concentration profiles of humid air, inlet air conditions are 78 F (26 C) 70% rh, linear (top), semi-log (bottom).

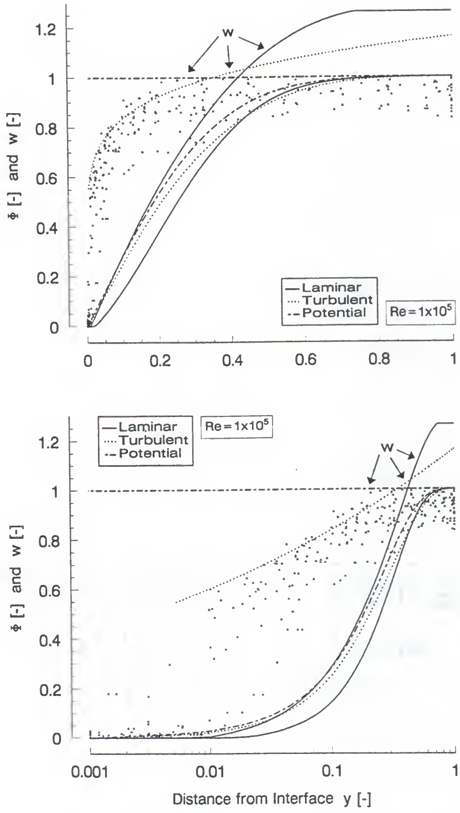

Figure 4-2. Effect of specified velocity distribution, w, on concentration distribution, Φ, linear scale (top), semi-log scale (bottom).

This page intentionally left blank.

Finite Element Model

Laminar steady state heat convection in a channel, considering natural plus forced convection, are the conditions considered by the three dimensional FEA model. A CAD-type pre-processor was used to specify the geometry and boundary conditions, and generate the mesh.[11] The input deck is described in Appendix A as part of a sample output listing.

The cartesian orientation chosen for this analysis is consistent with heat transfer literature[12] (the software used was incapable of considering mass transfer, this was not necessary to study buoyancy effects nevertheless): x is the mixture flow direction, y is the gravity force direction, and z is the direction normal to the surface. A channel with dimensions of $X=4.0$ ft (121.9 cm), $Y=1.5$ ft (45.72 cm) and $Z=0.1$ ft (3.048 cm) was specified based on the experimental apparatus of the present work. The boundary conditions considered specify low speed ($U<3$ m/s) forced convection with one cooled or heated surface, the remaining surfaces are maintained at inlet temperature. The boundary conditions of the example provided are $U(0,y,z)=2$ ft/s (0.6 m/s), $T(0,y,z)=80$ F (26.7 C), and $T(x,y,0)=35$ F (1.7 C).

The mesh type and size were restricted by the capabilities of the available software/hardware.[13] The mesh was limited to a 25 × 15 × 10 XYZ grid of linear quadrilateral elements. See Chapter 7 and Appendix A for further discussion.

---

[11] The software used was DISPLAY-PRE, NISA/3D-FLUID, and DISPLAY-POST by Engineering Mechanics Research Corporation of Troy Michigan.

[12] The mathematical model is based on a different orientation since it considers condensation.

To qualify the model several cases were analyzed for agreement with expected results. For the trivial case of all temperature boundary conditions being equal, the predicted temperature was uniform as expected. Results using the boundary conditions referred to previously are shown in Figure 4-3 and Figure 4-4. The xz-plane velocity vectors, viewed from above, show the expected velocity distribution. The x-direction velocity and temperature contours show the expected developing boundary layers. The indicated y and z direction velocities disappear (except in the inlet region) when buoyancy was neglected; this is discussed further in Chapter 6. The expected boundary-layer development at the top and bottom of the enclosed channel can be seen in the yz-plane contours, viewed into the flow. Also evident is the increase in core velocity satisfying the conservation of mass.

One unexpected result is the shortness of the inlet region: the flow becomes fully developed by $x = 0.5$ ft (15.2 cm). This is partially due to the computed Reynolds number; the software uses an arbitrary reference length and reference velocity. After several verifications, it was concluded that this incredulity is a peculiarity of the software and does not appear to affect its ability to predict buoyancy effects.

---

[13] A Hewlett Packard/Apollo model 3500 was used, capable of approximately 2 mips.

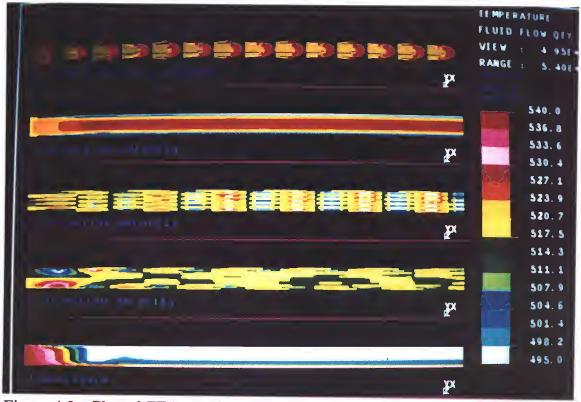

Figure 4-3. Plot of FEA predicted velocity and temperature in the xz-plane, scale units are R.

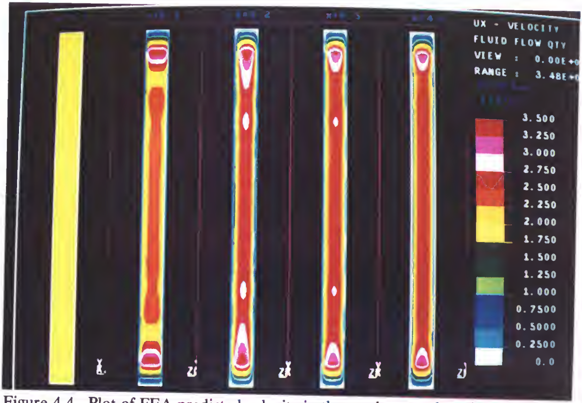

Figure 4-4. Plot of FEA predicted velocity in the yz-plane, scale units are ft/s.

CHAPTER 5
EXPERIMENTAL METHODOLOGY

The physical situation studied is heat and mass transfer to the flat wall of a channel under forced convection. The temperature and concentration gradient is induced by one surface. The opposite surface is adiabatic and impermeable and thus simulates the centerline of symmetric flow between two cooled walls. A mixture of water vapor and air is introduced at the entrance to the channel and flows parallel to it. The inlet velocity, temperature, and concentration are uniform and the flow condition is laminar. Development of velocity, temperature, and concentration boundary layers occurs downstream from the leading edge of the wall. The two velocity boundary layers over the opposite walls of the channel cause an increase in core velocity. As illustrated in Chapter 4, this has a minimal effect on the concentration distribution results.

Design and construction of the experimental system used to study this situation was a significant effort of this work. Components of the system can be grouped into three primary subsystems: (1) the cooled wall channel and associated temperature control equipment, (2) the miniature concentration probe and associated positioning and signal conditioning equipment, and (3) instrumentation for temperature, humidity, dew point, flow, and pressure measurement. A schematic of the experimental system is provided in Figure 5-1; and photographs

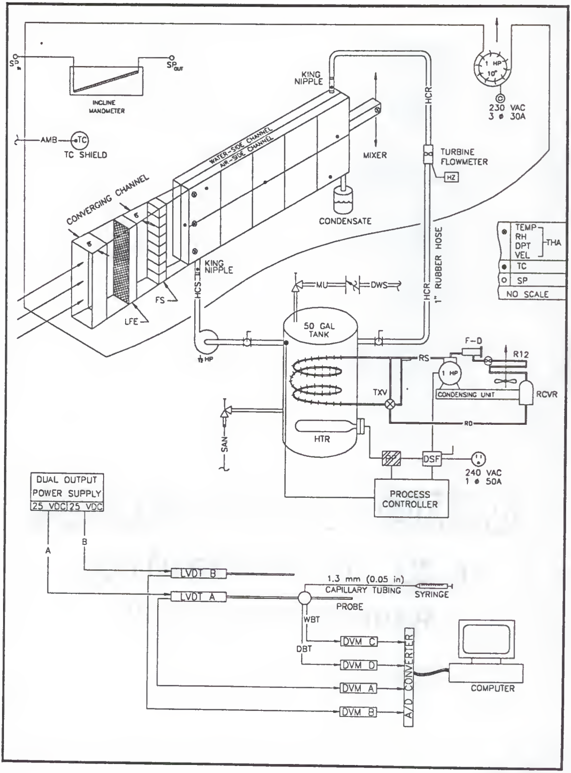

Figure 5-1. Schematic diagram of the experimental system used in this work.

of the laboratory installation are shown in Figure 5-2 and Figure 5-3. The channel and probe subsystems will be described in the sections to follow. The standard instrumentation is described in Appendix F along with the data collection procedure.

Upon completion and adjustment of the system, 53 qualification trials and tests under adiabatic conditions or using a heated plate were performed. Finally, a total of 120 trials at twelve air flow rates and two plate temperatures were performed using an efficient data collection and analysis procedure.

Cooled-Wall Channel Subsystem

This subsystem consists of the air-side channel, the coolant-side channel, and the coolant delivery equipment. The capabilities of the subsystem are listed in Table 5-1.

Table 5-1. Capabilities of the cooled-wall channel subsystem.

QUANTITY	SPECIFICATION
Coolant Liquid Limits	-1 to 99 C (31 to 210 F)
Coolant Capacity	230 ℓ (60 gal)
Chiller Range	-20 to 20 C (-5 to 68 F)
Chiller Capacity 7 C (45 F)	3.5 kW (12,000 Btuh)
20 C (-5 F)	1.5 kW (5180 Btuh)
Heater Range	20 to 140 C (68 to 284 F)
Heater Capacity	3.0 kW (10,240 Btuh)
Coolant Flow Rate	0 to 0.2 ℓ/s (3.4 gpm)
Air Velocity	0 to 14 m/s (2750 fpm)
Coolant to Surface ΔT	2.2° C (4° F)

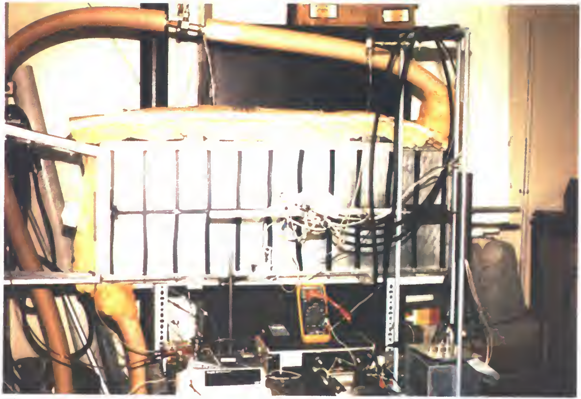

Figure 5-2. Photograph of the cooled-wall channel and associated equipment.

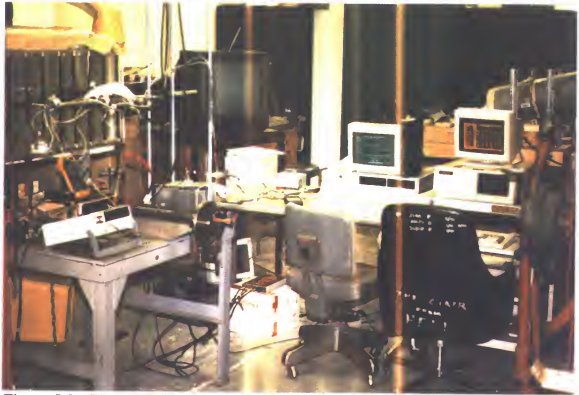

Figure 5-3. Photograph of the laboratory installation.

Humid air flows through the air-side channel and condensation occurs on the cooled wall. The coolant-side channel runs parallel to the air side channel, separated by the condensing surface. Coolant is pumped from a tank through the coolant-side channel. Coolant temperature is maintained with an in-tank chiller system and heater. A cross section of the channel assembly is shown in Figure 5-4, the air-side and coolant-side channels are the principal features of this assembly.

Air-Side Channel

The condensing surface is an aluminum flat plate measuring 122.9 cm long × 45.7 cm high × 0.476 cm thick (48 × 18 × 0.1875 in). The plate forms one vertical surface of the 2.54 cm (1.0 in) wide channel. The other three surfaces are of 1.3 cm (0.5 in) thick clear Plexiglass to permit flow and condensate visualization studies. Since air temperature outside the channel is within 1° C (1.8° F) of channel inlet conditions, the temperature gradient across the Plexiglass walls is negligible. Thus, the concentration and temperature symmetry between two cooled walls is duplicated since there is negligible heat transfer, and no mass transfer across the Plexiglass walls. The Plexiglass wall is grooved to permit probe traverses. There is one central horizontal groove and 12 vertical groves.

The dimensions of the plate were based on three factors. Plate thickness was chosen as a compromise between resistance to deformation and to conduction. Plate length was chosen to expand the boundary layer to 25 times

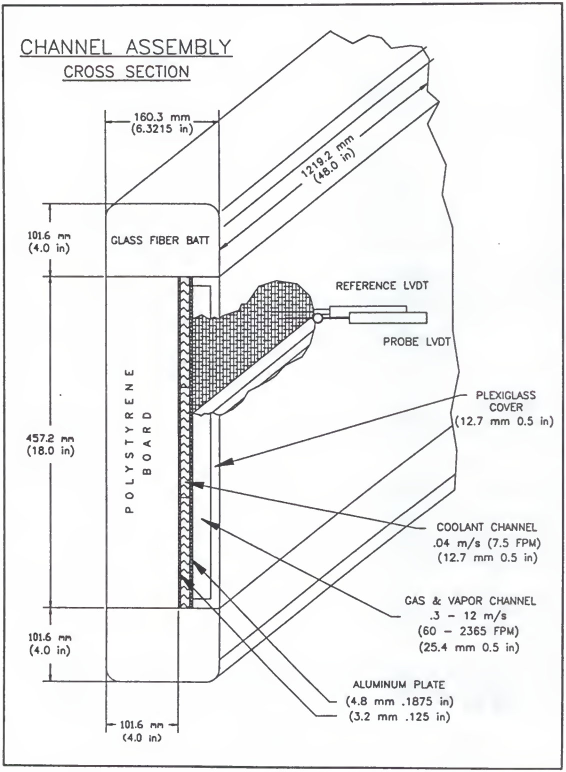
CHANNEL ASSEMBLY
CROSS SECTION
160.3 mm (6.3215 in)
1219.2 mm (48.0 in)
101.6 mm (4.0 in)
GLASS FIBER BATT
REFERENCE LVDT
PROBE LVDT
457.2 mm (18.0 in)
POLYSTYRENE BOARD
PLEXIGLASS COVER (12.7 mm 0.5 in)
COOLANT CHANNEL .04 m/s (7.5 FPM) (12.7 mm 0.5 in)
GAS & VAPOR CHANNEL .3 - 12 m/s (60 - 2365 FPM) (25.4 mm 0.5 in)
101.6 mm (4.0 in)
ALUMINUM PLATE (4.8 mm .1875 in) (3.2 mm .125 in)
101.6 mm (4.0 in)

Figure 5-4. Cross section drawing of the channel assembly.

that of a condensing heat-exchanger fin. This provides increased resolution of the noncondensable gas film. Plate height was based on that of a small dehumidifying heat exchanger.

The channel is situated between two rooms in the laboratory building. Flow through the channel is induced by lowering the pressure in the outlet-side room with a 746 W - 25 cm (1 hp - 10") centrifugal blower and adjusted by positioning a relief door. This provides a flow that is virtually free of fan disturbances. Additionally, air at inlet conditions flows into the outlet-side room through the relief door and surrounds the channel.

An inlet converging-channel reduces inlet disturbances. A laminar flow element and a grille ensure parallel flow conditions at the channel inlet. The converging channel consists of two sections: a 14 cm (5.5 in), 8° inlet section and a 40.cm (16 in), 6° section containing the stainless steel and plastic flow straighteners. The straighteners are described in Table 5-2. There proper size and placement was found using smoke visualization.

Table 5-2. Specifications of flow straighteners used at channel inlet.

Specification	HONEYCOMB	GRID
MATERIAL	Stainless Steel	Plastic
DEPTH	5 cm (2 in)	1.9 cm (0.75 in)
CELL SHAPE	Hexagon	Square
CELL SIZE	0.64 cm (0.25 in)	1.3 cm (0.5 in)
WALL THICKNESS	0.05 mm (0.002 in)	0.1 mm (0.04 in)

Coolant-Side Channel

The condensing surface of the air-side channel forms one wall of this channel; the opposite wall is of 0.32 cm (0.125 in) aluminum and the edges are of 1.3 cm (0.5 in) square tubing. The two vertical tubes are perforated with sixteen 0.8 cm (0.3125 in) holes serving as inlet and outlet manifolds. The inlet and outlet of the manifolds are at the bottom and top, respectively. This arrangement encourages even flow and facilitates bleeding air from the system. The channel is partially divided into three sections to promote a uniform velocity distribution.

The channel width was chosen to foster a small temperature rise and high heat transfer coefficient. Small coolant temperature rise produces an isothermal plate. The predominant heat transfer resistance should be the air-side film coefficient. Additionally, a high heat transfer coefficient results in a cooler plate for a given coolant temperature. The thinner the channel, the greater the temperature rise (due to lower mass flow rate) or the greater the heat transfer coefficient (due to higher velocity).

Channel design conditions were the following: the design heat transfer was 1.5 kW (2500 Btuh) using an air-side coefficient of $h=60\ \mathrm{W/m^2/^\circ C}$ (10 $\mathrm{Btuh/ft^2/^\circ F}$), and the maximum permissible coolant temperature rise was 0.6°C (1°F). Thus, a required coolant flow rate of 0.3 ℓ/s (5 gpm) was calculated. Selecting a coolant-side coefficient of three times the air side coefficient ensured a small coolant-side resistance. Thus for $h=180\ \mathrm{W/m^2/^\circ C}$ (30 $\mathrm{Btuh/ft^2/^\circ F}$) the required velocity, based on laminar flow theory, is 4.2 cm/s (8.2 fpm). In turn, the required channel width is 1.75 cm (0.69 in). The next smallest nominal tube size was one-half inch (1.3 cm). Using this tubing, the predicted heat transfer coefficient was 203 $W/m^2/^\circ C$ (35.7 $Btuh/ft^2/^\circ F$).

The coolant and air flow in the same direction, as in a parallel flow heat exchanger. This arrangement promotes an isothermal surface by partially offsetting (by approximately 25%) the decrease in local heat transfer coefficient along the flow direction. At a distance of 2.5 cm (1 in) downstream from the leading edge, the local h is typically 2 to 2.5 times that at the trailing edge. This tends to increase the plate surface temperature there. The parallel flow provides a higher coolant side h and colder coolant near the leading edge.

The final size and number of manifold holes was based on their outlet velocity. An experimental trial and error method was employed. Using a tap water connection and valve, the flow rate through the manifold was set to 0.3 ℓ/s (5 gpm) using a catch bucket and a timer. Hole size and number were adjusted to obtain even jet distribution and a penetration of approximately 10 cm (4 in).

Coolant Delivery Equipment

The coolant is chilled or heated, and stored in a 190 ℓ (50 gallon) coated-steel tank. The tank was sized to accommodate an evaporator coil and a resistance heater, and to provide a large thermal mass. Partial freezing of the coolant provides additional thermal stability during cooling. The tank is insulated with a 10 cm (4 in) thick fiberglass batt and the piping is insulated with 1.3 cm

(0.5 in) thick urethane foam. The coolant is tap water and 1% chlorine bleach treated with silicone pump-lubricant/rust-preventive.

The chiller system is based on a 1 hp R-12 air-cooled condensing unit. The unit was sized to chill the coolant from 24 C to 0 C (75 F to 32 F) in fewer than 3 hours, and then freeze half the coolant in the tank in an additional 5 hours to facilitate overnight readiness. The evaporator coil was built from 8.5 m (28 ft) of 1.3 cm (0.5 in) copper tubing with 10 cm long by 0.6 cm wide (4 × 0.25 in) galvanized steel fins, spirally wrapped, to facilitate ice building. The estimate of required heat transfer area was based on a commercially available water cooled condenser.

Heating is provided by a 3 kW (10,240 Btuh) immersion resistance heater. The unit was sized to offset the available cooling capacity for temperature control, and to heat the coolant from 24 C to 100 C (75 F to 212 F) in fewer than 8 hours. Tank outlet temperature is controlled by a self-tuning programmable PID process controller that cycles the immersion heater only via a solid state relay. The chiller system response is too slow for effective use in temperature control.

The coolant is pumped from the tank to the channel by a 62 W (1/12 hp) centrifugal pump. The pump was sized based on head loss estimations of the system's valves, fittings, piping, the channel, and the manifold outlet orifices: a total head of 2.4 m (8 ft) of water.

Concentration Probe Subsystem

This subsystem consists of the miniature wet-bulb/dry-bulb concentration probe, the positioning equipment, and the signal conditioning and data acquisition equipment (which is diagramed in Figure 5-1). The probe is inserted through the Plexiglass wall of the air-side channel and traversed through the boundary layer until it contacts the wall. The probe outputs are linearized and amplified, and then routed to a data acquisition system with the position-transducer outputs.

Concentration Probe

The initial concept for this type of probe followed the work of Peterson and Tien (1987), described in Chapter 3. (Several other concentration measurement techniques are also evaluated in Chapter 3.) This type was selected because it is small, simple, and accurate. After a few prototypes were tested, the design evolved into the instrument described here. A diagram of the probe is provided in Figure 5-5.

The purpose of this subsystem is the measurement of wet-bulb and dry-bulb temperature distribution through a boundary layer of 25 mm (1 in) or less and a gas film layer of 1 mm (0.04 in) or less. The typical expected concentration difference was 4.3 g/kg (30 gr/lb). Limiting the concentration error to 10% required position resolution to within 0.1 mm (0.004 in) and temperature accuracy to within 0.84° C (1.5° F). A simple analysis of the error due to radiation heat transfer is presented in Appendix D.

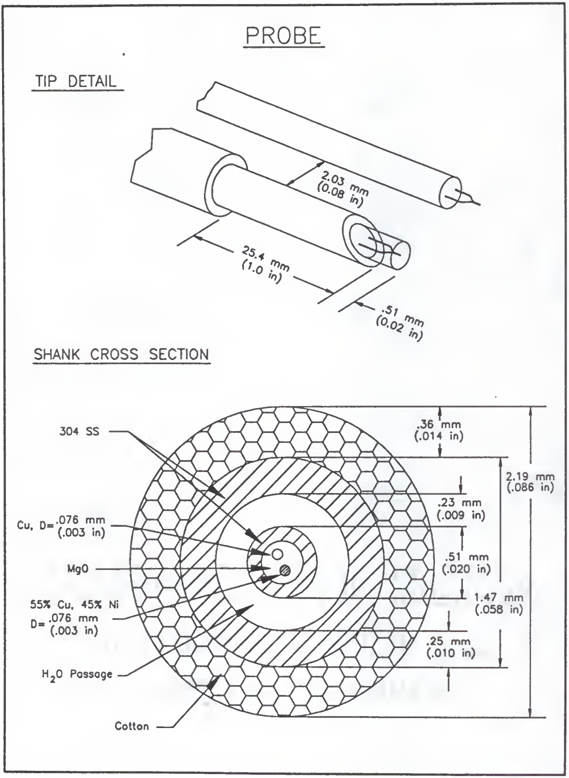

Figure 5-5. Drawing of concentration probe tip detail and shank cross section.

Thermocouples were selected to measure temperature since they are available in sizes as small as 0.025 mm (0.001 in). Type T thermocouple wire (copper-Constantan) was selected because it has the lowest ASTM standard error (±0.8° C, ±1.44° F) and one of the highest Seebeck coefficients (38 μV/° C, 21 μV/° F). After several fatigue failures, it was concluded that 0.025 mm (0.001 in) wire was too delicate. Wire size 0.076 mm (0.003 in) was substituted. The wet-bulb thermocouple was implanted in a 1.6 mm (0.064 in) fine-cell urethane foam sphere under a light microscope. Stainless steel was selected for the probe body for its rigidity, resistance to corrosion, and availability. The leads of both thermocouples pass through a 0.5 mm (0.02 in) 304-SS sheath. The wet-bulb sheath passes through a 1.6 mm (0.064 in) hypodermic needle, through which $H_2O(\ell)$ is supplied to the urethane sphere. Liquid is fed to the other end of the needle through a 1.3 mm (0.05 in) Tygon capillary tube connected to a 3 mℓ syringe which is elevated to provide a constant head. The wet-bulb shank is insulated with a 0.36 mm (0.014 in) cotton jacket. Moistening the jacket reduces heat conduction between the probe body and the wet-bulb tip by reducing their temperature difference.

The probe was calibrated by Jackson (1992). The systematic error was found to be -0.72° C (-1.3° F) for the dry-bulb and +1.09° C (+1.97° F) for the wet-bulb. The precision was reported as ±0.65° C (±1.18° F) for the dry-bulb and ±0.46° C (±0.83° F) for the wet-bulb. This results in a concentration precision of ±0.34 g/kg (±2.39 gr/lb), or about 8% of the expected concentration range.

Positioning Equipment

The probe body is coupled to an LVDT (linear variable differential transformer) and a precision threaded rod. The LVDT provides an output voltage linearly related to position of the probe relative to the traverse support structure. A second LVDT is used as a reference. It continuously measures the distance between the support structure and the plate surface, accounting for deformation of both. When rotated, the precision threaded rod (similar to those found in a milling machine table) moves the probe. The LVDTs are powered by a variable dual-output isolated power supply set to 25.000 VDC.

The accuracy of the LVDT depends on its linearity, the accuracy of the calibration standards, and the accuracy of the input and output voltage measurements. While in use, accuracy is a function of the distance measured as well. Calibration was done with a mechanical standard resolution of 1 μm (0.00004 in) and a digital volt meter accurate to 0.5 mV. The resulting calibration accuracy was 5 μm/V (0.0002 in/V). With an input voltage resolution of 0.5 mV and A/D voltage resolution of 5 mV, the maximum displacement error is 5.8 μm (0.00023 in) at the cooled wall, increasing to 109 μm (0.004 in) at the opposite wall of the channel. This corresponds to roughly a 10% maximum error in the gas film thickness, and a 1% maximum error in the boundary-layer thickness.

Signal Conditioning Equipment

The outputs from the probe thermocouples are linearized and amplified by a signal conditioner that provides a 0 to 10 V output corresponding to 0 to 200 C

(32 to 392 F). The combined accuracy and nonlinearity of the circuit is 0.22° C (0.4° F). The total estimated accuracy of the system output at this stage is slightly less than 0.83° C (1.5° F). The outputs from the signal conditioner, and the output of the LVDTs, are routed to an A/D (analog to digital) converter and to four electronic multi-meters. The digital signal is collected by a PC running a digital oscilloscope software package.[14]

Only an 8-bit A/D converter was available for this work, adding an uncertainty of ±0.4° C (±0.72° F) to the temperature measurements. A standard 12-bit A/D converter would not appreciably increase the error of the system. Thus, the total estimated accuracy of the system is 0.92° C (1.7° F) or 0.54 g/kg (3.8 gr/lb). The corresponding estimated concentration difference uncertainty is an acceptable ±9%.

Data Analysis

The cartesian orientation chosen for this analysis is consistent with the analytic analysis of this work: x is the condensate flow direction, y is the direction normal to the surface, and z is the mixture flow direction (Kotake, 1980).

The equations employed were adapted from basic relations found in the ASHRAE Handbook of Fundamentals (1985) and heat transfer texts (Incropera and DeWitt, 1985; Welty et al., 1976).

The raw data was used to determine the temperature and concentration distribution in the channel, *C*(y,z), and the average Nusselt and Sherwood number as a function of Reynolds number. These dimensionless quantities are defined by the relations given in equation (5-1).

---

[14] R1005 Digital Oscilloscope, Version 3.1, by Rapid Systems, Inc., Seattle WA.

$$\mathrm{Re}_z = \frac{W z^*}{\nu} \qquad \overline{\mathrm{Nu}_z} = \frac{\overline{h_z} z^*}{k} \qquad \overline{\mathrm{Sh}_z} = \frac{\overline{h_{m,z}} z^*}{D_{ij}} \tag{5-1}$$

The inlet velocity, W, is the average of vane anemometer measurements at three x locations. The heat and mass transfer coefficients are found using

$$h_z = \frac{Q}{A_{xz}(T_i - T_w)} \qquad h_{m,z} = \frac{Q_{cond}}{h_{fg} A_{xz}(\rho_{H_2O,i} - \rho_{H_2O,w})} \tag{5-2}$$

The wall temperature is the average of thermocouple measurements at three locations. The inlet temperature is measured using the probe or the hygrothermoanemometer.

The density of water vapor in air is given by

$$\rho_{H_2O} = \frac{C}{1-C} \rho_{air} \tag{5-3}$$

and the density of air is given by

$$\rho_{air} = \frac{P}{R T_i [1 + 1.6078(\frac{C}{1-C})]} \tag{5-4}$$

The concentration at the wall is found from the specific humidity $W_{sp,w}$ using

$$W_{sp,w} = \frac{C_w}{1-C_w} = 0.62198 \frac{P_{H_2O,s}}{P - P_{H_2O,s}} \tag{5-5}$$

where the saturated partial pressure of water vapor at any temperature above freezing is given by the polynomial regression of equation (5-6).[15]

$$\begin{gathered}P_{H_2O} = \exp\left(\frac{c_1}{T}+c_2+c_3T+c_4T^2+c_5T^3+c_6\ln T\right)\\ c_1=-10440.4 \qquad c_2=-11.2946669 \qquad c_3=-0.02700133\\ c_4=0.12897060\cdot10^{-4} \quad c_5=-0.2478068\cdot10^{-8} \quad c_6=6.5459673\end{gathered} \tag{5-6}$$

The values 0.62198 and 1.6078 are ratios of the molecular mass of H_2O, 18.01534 g/g·gmol, and the apparent molecular mass of dry air, 28.9645 g/g·gmol.

The specific humidity at the inlet is found from the probe dry/wet bulb measurements, or from the hygrothermoanemometer humidity or dew point measurements. Specific humidity is found from the partial pressure of water at the dew point temperature using the relation expressed in equation (5-5). The partial pressure of water, in turn, is given by the polynomial regression of equation (5-6). Specific humidity is found from relative humidity using the relation of equation (5-5) also. In this case, the water vapor partial pressure is found from the relative humidity ϕ using

$$P_{H_2O} = \phi P_{H_2O,s} \tag{5-7}$$

where the saturation partial pressure is found by substituting the dry-bulb temperature into equation (5-6).

The sensible heat transfer is found from the equation

$$Q_{sens} = W\rho_{air}A_{xy}c_{p,mix}(T_m-T_i) \tag{5-8}$$

---

[15] Units are T [R] and P [psia], see the ASHRAE Handbook of Fundamentals, 1985, p.6.6.

where the mean temperature is found by integrating the measured temperature profile

$$T_m = \int_0^Y T dy \tag{5-9}$$

with the simplification that the velocity profile is linear and equal to the mean velocity. This assumption produces a mean temperature that is less than 4% lower than the true mean temperature in the range of conditions considered.

The latent heat transfer is found using the equation

$$Q_{cond} = W \rho_{air} A_{xy} h_{fg} (W_{sp,i} - W_{sp,m}) \tag{5-10}$$

where mean specific humidity is found by integrating the specific humidity distribution measured by the probe. Specific humidity is found from the dry-bulb and wet-bulb temperature using the equation

$$W_{sp} = \frac{(1093 - 0.556T^*) W^*_{sp,s} - 0.240(T - T^*)}{1093 + 0.444T - T^*} \tag{5-11}$$

which was derived assuming perfect gas behavior. The saturation partial pressure is evaluated using equation (5-6) at the wet-bulb temperature.

The coolant-side heat transfer is evaluated using the relation

$$Q_{H_2O(\ell)} = \Lambda \rho_{H_2O(\ell)} c_{p,H_2O(\ell)} (T_{in} - T_{out}) - Q_{gain} \tag{5-12}$$

where the temperature difference is measured using the comparison function of the thermocouple thermometer, or by connecting the coolant inlet and outlet thermocouple in series and measuring the voltage. Heat absorbed by the coolant from radiation and through the plate back, sides and supports is accounted for by Q_{gain}. A simple radiation analysis is discussed in Appendix D. Conduction gain is estimated using the measured temperature differential across the plate back and side insulation.

Uncertainty in the sensible heat transfer coefficient was estimated to be about ±10%, based on propagation of error from each independent measurement. Latent heat transfer, much more difficult to measure accurately, was estimated to have an uncertainty of at least ±10% and up to ±25%. This high uncertainty is mainly due to the low accuracy of the measured specific humidity and the small and not easily measured coolant temperature differential.

System Qualification

Each of the subsystems was thoroughly tested. Modifications were made, as necessary, to realize design specifications. Next, the entire system was tested by collecting data for some trivial limiting cases and for some dry-heat transfer cases (for which the plate temperature was above the dew point). The procedure used is described in Appendix F. A total of 53 heated-plate qualification trials were completed.

Cooled-Wall Channel Subsystem

The plate was checked for flatness under full coolant pump pressure and found acceptable. An infrared thermometer was used to verify an isothermal surface to within 1.7C±0.6° C (35F±1.0° F) with no air flow. A 0.8 mm (0.03 in) thermocouple probe was used to measure the plate surface temperature at 12 *z* and 7 *x* locations (an 84 location grid) with air flow (Jackson, 1992). This method is relatively inaccurate due to contact resistance, conduction through the leads, and the large size of the probe relative to the upstream boundary layer. Used to compliment an analysis of plate surface temperature, however, it was found to be simple and efficient. The surface was measured to be isothermal within 3.9C±1.0° C (39F±1.8° F) in the x-direction and 3.9C±2.9° C (39F±5.2° F) in the flow direction.

A heat transfer analysis of the complete channel assembly using measured ambient, insulation, aluminum, coolant inlet and outlet, and air inlet temperatures was performed. The difference between the surface temperature 2.5 cm (1 in) from the leading edge and at the trailing edge, 119.4 cm (47 in) downstream, was determined to be 0.8° C (1.4° F) at 1.2 m/s (240 fpm). This corresponds to $\mathrm{Re}_L = 10^5$, for which the difference in respective local heat transfer coefficients is 2.3 times, and the isothermal condition is 3.9C±0.4° C (39F±0.7° F). The maximum difference in local *h*, occurring at $\mathrm{Re}_L = 9 \times 10^5$, is 2.5 times. The true surface temperature difference is between the calculated and measured values.

Considering the inaccuracy of the measurement method it is most likely close to the calculated value, which was deemed acceptable.

Smoke visualization was used to verify uniform inlet flow and laminar conditions through the channel with no temperature difference. The smoke lines were straight and coherent. Condensation was observed to be drop-wise which is consistent with operating dehumidifying heat exchangers and observations reported by Raffellini and Tarabusi (1980), and Sandararaman and Venkatram (1977).

Coolant flow was measured to be 0.2 ℓ/s (3.3 gpm). This is 34% below design conditions because the slope of the pump curve is small at the design pressure drop. Fortunately, heat transfer rate was also well below design conditions for all but the highest air flow rates, so the low coolant flow rate was found acceptable. The chiller system was able to cool then freeze about half the coolant in the tank overnight, as designed. Coolant temperature was found to be very stable, varying no more than $\pm 0.2^\circ$ C ($\pm 0.3^\circ$ F) during trials.

Concentration Probe Subsystem

The dew point of air flowing through the channel, with no heat transfer, was measured with the concentration probe and a dew point hygrometer (the secondary standard used to calibrate the probe). The measured uncertainty was approximately ±7.5%, somewhat better than expected. Air velocity had no measurable effect on probe accuracy. This is supported by a heat and mass transfer analysis of the probe. As indicated in Appendix C, changing air velocity changes the heat and mass transfer coefficients proportionally according to the Lewis relation, which holds for air and water vapor mixtures. Of course, at very low flow rates (lower than those considered here), heat and mass transfer at the probe tip can produce a local increase in humidity.

Sensitivity to body conduction effects was tested by focusing a 63 C, 6 m/s (145 F, 1200 fpm) air jet at the probe shank and observing the probe outputs. The air velocity in the channel was 0.9 m/s (170 fpm). Temperature rose by less than 0.1° C (0.2° F) after two minutes.

Probe time constant was measured by quickly traversing the probe into the condensing boundary layer, approximating a step input. Dry-bulb time constant was measured to be 1.0 s, and wet-bulb time constant was measured to be 4.4 s using a digital oscilloscope to measure response to a simultaneous step change in temperature and concentration. These values are of the same order of magnitude predicted by the transient analysis given in Appendix C. Time response was not significantly affected by air velocity.

Standard Instrumentation

First, all thermocouples and RTDs were checked against an NBS-150 mercury-in-glass thermometer in distilled water at the ice point and at ambient temperature. Only those with a deviation less than 0.2° C (0.3° F) were passed.

Next, the apparatus was allowed to stabilize at room temperature for 3 days, then the coolant inlet and outlet thermocouples were checked for zero potential when wired in series. Even with the thermocouple inputs shunted, a varying potential was indicated by the voltmeter. This was compensated by taking an additional voltage data point with the amplifier input short circuited, and subtracting this from the measured voltage differential.

Dry Heat Transfer Trials

The experimental system was qualified by running a series of limiting trials having easily predicted trivial results. The first set of trials had inlet temperature equal to wall temperature, and the second set of trials used a heated plate. This was done to preclude mass transfer due to condensation while producing heat transfer across a similar temperature gradient.

Concentration and temperature distribution was constant within experimental error for the first set, as shown in Figure 5-6. Heat transfer rate was calculated to be zero, within experimental error, using measured data from several averaged trials at four air velocities. For one run, with $Re_L = 3 \times 10^4$, the plate temperature was dropped to 4.4 C (40 F) immediately after an adiabatic trial (with no change in flow and inlet conditions) to confirm that the change in profile, shown in Figure 5-6, was due to condensation.

A series of complete trials were performed with a plate temperature of 49 C (120 F) and 88 C (190 F) across the full range of inlet velocity. The measured heat transfer coefficients agreed well with the experimental findings of Jurges

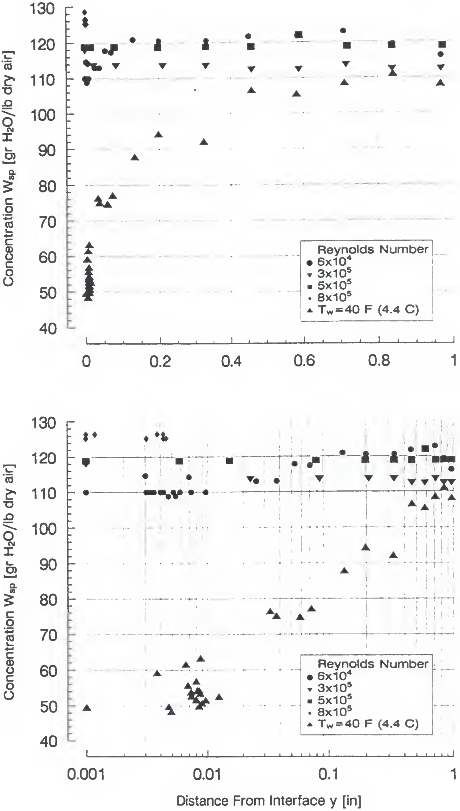

Figure 5-6. Measured adiabatic and cooled-plate specific humidity profiles.

(McAdams, 1954) and the correlation of Colburn (Incropera and DeWitt, 1985). Further discussion of these results, and a plot of the data, is given in Chapter 6. Temperature distribution was between that predicted by laminar and turbulent flow theory. Measured profiles for one inlet velocity, 1.2 m/s (240 fpm), are shown in Figure 5-7. Based on the predictions of the finite element model and smoke visualization studies, it was concluded that the flow is neither genuinely laminar because of buoyancy effects, nor is it turbulent.

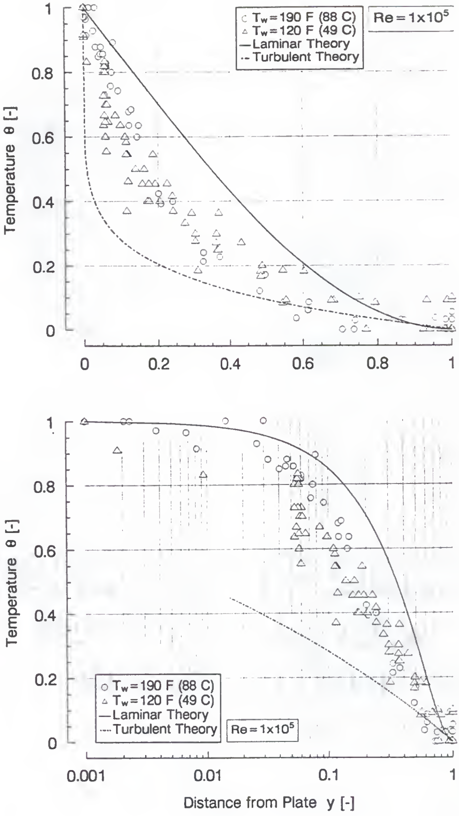

Figure 5-7. Heated-plate temperature profiles at $Re_L = 10^5$.

CHAPTER 6
RESULTS

All three investigative tools produced valuable material. Finite element analysis (FEA) supported a hypothesis that buoyancy driven vorticity prevented two dimensional laminar flow under the conditions considered. The mathematical boundary-layer model successfully predicted the effect of velocity, diffusion rate, and wall conditions on concentration distribution and mass transfer. The experimental investigation enhanced and validated the model, and supplied data not found in the literature.

Finite Element Analysis

The finite element model predicted buoyancy driven vorticity near the plate surface. At 1.50 cm (0.60 in) from the plate (the channel center), the finite element model predicted no y or z component to the velocity. However, near the plate surface at $y = 0.30$ cm (0.12 in), components in all three directions were predicted. It was apparent that this three dimensional flow was caused by buoyancy forces.

Velocity Vectors

A velocity vector plot at $y = 1.5$ cm (0.05 ft) is shown in Figure 6-1. The inlet velocity is shown in the figure as 2 ft/s (0.61 m/s), corresponding to $Re_L = 5 \times 10^4$. The inlet temperature is 27 C (80 F) and the plate temperature is 1.7 C (35 F). Flow is in the positive x-direction. The velocity increase predicted along the channel core is due to growth of the momentum boundary layer. The velocity vectors have negligible *y* and *z* components.

Another velocity vector plot near the plate surface at $y = 0.30$ cm (.01 ft) is shown in Figure 6-2. The vectors have *y* and *z* components, as well as the *x* component. This prediction was experimentally verified using smoke to mark streamlines.[16] The *y* component is one order of magnitude smaller, and the *z* component is two orders of magnitude smaller than the *x* component. When buoyant forces were neglected in the analysis, the model predicted a negligible *y* component. The *z* component remained to satisfy conservation of mass in the developing boundary layer.

Buoyancy

The effects of combined inertial and buoyant forces are normally considered for heat transfer when the Grashof number is same magnitude as the square of the Reynolds number. This indicates comparable buoyancy and inertial forces (Incropera and Dewitt, 1985). For the case considered here the ratio is

$$\frac{Gr_L}{Re_L^{\,2}} = \frac{g\beta(T_s - T_\infty)L}{u^2} = 0.88 \approx 1 \tag{6-1}$$

---

[16] See the Experimental Investigation section of this chapter for a detailed description.

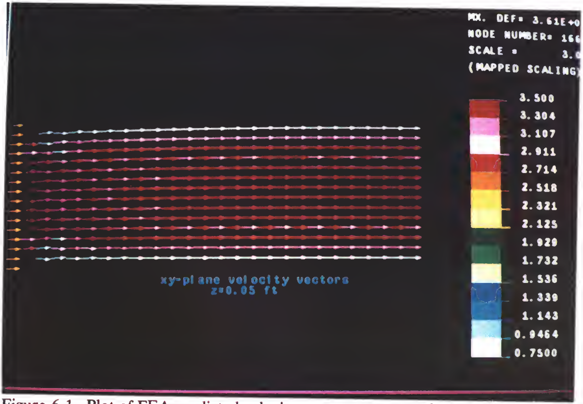

Figure 6-1. Plot of FEA predicted velocity vectors at center of channel. Scale units are ft/s.

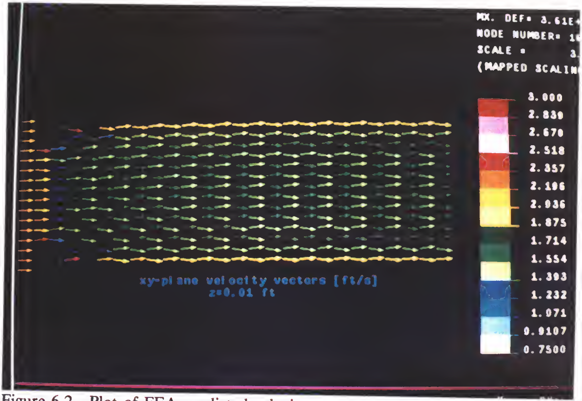

Figure 6-2. Plot of FEA predicted velocity vectors near the plate surface. Scale units are ft/s.

The relationship of equation (6-1) supports the FEA prediction that temperature induced density differences add significant *y* and *z* components to the flow velocity. For the forced convection velocity range 0.3 to 12 m/s (60 to 2360 fpm), plate length of 43.2 cm (17 in), and temperature difference of 22° C (40° F), the ratio for this work is in the range

$$2.4 > \frac{Gr_L}{Re_L^2} > 0.002 \qquad (6\text{-}2)$$

This establishes that buoyancy effects existed for forced convection velocities less than 2.5 m/s (492 fpm). For higher velocities, inertial forces overshadowed buoyancy forces.

The velocity component due to free convection predicted by the model is significant relative to the velocity component due to forced convection . Under pure free convection conditions, the boundary-layer thickness is

$$\delta_L = \frac{6L}{(\frac{Gr_L}{4})^{\frac{1}{4}}} = 2.84\,\text{cm}\ (1.12'') \qquad (6\text{-}3)$$

The equivalent Reynolds number of this buoyancy driven flow is

$$Re_L = (\frac{5L}{\delta_L})^2 = 5780 \qquad (6\text{-}4)$$

corresponding to a velocity of 0.2 m/s (39 fpm). This buoyancy driven velocity is almost one-third the forced convection inlet velocity specified for this example.

The finite element model's predictions verify that the subject flow is not genuinely laminar. Buoyancy driven vorticity can be expected to change the shape of the laminar boundary-layer profiles by convecting the free stream into the boundary layer. This results in higher heat and mass transfer rates than laminar flow theory predicts.

Experimental Investigation

The experimental system was successfully developed and used to study surface condensation on a vertical flat plate. It revealed several interesting characteristics of the concentration boundary layer. Observed buoyancy-induced convection-currents and vortices increased profile slope and mass transfer rate. Concentration and temperature profiles across the boundary layer, and heat and mass transfer rates were measured at a series of Reynolds numbers between 3×10^4 and 9×10^5. Measurements were made at inlet velocities ranging from 0.35 to 11.0 m/s (69 to 2165 fpm). Two plate temperatures were used: 11 C (52 F), just above the dew point of the inlet air, and 2.8 C (37 F).

Buoyancy

Smoke injected into the flow confirmed that buoyancy induced convection currents disturbed the otherwise laminar boundary layer. With plate temperature less than inlet temperature, downward flow at the surface was clearly visible, and falling vortices were observed periodically. The same phenomena were observed when the plate was heated, and the surface flow and vortices moved upward as expected. With no temperature difference, the smoke streams were straight; they indicated a negligible degree of intermittent turbulence and no velocity component in the direction of gravity, as discussed in Chapter 5.

The concentration gradient due to condensation augments temperature induced buoyancy. Lowered concentration at the surface raises the density of the mixture near the surface even higher above the inlet condition. Typically, the density increase at the wall due to cooling was on the order of 9%, with an additional 1% due to condensation.

Concentration and Temperature Profiles

Concentration and temperature profile data was nondimensionalized to remove the effect of plate temperature and inlet conditions. This established the effect of Reynolds number and diffusion parameters. Nondimensional ($\delta_n=\delta_n^*/Y$) boundary-layer thicknesses decreased from $\delta_t=1=\delta_c$ at $Re_L=3\times 10^4$ to $\delta_t=0.5 > \delta_c=0.1$ at $Re_L=9\times 10^5$. As expected, δ_t and δ_c decreased with increasing Reynolds number, as exampled by a comparison of Figure 6-3 with Figure 6-4.

Of special interest is the observed increase in Lewis number

$$Le = \frac{Sc}{Pr} = \frac{\alpha}{D_{ij}} \propto \left(\frac{\delta_t}{\delta_c}\right)^n \tag{6-5}$$

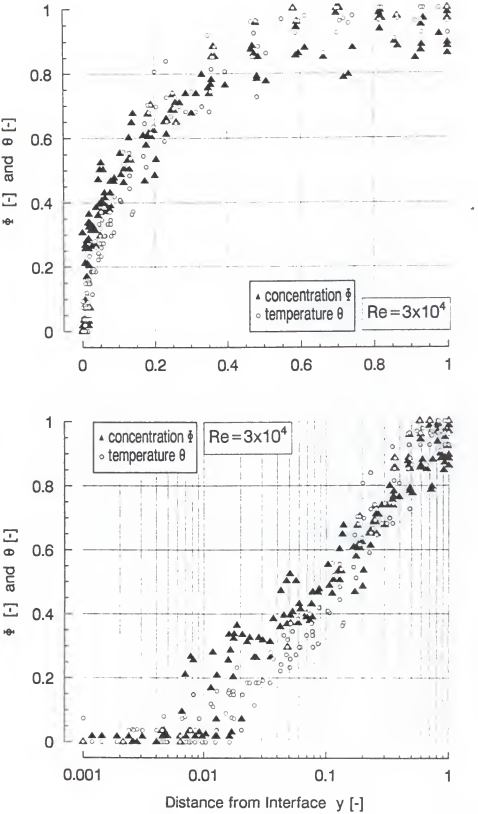

Figure 6-3. Measured concentration and temperature profiles at Re_L=3x10^4, linear scale (top), semi-log scale (bottom).

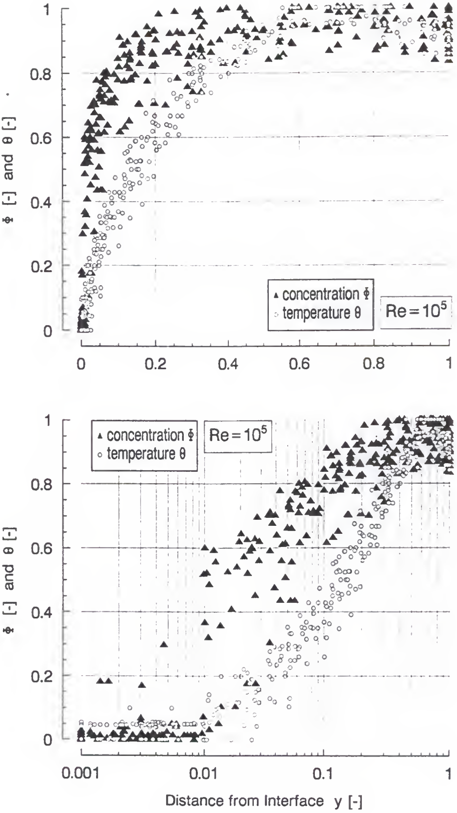

Figure 6-4. Measured concentration and temperature profiles at $Re_L = 10^5$, linear scale (top), semi-log scale (bottom).

with Reynolds number. At $\mathrm{Re}_L = 3\times10^4$ the temperature and concentration data indicate that the two boundary layers are spatially congruent. At increasing Re_L, the concentration boundary-layer profile separates from the temperature boundary-layer profile and moves towards the interface. This is also evidenced by a comparison of Figure 6-3 and Figure 6-4. So, the concentration boundary layer becomes thinner relative to the temperature boundary layer as Re_L is increased. This effect is not due to the transverse velocity of vapor migration towards the wall which thickens the concentration boundary layer as Re_L is increased (Welty et al., 1976). Also, there is an opposing transverse velocity of gas migration away from the wall.

In order to conveniently quantify this relative change in boundary-layer thickness, the diffusion factor, C_D, was introduced and defined as

$$C_D = \frac{Le}{Le_n} \tag{6-6}$$

so that the diffusion factor decreases with increase in measured Lewis number, $Le_{\underline{n}}$. The Lewis number in the numerator, Le, is calculated using handbook property values. The relationship between C_D and Re_L is plotted in Figure 6-5; three hypothesis were conceived to explain this relationship.

An inhibited diffusion hypothesis is a plausible explanation of the thinning concentration boundary layer based on Equation (6-5). The interpretations of the change in Lewis number, to follow, are suggested by two facts: (1) the vapor molecules must cross a velocity and a temperature gradient as they move towards

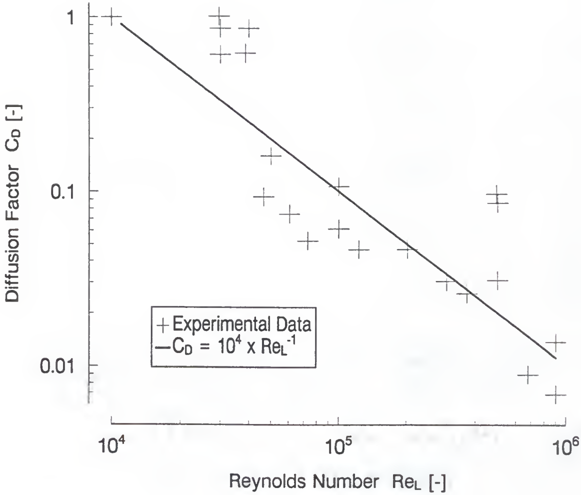

Figure 6-5. Correlation of measured difference between concentration and temperature boundary layer thicknesses.

the plate, and (2) published values and relations for mass diffusivity, D_{ij}, typically apply to stagnant isothermal conditions.

Theoretically, mass diffusivity decreases with temperature linearly in the range 30 to 0 C (86 to 32 F): from 2.65×10^{-5} to 2.17×10^{-5} m^2/s (1.03 to 0.84 ft^2/hr). Thus, diffusion is retarded as the molecules progress through the temperature boundary layer. Regardless, this effect alone does not resolve the large apparent reduction in diffusion indicated by Figure 6-5.

Thermal diffusion also contributes to the observed inhibition. Smaller, lighter molecules diffuse toward warmer regions (Chapman and Cowling, 1970). Since H_2O is smaller and lighter than both O_2 and N_2, gas theory predicts that water vapor molecules will tend to thermally diffuse away from the plate. This is in the opposite direction of ordinary diffusion. Additionally, the larger, heavier air molecules will stay near the cool gas film, increasing its thickness and further inhibiting diffusion. Unfortunately, the magnitude of this effect, under the conditions considered here, is not readily obtained, nor has any experimental work on H_2O-air been located (Chapman and Cowling, 1970).

A third hypothesis attributes inhibited diffusion to the velocity gradient in the momentum boundary layer. Using a coordinate system attached to a vapor molecule, it is clear that any vapor molecule has a higher velocity than any neighboring molecule that is closer to the plate. As a vapor molecule diffuses towards the plate, its greater velocity increases the probability of a collision with a slower moving air or vapor molecule. Its greater kinetic energy causes the result of these collisions to be unlike that of collisions in a stagnant fluid. The same would be true of air molecules diffusing away from the plate. Additionally, the direction of the transverse velocity manifested by conservation of mass in the boundary layer opposes that of the diffusing vapor molecules. Thus, diffusion is retarded across the momentum boundary layer.

If the above suppositions are sound, the magnitude of the effect would increase with increasing Re_L. At higher Re_L, the kinetic energy difference between neighboring molecules is larger and the temperature gradient is greater, intensifying the inhibition effect. The dependence of the apparent mass diffusivity, experimentally measured via the diffusion factor C_D, on Re_L is significant as shown in Figure 6-5. Negligible inhibition is indicated by $C_D = 1$, a decreasing diffusion factor indicates a decrease in diffusion. This correlated phenomena, together with Equation (6-5), suggested an inhibited diffusivity relation of the form

$$D_{ij,n} \propto \mathrm{f}\{Re_L^n\}\ D_{ij} \qquad (6\text{-}7)$$

that is supported by this measured correlation with Reynolds number:

$$C_D = \frac{10^4}{Re_L} = \frac{D_{ij,Re_L}}{D_{ij}} \qquad Re_L \in [1.1\times10^4, 10^6] \qquad (6\text{-}8)$$

A noncondensable film is distinctly visible in the experimental data, this can be seen in the semi-log plots of Figure 6-3 and Figure 6-4. The film thickness is 0.38 mm (0.015 in) at $\mathrm{Re}_L = 3\times10^4$ and decreases to 0.05 mm (0.002 in) at $\mathrm{Re}_L = 9\times10^5$. This thickness is about 1.8×10^5 to 2.4×10^4 average molecular diameters, respectively. At higher Re_L, measured film thickness is equal to that predicted by the mathematical model[17]. At low R_L, buoyancy effects reduce the film thickness below the model's prediction.

Heat and Mass Transfer Rates

Measured Nu_L and Sh_L were compared with the predictions of relations for $Nu_L(Re_L,Pr)$ and $Sh_L(Re_L,Sc)$ derived using the Blasius solution of the hydrodynamic boundary layer, the heat and mass transfer analogies to it, and Fick's Law.

$$\begin{aligned} Nu_L &= 0.664\, Re_L^{\frac{1}{2}}\, Pr^{\frac{1}{3}} \\ Sh_L &= 0.664\, Re_L^{\frac{1}{2}}\, Sc^{\frac{1}{3}} \end{aligned} \qquad (6\text{-}9)$$

These relations largely under predicted both Nu and Sh, probably due to the observed buoyancy induced vorticity.

Comparison of Nu_L and Sh_L to two empirically derived correlations, given in Equation (6-10), are shown in Figure 6-6.

$$\begin{aligned} Nu_L &= 0.055\ Re_L^{0.78} Pr^{0.33} \\ Sh_L &= 0.036\ Re_L^{0.80} Sc^{0.33} \end{aligned} \qquad (6\text{-}10)$$

The first is by Jurges (McAdams, 1954) and the second is by Colburn (Incropera and DeWitt, 1985). The data agrees with these correlations within experimental error. Heat and mass transfer rates were considerably higher than predicted by

---

[17] See the Fortran Model section of this chapter for a more detailed comparison.

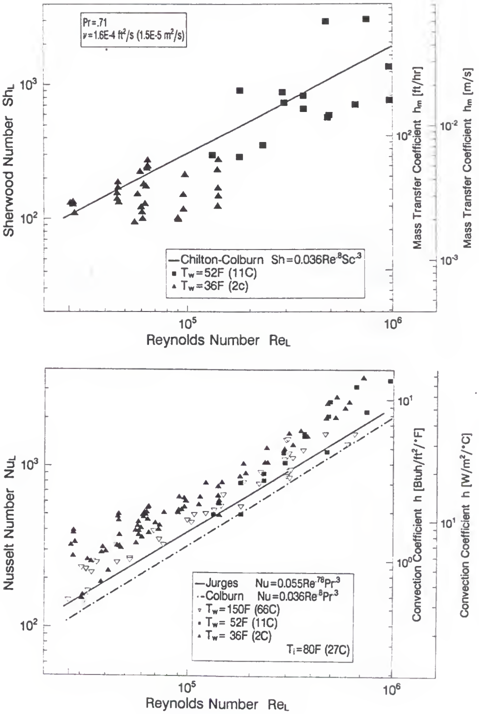

Figure 6-6. Comparison of measured Nusselt number and Sherwood number with published empirical correlations.

laminar flow theory. These empirical correlations from the literature more closely matched measured heat and mass transfer rates.

Measured Nusselt and Sherwood numbers showed no definite dependence on plate temperature. There appears to be an increase in Nu_L of approximately 5% due to a decrease in plate temperature from 11 C to 2 C (52 F to 36 F), however this difference is smaller than the experimental uncertainty. Since buoyancy was shown to influence the measured boundary-layer profiles, the expected effect of temperature difference on Sh_L was evidently less than the resolution of the apparatus. The existence of mass transfer appears to increase Nusselt number by approximately 10%, however this increase is also comparable to the experimental uncertainty.

Mathematical Model

An exact explicit solution to the concentration equation was found and verified. The solution is the core of a mathematical model, executed in Fortran, of forced-convection condensation from a mixture of vapor and noncondensable gas over a plate or in a channel. The model can calculate velocity, temperature, and concentration profiles as well as heat and mass transfer to or from the walls. Most importantly, the model can estimate the effect of changing inlet velocity, diffusion rate, or wall conditions on condensation rate.

Concentration Solution

A closed form solution to the concentration equation was found to be

$$\Phi = \Gamma^{\frac{1}{2}} = \frac{2}{\pi} e^{-\frac{py}{2}} \sum_{n}^{\infty} \frac{n}{n^2+\alpha^2} [1-(-1)^n e^{\alpha\pi}] e^{-\beta_n z} \sin(\frac{n\pi Y}{2R_o} y) \qquad (4\text{-}21)$$

WHERE

$$\alpha = \frac{pR_o}{\pi Y} \qquad \beta_n = \frac{n^2+\bar{p}}{\bar{r}}$$

$$p = -VY\frac{Sc}{\nu}v \qquad \bar{p} = (\frac{pR_o}{\pi Y})^2 \qquad r = \frac{WY^2}{Z}\frac{Sc}{\nu}w \qquad \bar{r} = r(\frac{2R_o}{\pi Y})^2$$

as discussed in Chapter 4. The solution is plotted as nondimensional concentration over the cartesian plane in Figure 6-7 and Figure 6-8. The flow direction is along the positive z-axis, shown as Re_x. The x-coordinate originates at the onset of condensation. The y-axis originates at the vapor-liquid interface and is normal to it. The shaded bands cover a nondimensional concentration range of 0.1, except the highest and lowest bands which indicate vapor concentrations of $\Phi > 0.99$ and $\Phi < 0.01$, respectively. These bands indicate the boundary layer and gas film thicknesses, respectively. The concentration gradient is

$$\frac{\partial \Gamma^{\frac{1}{2}}}{\partial y} = \sum_{n}^{\infty} e^{-(\frac{py}{2}+\beta_n)} (1-(-1)^n e^{\alpha\pi}) [\frac{Yn^2 \cos(\frac{n\pi Y}{2R_o} y)}{R(n^2+\bar{p})} + \frac{np \sin(\frac{n\pi Y}{2R_o} y)}{\pi (n^2+\bar{p})}] \qquad (6\text{-}11)$$

The solution accurately follows the prescribed boundary conditions at $x=0$ and $y=0$. The region $Re_x < 3\times 10^5$ was studied experimentally. A trivial discontinuity at $Re_x = 1.6\times 10^5$ is due to the switch from entrance to fully developed velocity profile. Another small discontinuity at $Re_x = 7\times 10^5$ is caused by the

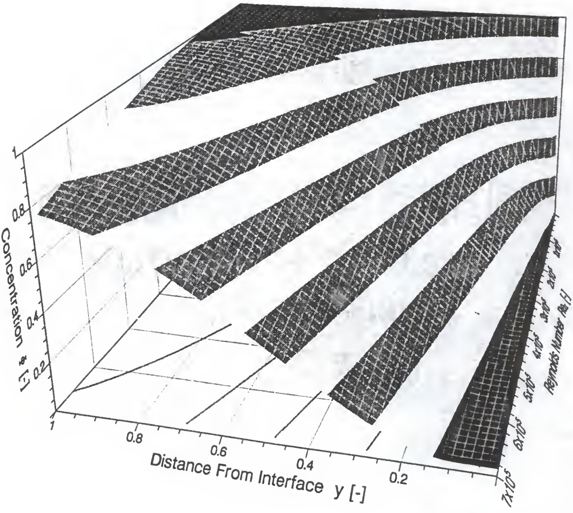

Figure 6-7. Solution to the concentration equation plotted for $Re_x < 7x10^5$.

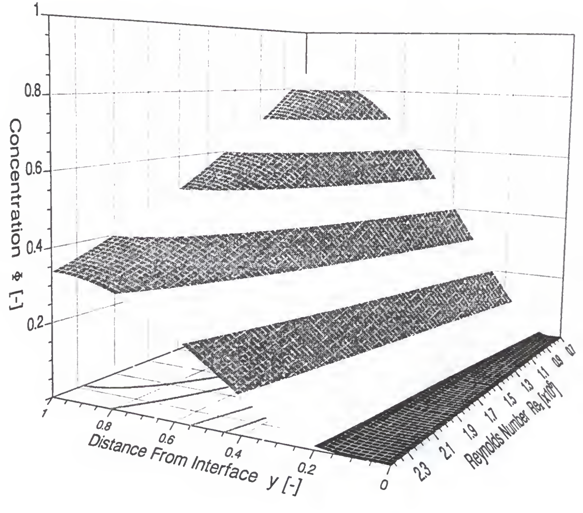

Figure 6-8. Solution to the concentration equation plotted for $7x10^5 < Re_x \leq 2.42x10^6$.

transition to turbulent flow. The concentration profile is fully developed for $Re_x > 2\times 10^5$, as shown by the top-most band in Figure 6-7. The growth of the noncondensable film is represented by the bottom-most band. Near the leading edge, for $Re_x < 8\times 10^4$, vapor concentration near the interface drops abruptly and the noncondensable film grows rapidly. As the noncondensable film thickens, the reduction in concentration becomes less exceptional. The centerline ($y=1$) concentration dissipates sluggishly. This solution to the concentration equation was used in the Fortran model listed in Appendix B.

Concentration Profiles

Two families of concentration profiles were useful in testing the experimentally obtained diffusion factor. The first shows the variation with Reynolds numbers in the range $3\times 10^4 \leq Re_L \leq 9\times 10^5$. The second shows variation with the diffusion factor, $0.05 \leq C_D \leq 10$, the quantity suggested by the experimental portion of this work.

As expected, the concentration boundary-layer thickness decreases with increasing Re_L, as shown in Figure 6-9. This means that as the inlet velocity increases, the mass of vapor condensed from any moving control volume decreases. However, the total mass transfer rate does not decrease since the reduction in boundary-layer thickness is offset by the increased inlet mass flow rate. This correlation is discussed further in the section on heat and mass transfer rates.

Assuming a constant diffusion factor C_D, the model indicates that the diffusion of noncondensable gas away from the wall occurs more quickly at higher Re_L since the concentration gradient is larger. As the inlet velocity is increased, both the concentration boundary layer and the gas film become thinner. A noncondensable gas film is distinctly visible in the semi-log plot of Figure 6-9. The film thickens from 0.05 mm (0.002 in) at $Re_L=9\times10^5$ to 1.0 mm (0.04 in) at $Re_L=3\times10^4$ in the family of profiles. The same trend was observed in the experimental data. As shown in Table 6-1, the predicted film thickness is closer to the experimental data at high Re_L.

Table 6-1. Comparison of predicted non-condensable gas film thickness with experimental data.

Re_L	DATA	MODEL	DIFFERENCE
9×10^5	0.05 mm 0.002 in	0.05 mm 0.002 in	0.0%
1×10^5	0.20 mm 0.008 in	0.46 mm 0.018 in	56.5%
3×10^4	0.38 mm 0.015 in	1.02 mm 0.040 in	60.7%

Buoyancy induced convection probably removed part of the noncondensable film at lower Re_L.

The concentration boundary-layer thickness decreases as the diffusion factor is decreased, as shown in Figure 6-10. Decreasing the diffusion factor below 1.0 models an inhibition of diffusion (relative to diffusion in a stagnant isothermal isobaric medium) across the channel. Increasing C_D above 1.0, which

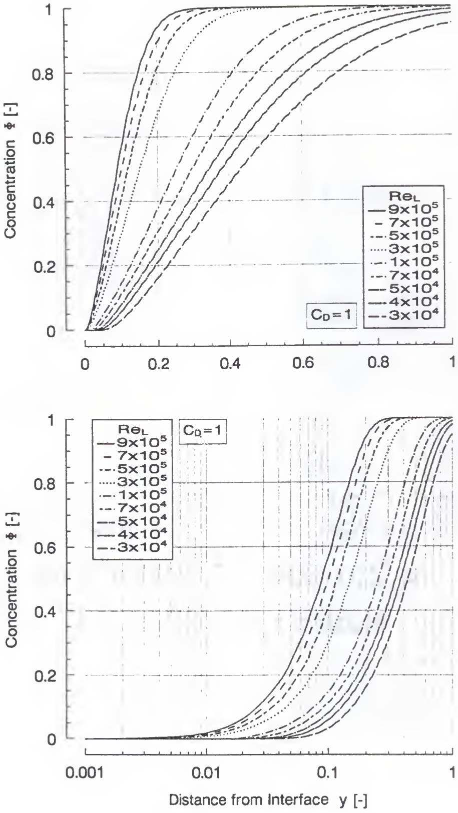

Figure 6-9. Family of concentration profiles for $3x10^4 \leq Re_L \leq 9x10^5$, linear scale (top), semi-log scale (bottom).

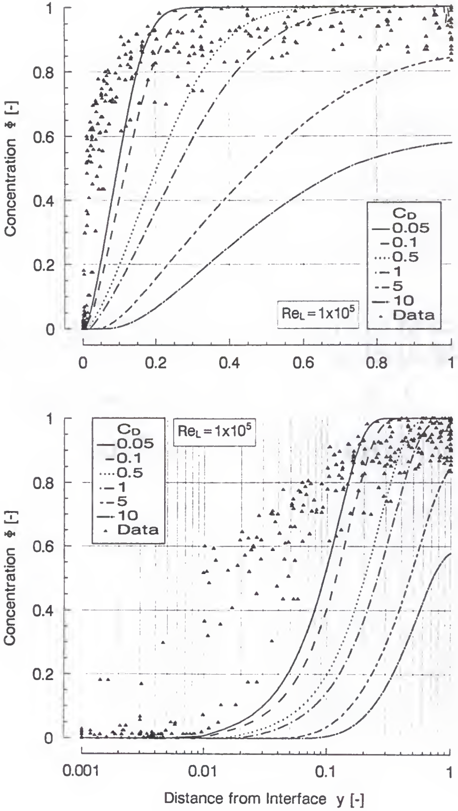

Figure 6-10. Family of concentration profiles for $0.05 \leq C_D \leq 10$, linear scale (top), semi-log scale (bottom).

models diffusion enhancement, causes a reduction in centerline ($y=1$) vapor concentration. Experimental data is also plotted in Figure 6-10, comparison reveals that diffusion was inhibited since the data is best described by the $C_D=0.1$ profile (given the $\delta_c<\delta_t$ relationship measured experimentally). Buoyancy driven vorticity and thermal diffusion probably caused the dissimilarity of shape between the $C_D=0.1$ profile and the experimental data.

The noncondensable film thickens as the diffusion factor is increased, as is apparent in the semi-log plot of Figure 6-10. Again, analogous to low Re_L, the decreased concentration gradient at high C_D slows the motion of gas molecules away from the gas film. The film is also evident in the experimental data of Figure 6-10, corresponding to the model profile for $C_D=0.1$.

The diffusive mass flux across the gas film, J_v, is given by Fick's law, which reduces to the relation

$$J_v = C_D D_{ij} \frac{\partial \rho_v}{\partial y^*} = C_D D_{ij} \frac{\partial(\rho_{v+g} C)}{\partial(yY)} \qquad (6\text{-}12)$$
$$\rho_v < \rho_{v+g} \,, \quad \Delta\rho_{v+g} < \Delta\rho_v$$

for the very low concentrations of vapor considered here. The results indicate that the concentration difference across the gas film is extremely small. Within the numerical accuracy of the series solutions (due to a finite number of series terms) and computer round-off error, this concentration difference is apparently not a strong function of diffusion factor or Reynolds number. In contrast, the film thickness varies significantly with diffusion factor and Reynolds number. Thus, it appears that the concentration gradient near the interface may be a strong function of film thickness.

Relative Humidity Profiles

Three families of calculated relative humidity profiles will be shown which will provide some insight into the condensing vapor -- noncondensable gas mixture boundary-layer behavior. The first set of profiles shows the effect of wall temperature and the second shows the effect of inlet relative humidity. The third shows the effect of the diffusion factor.

Moving from $y=1$ (the channel center) to the interface at $y=0$ (very near the wall), Figure 6-11 shows several important trends. Relative humidity boundary-layer thickness is unaffected by wall temperature. An increase in relative humidity with decrease in wall temperature is evident for $0.08 \leq y \leq \delta_c$. This is due to the saturation partial pressure decreasing more quickly than the vapor concentration as wall temperature is lowered. In the region $0.1 \leq y \leq 0.3$ for $T_w=1.7$ C (35 F), a local maximum exists since saturation partial pressure is reduced even further due to the thermodynamic properties of moist air, and the difference in shape between the temperature and concentration profiles. This is mostly due to the difference between δ_T and δ_c. This trend is reversed in the region $0 < y \leq 0.03$, where humidity decreases with wall temperature due to the decrease in wall concentration. All three profiles meet at ($y=0$, $\phi=1$) satisfying the corresponding boundary condition.

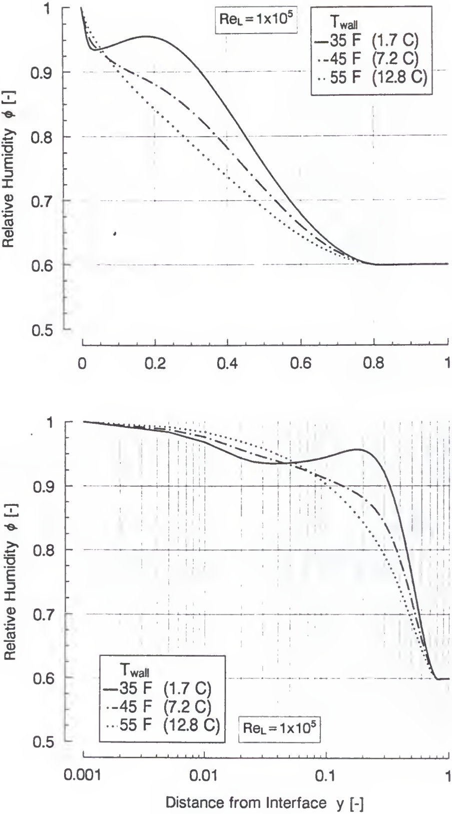

Figure 6-11. Family of relative humidity profiles for changing T_w, linear scale (top), semi-log scale (bottom).

The effect of increasing inlet relative humidity is analogous to that of decreasing wall temperature. However, the inverting trend near the interface is not an effect of changing ϕ_i, shown in Figure 6-12. Since T_w is identical for all three curves, they merge in the region of the gas film. Two interpretations of the local $\phi > 1$ maximum on the $\phi_i = 0.8$ profile are: (1) A state of metastable equilibrium exists allowing ϕ to exceed its saturation value of $\phi = 1$ temporarily, and (2) homogeneous condensation occurs in the vapor stream. The model considers phase change at the interface only.[18]

Experimental observations support (2) as fogging was noticed for $\phi_i > 0.8$. Nevertheless, the few observed fogging occurrences (five) do not disprove the first interpretation. The vapor may have existed in a metastable state for a very short period. Once the vapor molecules began to agglomerate, however, the transition from metastable supersaturation to homogeneous condensation would have occurred rapidly.

The effect of decreasing the diffusion factor is similar to that of increasing ϕ_i, as can be seen in Figure 6-13. Decreasing C_D effectively retards the progress of vapor molecules toward the wall. Since the concentration difference across the film is smaller than in the boundary layer, the vapor molecules accumulate, or queue, outside the gas film for $C_D \leq 0.5$.

---

[18] See assumption number 9 in Chapter 4.

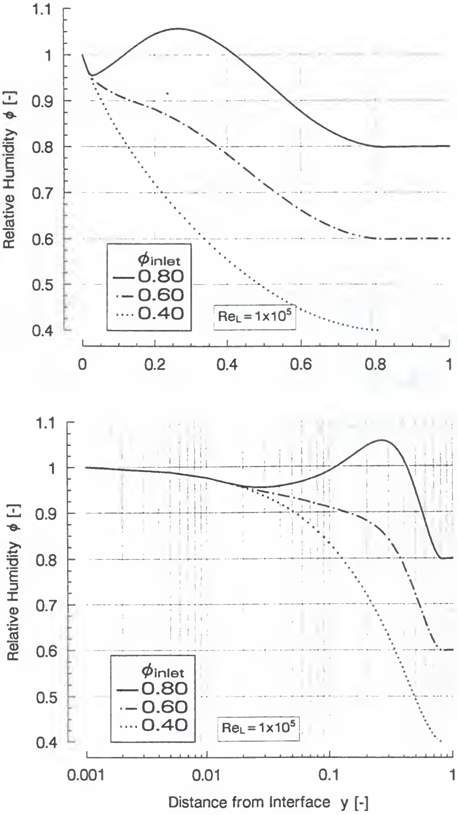

Figure 6-12. Family of relative humidity profiles for changing ϕ_i, linear scale (top), semi-log scale (bottom).

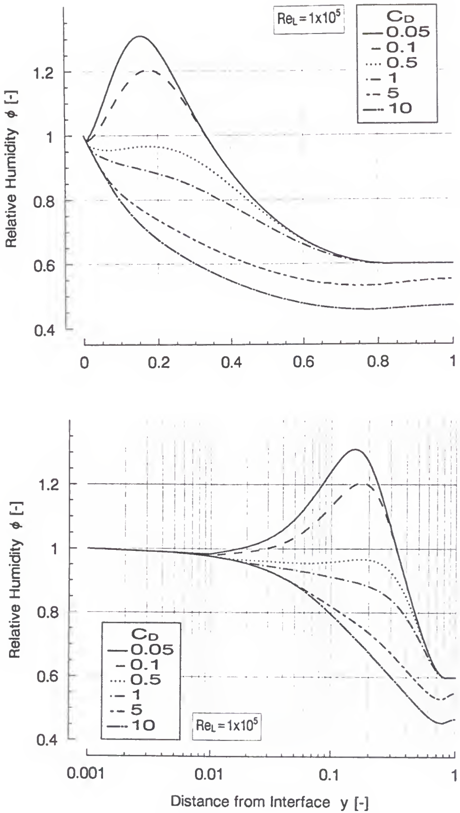

Figure 6-13. Family of relative humidity profiles for $0.05 \leq C_D \leq 10$, linear scale (top), semi-log scale (bottom).

Heat and Mass Transfer Rates

Overall heat and mass transfer rates were determined for various diffusion factors, wall temperatures, and Reynolds numbers using the model. The results were examined in the form of sensible heat ratio,

$$SHR = \frac{\dot{Q}_{SENSIBLE}}{\dot{Q}_{SENSIBLE} + \dot{Q}_{LATENT}} \qquad (6\text{-}13)$$

a standard measure of effectiveness for dehumidifying heat exchangers.

Figure 6-14 shows that mass transfer rate is a weak function of inlet velocity, *all other factors remaining constant*. For $\mathrm{Re_L} < 10^5$, which corresponds to an inlet velocity of $W < 1.2$ m/s ($W < 240$ fpm) at $z^* = 122$ cm ($z^* = 48$ in), *SHR* increases only slightly as Reynolds number is increased. Even for $\mathrm{Re_L} > 10^5$ the increase is only 10 percent at $\mathrm{Re_L} = 10^6$. This is evidence that, as inlet velocity is increased, the increase in total mass transfer due to increased gas-vapor mass flow rate essentially overwhelms the decrease in mass transfer indicated by the thinner concentration boundary layer.

In a real heat exchanger, however, the effect of inlet velocity on *SHR* is due to a combination of factors. For instance, real exchangers are rarely isothermal (as the model assumes). The wall surface temperature is elevated near the leading edge and decreases downstream. An increase in inlet velocity also results in an increase in average wall temperature. The model predicts that *SHR* decreases as wall temperature increases, *all other factors remaining constant*, as shown in Figure 6-15. As expected, both mass and heat transfer rate are reduced

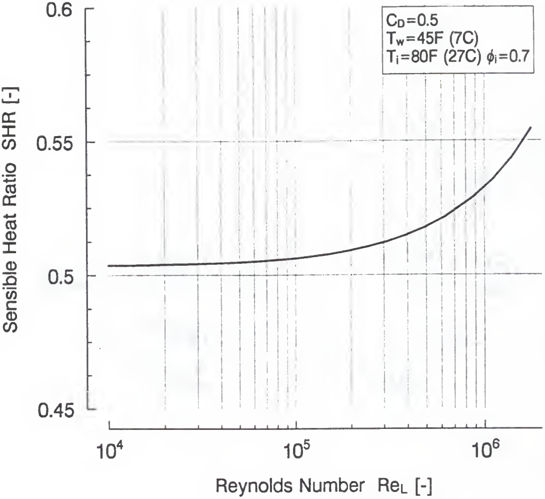

Figure 6-14. Sensible heat ratio versus Reynolds number with constant diffusion factor.

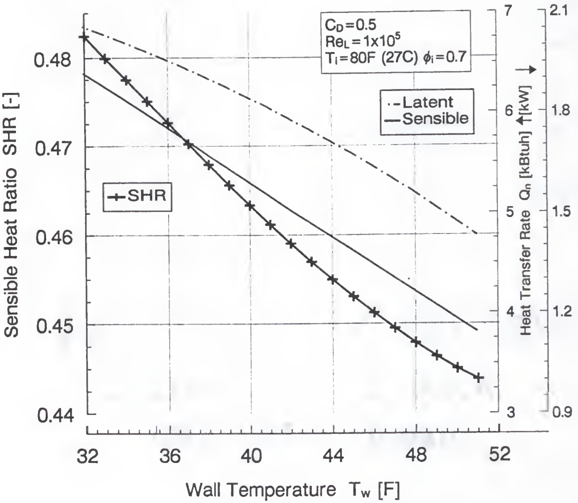

Figure 6-15. Sensible heat ratio versus isothermal wall temperature.

as wall temperature is increased. Unexpectedly, the reduction in heat transfer is greater -- but only about 10 percent greater over the entire serviceable range of a typical dehumidifying heat exchanger. So, *SHR* must be a strong function of an additional factor.

The experimental part of this work demonstrated that diffusion is inhibited as Re_L is increased, as previously discussed. Accordingly, the resulting empirical correlation between experimental C_D and Re_L was included in the model. Decreasing the diffusion factor decreases mass transfer, thereby increasing *SHR*, as shown in Figure 6-16. With this effect included, *SHR* increases significantly with Re_L as shown in Figure 6-17. The predicted behavior is comparable to that of a real dehumidifying heat exchanger.

The increase in *SHR* may be even larger at higher wall temperature. A further increase in temperature may result in zero mass transfer near the leading edge until, further downstream, the inner edge of the boundary layer is cooled below its dew point. This condition could cause an increase in *SHR* up to a maximum of $SHR=1$ for which the entire wall remains above the dew point.

In summary, a mathematical model was successfully developed and found be a valuable tool for the study of surface condensation. It revealed several interesting characteristics of the condensing boundary layer and their effects on mass transfer rate. It also spawned several enticing hypotheses describing mechanisms of mass transfer in the boundary layer. The model was enhanced based on experimental findings, giving it the ability to model more complex

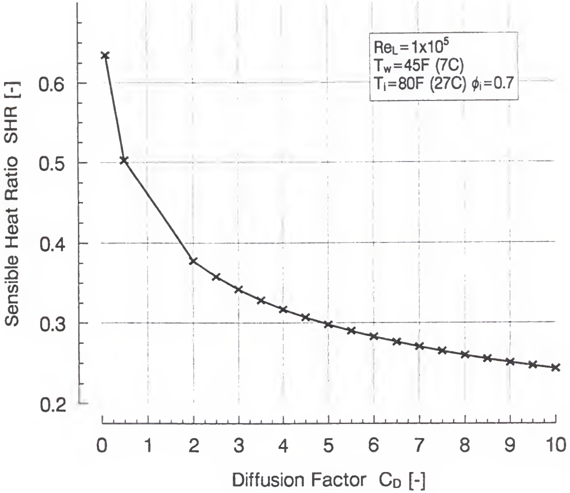

Figure 6-16. Sensible heat ratio versus diffusion factor C_D.

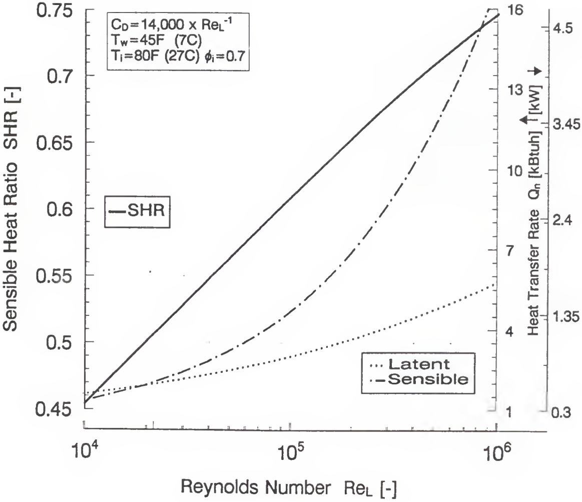

Figure 6-17. Sensible heat ratio versus Reynolds number with variable diffusion factor.

conditions. The predictions of the model at both the micro boundary-layer level and the macro heat-exchanger level are sound.

CHAPTER 7
CONCLUSIONS

A validated model of condensation from a mixture of vapor and non-condensing gas was produced. The results significantly contribute to the understanding of the heat and mass transfer processes occurring in a condensing heat exchanger. The performance of the model upholds the hypothesis that heat exchanger performance can be improved using a boundary layer type analysis. This was accomplished through successful completion of the many tasks necessary to satisfy the objectives of this work. The results provided an ability to determine resistances likely to inhibit mass transfer, and to suggest a means of condensation enhancement. Several recommendations to improve the models are made which should provide more detailed results.

Principal Conclusions

Based on the results of this work, the following conclusions are submitted.

1. An exact explicit two-dimensional solution to the concentration equation exists. The solution

$$\Phi = \frac{2}{\pi} e^{-\frac{py}{2}} \sum_{n}^{\infty} \frac{n}{n^2+\alpha^2} [1-(-1)^n e^{\alpha\pi}] e^{-\beta_n z} \sin(\frac{n\pi Y}{2R_o} y) \qquad (4\text{-}21)$$

was found using a cycle of transformations. It was verified by substitution into the differential equation.

2. Concentration and mass transfer data in the literature was extended. An experimental apparatus capable of measuring temperature and concentration profiles, and overall heat and mass transfer rates was developed to obtain the necessary data.

3. Condensation-driven diffusion across the boundary layer over a cooled vertical channel wall is inhibited according to

$$C_D = \frac{10^4}{\mathrm{Re}} = \frac{D_{ij,Re}}{D_{ij}} \qquad (6\text{-}8)$$

$$1.1\times10^4 \leq \mathrm{Re}_L \leq 10^6$$

4. A mathematical model of the condensing boundary layer in a channel was produced based on the solution. It was refined using the experimentally obtained inhibited diffusion correlation given in equation (6-8). The model can predict velocity, temperature, concentration, and relative humidity profiles; and sensible and latent heat transfer rates.

5. The increase in sensible heat ratio with inlet air velocity typical of dehumidifying heat exchangers is due partly to the inhibition of diffusion as described in equation (6-8).

6. The measured heat and mass transfer to or from a vertical channel wall exceeded the predictions of laminar flow theory. This is due to buoyancy induced convection caused primarily by temperature difference, and augmented by concentration difference when condensation is occurring.

7. During condensation from a mixture of vapor and noncondensable gas, a thin noncondensable gas film exists very near the wall and thickens downstream. The film thickness is on the order of
   0.5 mm (0.020 in) at $\mathrm{Re}_L=3\times10^4$ and
   0.05 mm (0.002 in) at $\mathrm{Re}_L=9\times10^5$
   for moist air. These results apply to the conditions
   $\nu=1.5\times10^{-5}$ m^2/s (1.6×10^{-4} ft^2/s),
   L=1.22 m (48 in), and
   0.35 and 11.0 m/s (69 and 2165 fpm) respectively.

8. Condensation rate is related to the gradient across the noncondensable film and the effective mass diffusivity of the vapor-gas mixture. It appears that the concentration gradient near the interface may be a strong function of film thickness.

9. Condensation rate may be significantly increased by increasing the diffusion rate through the boundary layer or decreasing the gas film thickness.

Relation to the Literature

The experimental apparatus recommences the work of Lebedev et al. (1969), Raffellini and Tarabusi (1980), Eckels and Rabas (1987), and Coney et al. (1989b) with a new emphasis on boundary layer examination. No other measurements of a concentration boundary layer, using either flat-plate or channel geometry, were reported in the literature reviewed. Temperature and concentration boundary-layer thicknesses were observed to decrease with increasing inlet velocity, as expected (Schlicting, 1955).

Measured Nusselt and Sherwood numbers satisfactorily agreed with empirical correlations published by McAdams (1954) and Welty (1976), although measured Sherwood number accuracy was low. Using the finite element model and smoke visualization, it was confirmed that buoyancy induced convection currents disturbed the laminar boundary layer. The effects of buoyancy were significant for inlet velocities of less than 2.5 m/s (492 fpm). This explains the low heat and mass transfer rate predictions of laminar flow theory and supports the similar finding of Coney et al. (1989b).

None of the authors of the literature reviewed had the intent or capability to study diffusion inhibition. The inhibited diffusion hypothesis supported by the experimental data, equation (6-8), proposes a relationship between the degree of diffusion inhibition and Reynolds number. Mechanisms explaining this relationship were postulated: (1) the temperature dependent mass diffusivity hypothesis, (2) the thermal diffusion hypothesis, and (3) the molecular momentum hypothesis. All were supported, to different degrees, by the boundary-layer measurements of this work. No other measurements of the gas film were reported in the literature reviewed, although its existence has been described.

No other exact explicit two-dimensional solution to the concentration equation for the conditions considered was reported in the literature reviewed. The solution provides concentration profiles from the inlet boundary condition to any point downstream, and shows the relationship among all of the relevant independent variables. The exact series solution adapted from Blasius's (1908) solution to the momentum boundary-layer equation does not possess these qualities. The solution compliments the numerical solution of Denny et al. (1971); and the analytic closed-form solution to the Graetz problem of Mansour (1989) and to the porous medium problem of Chaoyang and Chuanjing (1989).

Recommendations for Future Work

Investigation of the concentration boundary layer and mass transfer rate generated several interesting hypothesis which merit additional study. Further work should focus on verification of the causal relationships between changes in diffusion behavior (due to boundary condition changes) and the resulting changes in average mass transfer rate that were postulated in this work. If successful, many characteristics of dehumidifying heat exchangers could be precisely explained at the boundary-layer level, and ultimately at the molecular level.

Increased concentration precision and the addition of a pressure probe would permit more precise relative humidity profiles. The proposed explanations of humidity profile features predicted by the mathematical model could then be tested. Studies using high inlet humidity could identify homogenous condensation and metastable supersaturation.

Specific investigations of diffusion across a velocity gradient and across a temperature gradient would provide valuable insight into the diffusion phenomena observed in this work. This work on diffusion should focus on measurements of the mass diffusivity. An objective would be to determine the effect of velocity and temperature boundary layers on the effective mass diffusivity. A study of thermal diffusion in moist air would provide otherwise unavailable data. Although the results indicate thermal diffusion effects are minimal, the actual magnitude should be experimentally quantified.

Finally, a comparison between sensible heat ratio determined from boundary-layer measurements and from an entire heat exchanger should be undertaken. The fin model and exchanger should be operated at identical inlet and surface conditions. Tests at many conditions would connect the behavior of the bulk heat exchanger to measured changes in the boundary layer. This information could result in design features that would manage the boundary layer to improve the performance of condensing heat exchangers.

Recommendations for Improved Results

Future work should begin with an upgrade of the experimental apparatus to obtain more precise concentration and average mass transfer data. It is highly desirable to add a small multi-fin dehumidifying heat exchanger test section. The exchanger should operate simultaneously, at the same conditions as the existing fin model. Upgrading the analog-to-digital converter used in the experimental system from an 8-bit to a 12-bit unit would reduce the random error of the concentration and temperature profile measurements. The use of a laser holographic interferometer to provide sharper concentration resolution should be appraised. Measuring the density profile with the interferometer, and the temperature profile with the miniature thermocouple probe, may render a very accurate concentration profile. It would also permit visualization of the effect of flow dynamics on the concentration field. The use of an automated data acquisition system to collect overall heat and mass transfer related data is recommended. This would allow the determination of average steady-state heat transfer rates with finer precision and over longer intervals.

Faster hardware for the finite element analysis would be beneficial. The Hewlett Packard/Apollo 3500 used for this analysis ran 12.7 hours per 3750 linear element run, including 10.1 hours of CPU time. More capable hardware would allow a finer mesh. Dedicated software should be located, ideally with only the abilities necessary to perform this analysis . The software EMRC NISA 3-D FLUID V.91.0, used to solve the finite element model, is among the most general available, and it cannot solve simultaneous heat and mass transfer with phase change.

More capable hardware for execution of the Fortran model is recommended for calculation of many profiles or heat transfer rates per run. Calculation of 50 concentration profiles at 100 points per profile required one hour of CPU time on a DEC VAX 6320. Finer Blasius solution and laminar sublayer correlations may provide increased accuracy very near the wall.

APPENDIX A
FINITE ELEMENT MODEL

The following is a listing of the input for and output from the NISA finite element solver. (The input is echoed in this output listing.) Three dimensional mixed (free plus forced) convection is specified, along with the appropriate material properties. Nodal coordinates (units: [feet]) and boundary conditions (units: [ft/s], [R]) at each coordinate are specified, along with the desired solution method and number of iterations. The element type specified, NKTP 4, is a first order quadrilateral element with 8 nodes and three degrees of freedom per node. A 25 x 15 x 10 grid was created for a total of 3750 elements and 4576 nodes. Three velocity components, temperature, and pressure are output for each node. Lines have been removed from this abbreviated listing to conserve space.

```
                        PLATE8.OUT -- 3D CONVECTION IN A CHANNEL
                                   MICHAEL K. WEST

 LINE   1 ** EXECUTIVE
 LINE   2 FILE=PLATE8
 LINE   3 ANAL=FLUHT
 LINE   4 CONVECTION=MIXED,1
 LINE   5 SAVE=26,27
 LINE   6 DIME=3D
 LINE   7 *ELTYPE
                         AUG/ 7/1991  15:11:41
                         *NISA* COMPUTER PROGRAM RELEASE NO. 90.0
                         AUTHORIZED SITE : UNIVERSITY OF FLORIDA
                         ***** APOLLO PRODUCTION VERSION *****
                         LAST UPDATED : 07/24/90
                               FLUID  ANALYSIS
                               ---------------
                         Engineering Mechanics Research Corporation
                         P.O. Box 696, Troy, MI 48099 U.S.A.
                         Tel: 313/643-6222. Fax: 313/649-9380. Tlx: 469232.
 SELECTION OF ELEMENT TYPES FROM THE NISA ELEMENT LIBRARY (*ELTYPE DATA GROUP)

  NSRL      NKTP     NORDR  NODES/EL  DOF/NODE
  ----      ----     ----   --------  --------

    1         4        1        8        3

              -- NODAL COORDINATES (*NODES DATA GROUP ) --
NODE    COORD                                          ROTATED
 NO.   SYS. ID.                 COORDINATES             SYS. ID.
  1       0      0.00000E+00    0.00000E+00    1.00000E-01    0
  2       0      0.00000E+00    1.50000E+00    1.00000E-01    0
  3       0      4.00000E+00    1.50000E+00    1.00000E-01    0
 .
 . NODES 4 THRU 4573 REMOVED TO CONSERVE SPACE
 .
4574      0      1.60000E-01    1.20000E+00    0.00000E+00    0
4575      0      1.60000E-01    1.30000E+00    0.00000E+00    0
4576      0      1.60000E-01    1.40000E+00    0.00000E+00    0

ELEMENT DEFINITIONS (*ELEMENTS DATA GROUP)

ELEMENT  MATERIAL        REAL CONST ANISOTROPIC
NUMBER    INDEX   NSRL    INDEX      INDEX     --- E L E M E N T   N O D E   N U M B E R S ---
------    ----    ----    ----       ----      ------------------------------------------------
    1       1       1       1          0        80    81    43     4   496   497   459   420
    2       1       1       1          0        81    82    44    43   497   498   460   459
    3       1       1       1          0        82    83    45    44   498   499   461   460
 .
 . NODES 4 THRU 4573 REMOVED TO CONSERVE SPACE
 .
3748       1       1       1          0      4157  4158  4144  4143  4573  4574  4560  4559
3749       1       1       1          0      4158  4159  4145  4144  4574  4575  4561  4560
3750       1       1       1          0      4159  4160  4146  4145  4575  4576  4562  4561

MATERIAL PROPERTY TABLE  (*MATERIAL DATA GROUP)
-----------------------------------------
MATERIAL INDEX     1
 DENS    1  0 7.5000003E-02  0.0000000E+00  0.0000000E+00  0.0000000E+00  0.0000000E+00
 VISC    1  0 1.2200000E-05  0.0000000E+00  0.0000000E+00  0.0000000E+00  0.0000000E+00
 COND    1  0 4.1700000E-06  0.0000000E+00  0.0000000E+00  0.0000000E+00  0.0000000E+00
 SPEC    1  0 2.3999999E-01  0.0000000E+00  0.0000000E+00  0.0000000E+00  0.0000000E+00
 GRAV    1  0 3.2200001E+01  0.0000000E+00  0.0000000E+00  0.0000000E+00  0.0000000E+00
 BETA    1  0 2.2000000E-03  0.0000000E+00  0.0000000E+00  0.0000000E+00  0.0000000E+00
 TEMB    1  0 5.2200000E+02  0.0000000E+00  0.0000000E+00  0.0000000E+00  0.0000000E+00

    FLUID CONTROL FOR LOAD CASE ID NO.    1
    TOTAL NUMBER OF TIME STEPS .............(NLSTP) =   1
    MAXIMUM ITERATIONS IN EACH TIME STEP ...(ITMAX) =   1
    PRINTOUT CONTROL KEY ...................( NTPN) =   1
    TIME STEP ..............................(   DT) = 1.00000E+00
    TOLERANCE FOR EACH ITERATION ...........(  EPS) = 1.00000E-03
    PENALTY PARAMETER ......................( GAMA) = 1.00000E+08
    REFERENCE VELOCITY .....................( REFU) = 1.00000E+00
    REFERENCE LENGTH .......................( REFL) = 1.00000E+00
    REFERENCE TEMPERATURE (LOWER) ..........(REFT1) = 4.95000E+02
    REFERENCE TEMPERATURE (UPPER) ..........(REFT2) = 5.40000E+02

    SPECIFIED NODAL VALUE
    ---------------------
 NODE NO.  LABEL   NODAL VALUE   LAST NODE   INC      LABELS
     1  U       2.00000E+00       0      0
```

```
   1  V    0.00000E+00   0   0
   1  W    0.00000E+00   0   0
   1  T    5.40000E+02   0   0
   2  U    2.00000E+00   0   0
   2  V    0.00000E+00   0   0
   2  W    0.00000E+00   0   0
   2  T    5.40000E+02   0   0
   3  U    0.00000E+00   0   0
   3  V    0.00000E+00   0   0
   3  W    0.00000E+00   0   0
   3  T    5.40000E+02   0   0
   4  U    0.00000E+00   0   0
   4  V    0.00000E+00   0   0
   4  W    0.00000E+00   0   0
   4  T    5.40000E+02   0   0
   5  U    2.00000E+00   0   0
   5  V    0.00000E+00   0   0
   5  W    0.00000E+00   0   0
   5  T    5.40000E+02   0   0
   6  U    2.00000E+00   0   0
   6  V    0.00000E+00   0   0
   6  W    0.00000E+00   0   0
   6  T    5.40000E+02   0   0
   7  U    2.00000E+00   0   0
   7  V    0.00000E+00   0   0
   7  W    0.00000E+00   0   0
   7  T    5.40000E+02   0   0
   8  U    2.00000E+00   0   0
   8  V    0.00000E+00   0   0
   8  W    0.00000E+00   0   0
   8  T    5.40000E+02   0   0
   9  U    2.00000E+00   0   0
   9  V    0.00000E+00   0   0
   9  W    0.00000E+00   0   0
   9  T    5.40000E+02   0   0
  10  U    2.00000E+00   0   0
  10  V    0.00000E+00   0   0
  10  W    0.00000E+00   0   0
  10  T    5.40000E+02   0   0
   .
   .  NODES 11 THRU 4568 REMOVED TO CONSERVE SPACE
   .
4569  U    0.00000E+00   0   0
4569  V    0.00000E+00   0   0
4569  W    0.00000E+00   0   0
4569  T    4.95000E+02   0   0
4570  U    0.00000E+00   0   0
4570  V    0.00000E+00   0   0
4570  W    0.00000E+00   0   0
4570  T    4.95000E+02   0   0
4571  U    0.00000E+00   0   0
4571  V    0.00000E+00   0   0
4571  W    0.00000E+00   0   0
4571  T    4.95000E+02   0   0
4572  U    0.00000E+00   0   0
4572  V    0.00000E+00   0   0
4572  W    0.00000E+00   0   0
4572  T    4.95000E+02   0   0
4573  U    0.00000E+00   0   0
4573  V    0.00000E+00   0   0
4573  W    0.00000E+00   0   0
4573  T    4.95000E+02   0   0
```

```
     4574  U      0.00000E+00     0     0
     4574  V      0.00000E+00     0     0
     4574  W      0.00000E+00     0     0
     4574  T      4.95000E+02     0     0
     4575  U      0.00000E+00     0     0
     4575  V      0.00000E+00     0     0
     4575  W      0.00000E+00     0     0
     4575  T      4.95000E+02     0     0
     4576  U      0.00000E+00     0     0
     4576  V      0.00000E+00     0     0
     4576  W      0.00000E+00     0     0
     4576  T      4.95000E+02     0     0

SELECTIVE PRINTOUT CONTROL PARAMETERS (*PRINTCNTL DATA GROUP)
-------------------------------------------------------------
OUTPUT TYPE          -- SET NUMBERS (NEGATIVE MEANS NONE, ZERO MEANS ALL)

U-VELOCITY COMPONENT          0
V-VELOCITY COMPONENT          0
W-VELOCITY COMPONENT          0
TURBULENT KINETIC ENERGY     -1
DISSIPATION              -1
TURBULENT EDDY VISCOSITY     -1
STREAM-LINE              -1
TEMPERATURE               0
PRESSURE                 0
NORMAL STRESS SXX           -1
NORMAL STRESS SYY           -1
NORMAL STRESS SZZ           -1
SHEAR STRESS SXY           -1
SHEAR STRESS SXZ           -1
SHEAR STRESS SYZ           -1

      PROCESS NODAL COORDINATES DATA
      PROCESS ELEMENT CONNECTIVITY DATA
      TOTAL NUMBER OF ELEMENTS ...............=  3750
      TOTAL NUMBER OF NODES     ...............=  4576
      TOTAL NUMBER OF ACTIVE NODES ...........=  4576
      LARGEST NODE NUMBER       ...............=  4576

      MINIMUM X-COORD =   0.00000E+00  MAXIMUM X-COORD =    0.40000E+01
      MINIMUM Y-COORD =   0.00000E+00  MAXIMUM Y-COORD =    0.15000E+01
      MINIMUM Z-COORD =   0.00000E+00  MAXIMUM Z-COORD =    0.10000E+00

WAVE FRONT STATUS BEFORE MINIMIZATION
-------------------------------------
  MAXIMUM WAVE FRONT ..........=  3045
  RMS WAVE FRONT ..............=  2060
  AVERAGE WAVE FRONT ..........=  1938
  TOTAL NO. OF DOF IN MODEL ...=  13728

***** WAVE FRONT MINIMIZATION WAS SUCCESSFUL, ITERATION NO. 1 IS SELECTED
WAVE FRONT PARAMETERS ARE-
MAXIMUM WAVE FRONT=  741
RMS WAVE FRONT    =  548
AVERAGE WAVE FRONT=  537


     .....   THREE-DIMENSIONAL  FLUID  FLOW  .....

  TOTAL NUMBER OF ELEMENTS =  3750   TOTAL NUMBER OF NODES =  4576
  TOTAL NUMBER OF ELEMENT TYPES =  1
```

```
    TYPE  1 ......
    NKTP =  4   NORDR =  1   NPE =  8   NGPX =  2   NGPY =  2   NGPZ =  2

    TOTAL NUMBER OF MATERIAL TYPES =  1
    TYPE  1 ......
    DENSITY  = 0.750E-01   VISCOSITY = 0.122E-04
    CONDUCTIVITY =0.417E-05   SPECIFIC HEAT =0.240E+00
    GRAVITY =0.322E+02   VOLUME COEF. =0.220E-02
    REF. TEMP. =0.522E+03   ANGLE =0.000E+00
    RESISTANCE FACTOR =0.000E+00

       LOAD CASE =      1
       ------------------------

    INNER ITERATION =  1   TIME INCREMENT =0.100E+01
    TOTAL TIME STEP =  1   CONVERGENT TOLERANCE =0.100E-02
    PENALTY FACTOR =0.100E+09   PRINTCNTL =  1

    REF.T1  =0.495E+03      REF.T2  =0.540E+03
    REF.VEL  =0.100E+01     REF.LEN  =0.100E+01

    MATERIAL TYPE  1 ......
    REYNOLDS NUMBER =0.615E+04   PRANTL NUMBER =0.702E+00

    ------- BOUNDARY CONDITIONS -------
    NUMBER OF NODAL VELOCITY B.C.          =     4278
    NUMBER OF NODAL TEMPERATURE B.C.    =      1426
    NUMBER OF NODAL TURBULENT K B.C.    =        0
    NUMBER OF NODAL TURBULENT E B.C.    =        0
    NUMBER OF NODAL STREAMLINE B.C.     =        0
    NUMBER OF NODES ON TURBULENT WALL   =          0
    NUMBER OF HEAT SOURCES AT NODES     =        0
    NUMBER OF NEUMANN VELOCITY B.C.    =        0
    NUMBER OF NEUMANN TEMPERATURE B.C. =          0
    NUMBER OF NEUMANN TURBULENT  B.C.  =        0
    NUMBER OF NEUMANN STREAMLINE B.C.  =        0

** APPROXIMATE MEMORY REQUIREMENT      =  1255039 WORDS
** APPROXIMATE DISK SPACE REQUIREMENT  =    89.37 MEGABYTES

***  EXECUTING THE SOLVER OF NISA/FLUID  ***
      *** TIME STEP =     0.10000E+01 ***
 TEMP. ITERATION =   1   MAX ERROR =  0.845117E+00   AT NODE =   819
 VELOCITY ITERATION =1   MAX ERROR =  0.353969E+01   AT NODE =  2483

 NODE       U           V           W           T           P
   1 0.20000E+01 0.00000E+00 0.00000E+00 0.54000E+03 0.92965E+00
   2 0.20000E+01 0.00000E+00 0.00000E+00 0.54000E+03 0.92968E+00
   3 0.00000E+00 0.00000E+00 0.00000E+00 0.54000E+03 -.15570E+00
   4 0.00000E+00 0.00000E+00 0.00000E+00 0.54000E+03 -.15570E+00
   5 0.20000E+01 0.00000E+00 0.00000E+00 0.54000E+03 0.85096E+00
   6 0.20000E+01 0.00000E+00 0.00000E+00 0.54000E+03 0.83619E+00
   7 0.20000E+01 0.00000E+00 0.00000E+00 0.54000E+03 0.83524E+00
   8 0.20000E+01 0.00000E+00 0.00000E+00 0.54000E+03 0.83150E+00
   9 0.20000E+01 0.00000E+00 0.00000E+00 0.54000E+03 0.83195E+00
  10 0.20000E+01 0.00000E+00 0.00000E+00 0.54000E+03 0.83051E+00
   .
   .
   .
 414 0.00000E+00 0.00000E+00 0.00000E+00 0.54000E+03 0.81434E+00
 415 0.00000E+00 0.00000E+00 0.00000E+00 0.54000E+03 0.81677E+00
 416 0.00000E+00 0.00000E+00 0.00000E+00 0.54000E+03 0.82341E+00
 417 0.20000E+01 0.00000E+00 0.00000E+00 0.54000E+03 0.87646E+00
 418 0.20000E+01 0.00000E+00 0.00000E+00 0.54000E+03 0.87648E+00
 419 0.00000E+00 0.00000E+00 0.00000E+00 0.54000E+03 0.17482E-01
 420 0.00000E+00 0.00000E+00 0.00000E+00 0.54000E+03 0.17482E-01
 421 0.20000E+01 0.00000E+00 0.00000E+00 0.54000E+03 0.84756E+00
   .
   .
   .
 448 0.00000E+00 0.00000E+00 0.00000E+00 0.54000E+03 0.37253E+00
 449 0.00000E+00 0.00000E+00 0.00000E+00 0.54000E+03 0.33935E+00
 450 0.00000E+00 0.00000E+00 0.00000E+00 0.54000E+03 0.30474E+00
 451 0.00000E+00 0.00000E+00 0.00000E+00 0.54000E+03 0.27155E+00
 452 0.00000E+00 0.00000E+00 0.00000E+00 0.54000E+03 0.23695E+00
   .
   .
   .
4568 0.00000E+00 0.00000E+00 0.00000E+00 0.49500E+03 0.81151E+00
4569 0.00000E+00 0.00000E+00 0.00000E+00 0.49500E+03 0.81131E+00
4570 0.00000E+00 0.00000E+00 0.00000E+00 0.49500E+03 0.81132E+00
4571 0.00000E+00 0.00000E+00 0.00000E+00 0.49500E+03 0.81151E+00
4572 0.00000E+00 0.00000E+00 0.00000E+00 0.49500E+03 0.81205E+00
4573 0.00000E+00 0.00000E+00 0.00000E+00 0.49500E+03 0.81279E+00
4574 0.00000E+00 0.00000E+00 0.00000E+00 0.49500E+03 0.81434E+00
4575 0.00000E+00 0.00000E+00 0.00000E+00 0.49500E+03 0.81677E+00
4576 0.00000E+00 0.00000E+00 0.00000E+00 0.49500E+03 0.82341E+00

*** NORMAL COMPLETION

       O V E R A L L   T I M E   L O G   I N   S E C O N D S
       INPUT ( READ,GENERATE ) ....................... =   287.450
       DATA SORTING AND CHECKING ..................... =    55.983
       REORDERING OF ELEMENTS ........................ =   677.933
       PRE-FRONT ..................................... =   215.567
       FORM ELEMENT MATRICES (LINEAR PART)............ =  2649.183  =   0.736 HRS
       FORM ELEMENT MATRICES (NON-LINEAR PART)........ =  3703.940  =   1.029 HRS
       SOLUTION OF SYSTEM EQUATIONS .................. = 28466.263  =   7.907 HRS
       PRESSURE CALCULATION .......................... =   401.680
       RESULT PROCESSING ............................. =    45.184
       TOTAL CPU ..................................... = 36503.183  =  10.140 HRS

       TOTAL ELAPSED TIME IS ......................... = -45832.000  =  12.731 HRS
```

APPENDIX B
FORTRAN MODEL

The following is a Fortran code listing of the model of condensation from a mixture of vapor and noncondensable gas in a channel written for this work. It is based on an exact analytic solution to the concentration equation, completed as part of this work; and Blasius's laminar and the seventh-power turbulent hydrodynamic boundary-layer equations. The concentration solution is on lines 158-162, 169, and 182. The transverse velocity due to boundary layer growth is on line 142. The transverse velocity due to vapor migration is on lines 155 and 213. In this listing, all code lines are executable. However, in an actual run redundant routines are skipped; for example, the inviscid (line 144) and turbulent (line 136) profiles would not be employed simultaneously.

CONCENTRATION VERSION F;46
BY MICHAEL K. WEST

VARIABLE LISTING

NAME	SYMBOL	[UNITS]	DEFINITION
alpha	α	[ft/s]	artificial velocity
betan	β_n	[ft/s^2]	artificial acceleration
C	C	[-]	mass of vapor per unit mixture
Cb	C_b	[-]	average C between two y_j
CD	C_D	[-]	diffusion factor
Ci	C_i	[-]	C at inlet boundary condition
Cold	C_{old}	[-]	C at y_{j-1}
cond	m_v	[lb]	vapor condensed between two z_k
cp	c_p	[Btu/lb/F]	specific heat of gas

Cw	C_w	[-]	C at wall boundary condition
delta	δ	[ft]	momentum boundary layer thickness
deltat	δ_t	[ft]	thermal boundary layer thickness
detltc	δ_c	[ft]	species boundary layer thickness
Dij	D_{ij}	[ft^2/hr]	mass diffusivity
eps	ϵ	[-]	transformed distance into channel
eta	n	[-]	transformed distance from interface
F(eta)	f (n)	[-]	dimensionless stream function
FP(eta)	f' (n)	[-]	f prime, also from Blasius's equation
Pws(TR)	$P_{ws}(T)$	[psia]	saturation pressure over $H_2O(\ell)$
Fluxin	F_i	[lb/sec]	vapor entering channel
Fluxout	F_o	[lb/sec]	vapor leaving at z_k
FPM	U_o	[ft/min]	inlet velocity
grlb	W	[gr/lb]	mass of vapor per unit gas
lbi	W_i	[gr/lb]	grlb at inlet boundary condition
lbw	W_w	[gr/lb]	grlb at wall boundary condition
Mc	M_c	[lb]	mass of vapor in 1 × dy × dz
McOLD	$M_{c,old}$	[lb]	Mc in previous dz
mdot	m	[lb]	mass moving across 1 × dy
nu	ν	[ft^2/s]	kinematic viscosity of gas
Ny	N_y		highest y to be considered
p	p	[ft/s]	artificial velocity
pb	$\overline{p}$	[ft^2/s^2]	squared transformed artificial velocity
pi	π	[-]	ratio of circumference to diameter
Pr	Pr	[-]	Prandtl Number
Qcond	Q_{cond}	[Btu/hr]	total latent heat transfer
Qsens	Q_{sens}	[Btu/hr]	total sensible heat transfer
Qtot	Q_{tot}	[Btu/hr]	total heat transfer
r	r	[ft]	artificial distance
rb	$\overline{r}$	[ft]	transformed artificial distance
ReL	Re_L	[-]	Reynolds number at z=L
Ro	R_o	[ft]	wall to channel center
roh	ρ_{vapor}	[lb/ft^3]	characteristic density of vapor
row	ρ_{gas}	[lb/ft^3]	characteristic density of gas
Sc	Sc	[-]	Schmidt number
SHR	SHR	[-]	Sensible heat ratio
SIGMA	Σ	[-]	summation portion of concentration
sqgam	$\Gamma^{1/2}$	[-]	concentration excess
SURF	$\Gamma^{1/2}(y,z)$	[-]	matrix of concentration excess
tdelta	$\delta_{turbulent}$	[ft]	turbulent boundary layer thickness
theta	θ	[-]	temperature excess
Ti	T_i	[F]	inlet temperature boundary condition
TR	T	[R]	temperature in Rankine
Tw	T_w	[F]	wall temperature boundary condition

Tyz	T(y,z)	[F]	temperature
v	v	[-]	dimensionless transverse velocity
Vc	V	[ft/s]	characteristic transverse velocity
vdot	$v_{\dot{m}}$	[ft/s]	transverse velocity due to vapor
vstar	v^*	[ft/s]	transverse velocity due to conservation
w	w	[-]	dimensionless velocity
Wc	W	[ft/s]	characteristic velocity
wmax	w_{max}	[-]	dimensionless centerline velocity
Ws	W_s	[-]	humidity ratio at saturation
y	y	[-]	dimensionless length, y=0 at interface
Yc	Y	[ft]	characteristic length normal to wall
ydiv	N_{ydiv}		number of divisions in y-direction
yhat	$\hat{y}$	[ft]	length in direction normal to wall
z	z	[-]	dimensionless length, z=0 at inlet
z4	z_4	[-]	nondimensional z at $\hat{z}$=L
Zc	Z	[ft]	characteristic length in flow direction
zdiv	N_{zdiv}		number of iterations in z-direction

```
                                        5-Dec-1991 00:00:31    VAX
FORTRAN V5.6-119
                                        4-Dec-1991 12:40:27
DISK$USER:[MEFLUID]CONF.FOR;46 BY MICHAEL K.WEST
    -----------------------------------------------------------------------
C Calculates Concentration=C(y,z), Temp T(y,z), Velocity v(y,z) due
c to B.L. growth and vapor migration, entry or fully developed,
c velocity profiles w(y,z) and condensation and heat transfer rate.
    -----------------------------------------------------------------------
      OPEN (UNIT=1,FILE='B:CONC.DAT',STATUS='UNKNOWN')
      real lbw,lbi,nu,m(401,2),vdot(401),Mc,McOLD,mdot
      real betan,bug1,bug2,bug4,SURF(102,202)
      double precision SIGMA,bug3
C Laminar boundary-layer velocity solutions
      F(eta) = 1.86099E-2-9.12089E-2*eta+2.51852E-1*eta**2+
     1     -2.53447E-2*eta**3+9.39168E-4*eta**4
      FP(eta) = -2.37811E-2+4.10144E-1*eta-3.89629E-2*eta**2
     1      -1.79037E-3*eta**3+2.78840E-4*eta**4
C Saturation pressure over liquid water from 32F to 392F
      Pws(TR)=exp(c8/TR+c9+c10*TR+c11*TR**2+c12*TR**3+c13*log(TR))
      c8= -10440.4
      c9= -11.2946669
      c10=-.02700133
      c11= .12897060E-4
      c12=-.2478068E-8
```

```
       c13=6.5459673
C FP debug routine--for comparison with Schlicting's tabulated solutions
      Do 100 L=1,8
      e=(L-1)
      write(6,96)e,0.5*(e*FP(e)-F(e))
100   continue
96    format(2f12.5)
C constant values
      write(6,94)1
      IDL=100
      DO 5 ID=1,IDL
      tcond=0
C     y*[0,.08]; y[0,1]; w[0,1]; v[0,1]
C wall and inlet temperature
      Tw=32.+ID*1.
      Tw= 45.
      Ti= 80.
      pi=  3.141592654
C specified concentration at wall and at inlet gr H2O/7000 per lb dry air
c                                and lb H20 per lb mixture
      lbw= 39/7000
      lbi= 110/7000
      Cw=  lbw/(1+lbw)
      Ci=  lbi/(1+lbi)
C OR concentration at wall and inlet lb H20 per lb mixture
      if(ID.eq.1)Cw= .003
      if(ID.eq.2)Cw= .007
      Cw= .003
      Ci= .016
C OR concentration at wall is saturation concentration at Tw
       TR=Tw+459.67
       Ws=.62198*Pws(TR)/(14.696-Pws(TR))
       Cw=Ws/(1+Ws)
C channel thickness in inches/12
      Yc=  0.08/12.
      zs=  0.05
C channel width in inches/12
      Ro=  0.04/12.
C kinematic viscosity of air ft^2/sec
      nu=  0.00016
C Prandtl number
      Pr=  0.71
C specific heat of air
      cp=.24
```

```
C density of air
      row= 0.075
C density of water vapor
      roh= 0.03
C Reynold's number based on Length
      ReL=8.0E5/ID
C       ReL= 3*10**(2+.2*(ID-1))
C Diffusivity of species 'i' in species 'j' ft^2/hr
      Dij=.94
C Diffusivity Factor CD
      if(ID.eq.1)CD= .05
      if(ID.eq.2)CD= .1
      if(ID.eq.3)CD= .5
      if(ID.ge.4)CD= .5*ID
      CD=14000./ReL
      if(CD.gt.1)CD=1.
      Dij=Dij*CD
      write(6,94)
      write(6,94)ID,ReL
      SURF(1,ID)=ID
C Schmidt number
      Sc=  nu/Dij*3600.
C inlet velocity in FPM
      FPM=ReL*nu/4.*60.
C characteristic velocity [ft/s] in flow direction, *25 for similitude
      Wc=  FPM*25./60.
C characteristic value of flow direction coordinate z[0,inf]
      Zc= Yc**2*Wc/nu
C march in z direction (flow direction)
c .428544644=zdiv* for 48"@350FPM
c  @150 FPM zdiv= 5.*0.001843317972
C value of nondimensional z at z=L=4
      z4=4./25/Zc
      zdiv=z4/1.
      Mc=Ci/(1-Ci)*row*Yc*zdiv*Zc
      do 30 K=2,2
      z=zdiv*(K-1)
      write(6,*)
      McOLD=Mc
      Mc=0
      mdot=0
      Qsens=0
C characteristic value for transverse velocity v[0,1](y,z)
      Vc= nu/Yc
```

```
C B.L. thicknesses "delta" & turbulent thickness "tdelta"
C deltat=thermal B.L. thickness, deltac=concentration B.L. thickness
      delta= 5.0*sqrt(nu*(z*Zc)/Wc)
      deltat= delta*(Pr)**(-1./3.)
      deltac= delta*(Sc)**(-1./3.)
      if(z.gt.0) tdelta= 0.37*(z*Zc)*(nu/Wc/z/Zc)**(0.2)
      write(6,99) delta*12.*25.,deltat*12.*25.,deltac*12.*25.
     1        ,tdelta*12.*25.
      if(z.ne.0.and.delta/Yc.le.0.5)
     1        Vc= 0.8604*Wc*sqrt(nu/(z*Zc)/Wc)
C wmax is increase in centerline velocity due to displacement thickness
      eps=sqrt(nu*(z*Zc)/Ro**2/Wc)
      wmax=(1+1.7208*eps)
      write(6,96)eps,wmax
C march in y direction (through boundary layer)
      ydiv=100.
      Ny=ydiv
      Do 20 J=1,(Ny/2)+1
      y= 1./ydiv*(J-1)
C velocity and temperature profiles, check for fully developed flow
c w=velocity in flow direction z, v=BL transverse velocity in y direction
c theta = temeprature
c     v(y)[0,1]; w(y)[0,1]
      yhat= y*Yc
      if(y.gt.0.5) yhat= (1-y)*Yc
      if (z.eq.0) go to 40
      eta=yhat*sqrt(Wc/nu/(z*Zc))
      w= FP(eta)*wmax
C optional turbulent velocity profile:
      w= (yhat/tdelta)**(1./7.)*wmax
      theta= w/wmax*(Pr)**(-1./3.)/1.026
      if (w.gt.wmax)  w= wmax
      if (eps.ge.0.4) w= 1.68832*(1-(2*yhat/Yc-1)**2)
      if (deltat/Yc.gt.0.5) theta=  1-(2*yhat/Yc-1)**2
      vstar= 0.5*sqrt(nu*Wc/(z*Zc))*(eta*FP(eta)-F(eta))
      v= vstar/Vc
C optional linear inviscid velocity profile:
      w=1.
      v=0.
c no slip and symmetry conditions
      if (eps.gt.0.4) v=0.
40    if (z.eq.0)     w=1.
      if (z.eq.0.)    theta= 1.
      if (w.le.0.or.yhat.eq.0.)    w= 1E-9
      if (z.eq.0.or.yhat.eq.0.)    v=0.
      if (y.gt.0.5)                v=-v
C transverse velocity due to vapor migration
      v=v+vdot(J)/Vc
      if(v.gt.1)v=1.
C variable values needed for concentration solution
      p= -Vc*Yc*Sc/nu*v
      r= Wc*Yc**2/Zc*Sc/nu*w
      pb=(p*Ro/pi/Yc)**2
      rb=r*(2*Ro/pi/Yc)**2
      alpha=p*Ro/pi/Yc
      write(6,98)p,Vc,Yc,v
98     format(5f13.4)
      SIGMA=0.
C compute summation part of concentration for n terms in series
      DO 10 n=1,2000
      betan=(n**2+pb)/rb
      SIGMA=SIGMA+(n/(n**2+alpha**2)*(1-(-1)**n*exp(alpha*pi))*
     1 exp(-betan*z)*sin(n*pi*Yc/2./Ro*y))
C debug routine
      bug1= n/(n**2+alpha**2)
      bug2= (1-(-1)**n*exp(alpha*pi))
      bug3= exp(-betan*z)
      bug4= sin(n*pi*Yc/2./Ro*y)
      if(n.eq.2000)write(6,97)bug1,bug2,bug3,bug4,sigma
97     format(5e13.3)
97     format(f13.9,f13.9,f13.9,f13.9,f20.16)
10     CONTINUE
C calculate concentration C[lb H2O/lb mix], grlb[gr H2O/lb dry air]
c nondimensional concentration sqgam, and theta based on conc
      C=Cw+(Ci-Cw)*2./pi*exp(-p*y/2.)*SIGMA
      if(C.gt.Ci.or.C.lt.0.)C=Ci
      grlb=7000.*C/(1-C)
      sqgam=(C-Cw)/(Ci-Cw)
      if(sqgam.gt.0.9999.or.sqgam.lt.0.)sqgam=1.
      if(theta.gt.0.9999)theta=1.
      if(theta.lt.0.)theta=0.
      theta=sqgam*Sc**(1/3)*Pr**(-1/3)
      Tyz=theta*(Ti-Tw)+Tw
C calculation of vapor removal rate
c finds mass vapor contained in each dz by summing over dy
c vapor removed is difference between mass in dz and previous dz
C     m(y,t)= mass of vapor in volume 1 x dy x dz at time level t
C     Mc=mass of vapor in volume 1 x y x dz
```

```
      dy=Yc*25/ydiv
      dz=Zc*zdiv
      Cb=(C+Cold)/2.
      m(J,1)=m(J,2)
      m(J,2)=Cb/(1-Cb)*row*1*dy*dz
      if(J.eq.1) m(J,2)=0.
      Cold=C
      Mc=Mc+m(J,2)
C      Fluxout is total Flux leaving at z=z(K) [lb H20/sec]
      Fluxout=Mc/dz*Wc
      Qsens=Qsens+row*cp*Wc*3600*dy*1*(Ti-Tyz)
      write(6,99)z*Zc*12.*25.,y*Yc*12.*25.,w*Wc/25.*60,C,sqgam
      write(6,99)y*Yc*12.*25.,sqgam
      SURF(J+1,ID)=sqgam
 20    Continue
      Do 50 I=Ny/2+2,Ny+1
      mdot=m(I,2)-m(I,1)+mdot
      vdot(I)=mdot/roh/dz
 50    Continue
      vdot(Ny/2+1)=0.
      Do 55 I=1,Ny/2
      vdot(I)=-vdot(Ny+2-I)
 55    Continue
      cond=McOLD-Mc
C      cond is total lb H20 condensed in z(K)-z(K-1)
      write(6,94)z, 1E6*cond
 30    continue
      tcond=tcond+condtop
C      Fluxin is total Flux entering at z=0 [lb H20/sec]
      Fluxin=Ci/(1-Ci)*row*Wc*Yc*25/2
C      Qcond is total Btuh latent heat removed
      Qcond=(Fluxin-Fluxout)*3600*970
      Qtot=Qcond+Qsens
      SHR=Qsens/Qtot
      write(6,95)ReL,CD,Tw,Qsens,Qcond,SHR
 5    CONTINUE
      LN=0
 501   continue
      DO 500 JS=1,(Ny/2)+1+1
      if(JS.gt.1)write(6,93)    SURF(JS,LN+1),SURF(JS,LN+2),
     1            SURF(JS,LN+3),SURF(JS,LN+4),SURF(JS,LN+5),
     1            SURF(JS,LN+6),SURF(JS,LN+7),SURF(JS,LN+8)
      if(JS.eq.1)write(6,92)    SURF(JS,LN+1),SURF(JS,LN+2),
     1            SURF(JS,LN+3),SURF(JS,LN+4),SURF(JS,LN+5),
     1          SURF(JS,LN+6),SURF(JS,LN+7),SURF(JS,LN+8)
500   CONTINUE
      write(6,93)
      LN=LN+8
      if(LN.lt.IDL) goto 501
      CLOSE (1)
92     format(9f10.0)
93     format(9f10.6)
94     format(i8,f16.2,f16.8)
95     format(f10.0,f9.3,f9.1,2f12.6,f9.6)
99     format(f14.4,3f16.9)
      stop
      END
```

```
PROGRAM SECTIONS
  Name                              Bytes  Attributes
 0 $CODE     .                     2690   PIC CON REL LCL   SHR   EXE   RD NOWRT QUAD
 1 $PDATA                            25   PIC CON REL LCL   SHR NOEXE   RD NOWRT QUAD
 2 $LOCAL                         87356   PIC CON REL LCL NOSHR NOEXE   RD   WRT QUAD
  Total Space Allocated            9007
ENTRY POINTS
  Address  Type  Name
 0-00000000      CONF$MAIN
STATEMENT FUNCTIONS
  Address  Type  Name             Address  Type  Name             Address  Type  Name
 0-000009D6  R*4  F                **     R*4  FP          0-00000A2E  R*4  PWS
VARIABLES
 Address  Type  Name              Address  Type  Name              Address  Type  Name              Address  Type
Name

   **     R*4  ALPHA           **     R*4  BETAN           **     R*4  BUG1              **     R*4  BUG2

   **     R*8  BUG3            **     R*4  BUG4            **     R*4  C            2-000154CC  R*4  C10
 2-000154D0  R*4  C11         2-000154D4  R*4  C12         2-000154D8  R*4  C13        2-000154C4  R*4  C8

 2-000154C8  R*4  C9            **     R*4  CB              **     R*4  CI           2-00015520  R*4  COLD
   **     R*4  COND            **     R*4  CONDTOP          **     R*4  CP               **     R*4  CW
   **     R*4  DELTA           **     R*4  DELTAC           **     R*4  DELTAT           **     R*4  DIJ
   **     R*4  DY             **     R*4  DZ              **     R*4  EPS         AP-00000004@ R*4  ETA
AP-00000004@ R*4  ETA         2-00015508  R*4  ETA             **     R*4  FLUXIN         **     R*4FLUXOUT

   **     R*4  FPM            **     R*4  GRLB            **     I*4  I           2-000154DC  I*4  ID
   **     I*4  IDL        2-00015504  I*4  J             **     I*4  JS          2-000154EC  I*4  K
   **     R*4  LBI           **     R*4  LBW            **     I*4  LN          2-000154BC  R*4  MC
   **     R*4  MCOLD        2-000154C0  R*4  MDOT            **     I*4  N              **     R*4  NU
2-00015500  I*4  NY          2-00015518  R*4  P          2-0001551C  R*4  PB              **     R*4  PI
   **     R*4  PR            **     R*4  QCOND        2-000154F4  R*4  QSENS            **     R*4  QTOT

   **     R*4  R            **     R*4  RB            **     R*4  REL            **     R*4  RO
   **     R*4  ROH            **     R*4  ROW            **     R*4  SC             **     R*4  SHR
   **     R*8  SIGMA          **     R*4  SQGAM            **     R*4  TCOND           **     R*4  TDELTA

2-00015510  R*4  THETA            **     R*4  TI           2-000154E0  R*4  TR          AP-00000004@ R*4  TR

   **     R*4  TW            **     R*4  TYZ          2-00015514  R*4  V           2-000154F8  R*4  VC
   **     R*4  VSTAR       2-0001550C  R*4  W            2-000154E4  R*4  WC             2-000154FC  R*4  WMAX
   **      R*4  WS           **      R*4  Y            **      R*4  YC             **      R*4  YDIV
   **      R*4  YHAT       2-000154F0  R*4  Z             **      R*4  Z4          2-000154E8  R*4  ZC
   **      R*4  ZDIV         **      R*4  ZS

ARRAYS
  Address  Type  Name           Bytes  Dimensions

 2-00000000  R*4  M             3208  (401, 2)
 2-000012CC  R*4  SURF           82416  (102, 202)
 2-00000C88  R*4  VDOT            1604  (401)
LABELS

  Address   Label     Address   Label     Address   Label     Address   Label     Address   Label   Address Label


   **     5        **     10        **     20        **     30      0-000003B5  40        **     50
   **     55     1-00000004  92'   1-0000000A  93'   1-00000010  94'       **     95'        **     96'
   **     99'      **     500     0-000006A0  501


FUNCTIONS AND SUBROUTINES REFERENCED

 Type  Name          Type  Name          Type  Name          Type  Name

  R*4  MTH$ALOG       R*4  MTH$EXP        R*4  MTH$SIN        R*4  MTH$SQRT

COMMAND QUALIFIERS

  FORTRAN/CHECK/LIST CONF.FOR

  /CHECK=(BOUNDS,OVERFLOW,UNDERFLOW)
  /DEBUG=(NOSYMBOLS,TRACEBACK)
  /DESIGN=(NOCOMMENTS,NOPLACEHOLDERS)
  /SHOW=(NODICTIONARY,NOINCLUDE,MAP,NOPREPROCESSOR,SINGLE)
  /STANDARD=(NOSEMANTIC,NOSOURCE_FORM,NOSYNTAX)
  /WARNINGS=(NODECLARATIONS,GENERAL,NOULTRIX,NOVAXELN)
  /CONTINUATIONS=19  /NOCROSS_REFERENCE  /NOD_LINES  /NOEXTEND_SOURCE
  /F77  /NOG_FLOATING  /I4  /NOMACHINE_CODE  /OPTIMIZE  /NOPARALLEL
  /NOANALYSIS_DATA
  /NODIAGNOSTICS
  /LIST=DISK$USER:[MEFLUID]CONF.LIS;1
  /OBJECT=DISK$USER:[MEFLUID]CONF.OBJ;1

COMPILATION STATISTICS
 Run Time:          2.27 seconds
 Elapsed Time:      10.08 seconds
 Page Faults:       835
 Dynamic Memory:    676 pages
```

APPENDIX C
PROBE ANALYSIS

Water vapor concentration in a mixture of air and water vapor can be determined by measuring the wet-bulb temperature of the mixture. By definition, "thermodynamic wet-bulb temperature" is the adiabatic saturation temperature of the mixture, and is a unique property independent of mixture components, flow conditions, or measurement techniques (ASHRAE, 1985). The wet-bulb thermocouple does not measure adiabatic saturation temperature. The process occurring at the wet-bulb is not one of adiabatic saturation. It is influenced by heat and mass transfer rates, conduction, and radiation. Fortunately, for air-water vapor mixtures at atmospheric pressures and temperatures, wet-bulb temperature is approximately equal to adiabatic saturation temperature.

The wet-bulb thermocouple probe was analyzed to determine the influence of conduction, radiation, and heat and mass transfer rates on accuracy. An adiabatic saturation analysis was used to quantify conduction and radiation influences. A heat and mass transfer analysis was used to show the effect of convection coefficients and to estimate the difference between adiabatic saturation temperature and wet-bulb temperature.

Adiabatic Saturation Analysis

The adiabatic saturation process as applied to the probe is founded on conservation of mass and energy

$$\begin{gathered}\dot{m}_{g1} = \dot{m}_{g2} \\ \dot{Q}_{cv} + \Sigma \dot{m}_i h_i = \Sigma \dot{m}_j h_j\end{gathered} \tag{C-1}$$

an equation giving the vapor concentration is

$$W_1 = \frac{W_2(h_{v2}-h_{f3})+c_{pg}(T_2-T_1)}{h_{v1}-h_{f3}} - \frac{\dot{Q}}{\dot{m}_g(h_{v1}-h_{f3})} \tag{C-2}$$

where

- c_p = specific heat at constant pressure Btu/lb_m·°F
- h = enthalpy, Btu/lb_m
- m = mass flow rate through c.v., lb_m/h
- T = temperature
- W = humidity ratio, lb_m(water vapor)/lb_m(dry air)
- Q = heat added to c.v., Btu/h
- f - liquid
- g - gas
- v - vapor

The second term in the above equation accounts for conduction and radiation heat transfer to the wet-bulb.

Conduction heat transfer is found using the fin equation

$$\begin{gathered}\dot{Q}_c = M(T_\infty - T_2)\tanh(mL) \\ m^2 = \frac{hP}{kA_c} \\ M = \sqrt{hpkA_c}\end{gathered} \tag{C-3}$$

where

A_c = probe cross section area, ft^2
h = heat transfer coefficient, Btu/h•ft^2•°F
k = probe thermal conductivity, Btu/h•ft•°F
L = probe length, ft
P = probe perimeter, ft
T_∞ = bulk mixture temperature, F
T_2 = adiabatic saturation temperature, F

Radiation heat transfer is estimated using

$$\dot{Q}_r = A_s F \sigma \epsilon (T_\infty^4 - T_2^4) \tag{C-4}$$

where

A_s = probe tip surface area, ft^2
F = view factor
σ = Stefan-Boltzman constant, 0.1714 x 10^{-8} Btu/h•ft^2•°R
ϵ = hemispherical emittance
T_∞ = bulk mixture temperature, R
T_2 = adiabatic saturation temperature, R

The mass flow rate through the control volume is estimated using the Blasius series for symmetrical flow past a cylinder. The control volume need only contain the velocity, thermal and concentration boundary layers. The maximum boundary-layer thicknesses are estimated using the relations below (Schlichting, 1955).

$$\delta = 3.2\frac{R}{\sqrt{\mathrm{Re}_R}} \qquad \delta_t \approx \frac{\delta}{\mathrm{Pr}^{\frac{1}{3}}} \qquad \delta_c \approx \frac{\delta}{\mathrm{Sc}^{\frac{1}{3}}} \tag{C-5}$$

The following example demonstrates the relative magnitude of conduction and radiation effects on the adiabatic saturation temperature. For prescribed conditions of $T_1=75$ F, $\phi=0.35$, and $W_1=0.0065$ lb_m-H_2O/lb_m-da, the psychometric chart gives a wet-bulb temperature of 58.2 F. The measured saturation temperatures given by this analysis are shown in Table C-1.

Table C-1. Results of example perturbation calculation.

CONSIDERATION	T_2 [F]	ERROR
Adiabatic	58.239	--
Radiation	58.245	0.01%
Conduction	58.498	0.44%
Cond + Rad	58.504	0.46%

Conduction's effect is of the same order of magnitude as the accuracy of the calibration standard used to calibrate the probe, a dew point hygrometer with accuracy of ±0.5° F. Radiation heat transfer has a negligible effect.

Heat and Mass Transfer Analysis

Using conservation of energy with latent heat being supplied by conduction and convection, and conservation of mass across the control surface for vapor and gas:

$$h_c A_s (T_\infty - T_{wb}) = M_v \dot{c}_f'' h_{fg} A_s$$

$$\dot{c}_f'' = C_v V_m - CD\frac{\partial(\frac{C_v}{C})}{\partial r} \qquad \dot{c}_g'' = 0 = C_g V_m - CD\frac{\partial(\frac{C_g}{C})}{\partial r} \tag{C-6}$$

where

A_s = surface area available to heat and mass transfer, ft^2
C = molal concentration, $lb\text{-}mol/ft^3$
D = mass diffusivity, ft^2/h
h_c = heat transfer coefficient, $Btu/h\cdot ft^2\cdot {}^\circ F$
h_{fg} = latent heat of vaporization, Btu/lb_m
M_v = molecular weight, $lb_m/lb\text{-}mol$
r = radial coordinate direction, ft
V_m = mean advection velocity, ft/h
c'' = molar flux, $lb\text{-}mol/ft^2\cdot hr$

a mass transfer coefficient, h_m [ft/h], can be defined after substitution of the gas mole balance into the vapor mole balance

$$\dot{x}_f'' = -\frac{C}{C_v} D \frac{\partial C_v}{\partial r} = -\frac{D\frac{\partial C_v}{\partial r}}{x_v} = \frac{h_m(C_v - C_{v,\infty})}{1 - x_g} \tag{C-7}$$

Using Dalton's Law of partial pressures and the ideal gas law, the mole balance is substituted into the energy balance to give a relation for the mole fraction of vapor in the mixture, $x_{v,\infty}$.

$$x_{v,\infty} = x_{v,wb} - \frac{h_c}{h_m} \cdot \frac{R_o T_{wb}}{M_v h_{fg} P_T} \cdot \frac{P_{v,wb}}{P_T} (T_\infty - T_{wb}) \tag{C-8}$$

The reading of the wet-bulb thermocouple probe will be the adiabatic saturation temperature if the Lewis number, α/D, is unity. The Lewis relation between the heat and mass transfer coefficients is

$$\frac{h_c}{h_m} = \rho c_p \frac{\alpha}{D} \tag{C-9}$$

For Le = 1, $h_c/h_m = 0.018$ Btu/ft^3•°R. Using published correlations for the heat and mass transfer coefficients at the probe tip (Incropera and DeWitt, 1985) $h_c = 14$ Btu/h•ft^2•°F and $h_m = 872$ ft/h. Thus $h_c/h_m = 0.016$ Btu/ft^3•°R and Le = 0.84. The difference between the adiabatic saturation temperature and the wet-bulb temperature due to Le < 1, for the conditions considered previously, is a decrease of approximately 1°F.

In summary, the effects of conduction, radiation, and heat and mass transfer coefficients on the difference between wet-bulb temperature measured with the probe and thermodynamic wet-bulb (or adiabatic saturation) temperature was quantified. The effects of conduction are minimal. Conduction can be expected to offset the difference between measured and thermodynamic wet-bulb temperature. The effects of radiation are negligible.

Transient Response

The effect of probe size, flow velocity, and material properties on response time can be approximated using a simple lumped capacitance method. A rigorous transient solution to the conservation of energy equation is not necessary to estimate the magnitude of the time constant. Analysis of the two limit cases, (1) change in concentration with no change in temperature, and (2) change in temperature with no change in concentration, gives (Peterson and Tien, 1987)

$$\frac{T-T_\infty}{T_0-T_\infty} = e^{-\frac{t}{\tau}} \qquad \text{(C-10)}$$

where

$$
\begin{aligned}
\tau_{heat} &= \frac{\rho_f c_f \forall}{h_c A} = \frac{2}{3} \cdot \frac{\rho_f\, c_f\, r^2}{k_g [2 + (.4Re^{\frac{1}{2}} + .06Re^{\frac{2}{3}}) Pr^{\frac{2}{5}} (\frac{\mu}{\mu_s})^{\frac{1}{4}}]} \\
\tau_{mass} &= \frac{\rho_f c_f \forall \theta}{h_m h_{fg} \rho_v A} = \frac{2}{3} \cdot \frac{\rho_f\, c_f\, r^2\, \theta}{\rho v h_{fg} D [2 + (.4Re^{\frac{1}{2}} + .06Re^{\frac{2}{3}}) Sc^{\frac{2}{5}} (\frac{\mu}{\mu_s})^{\frac{1}{4}}]}
\end{aligned}
\qquad \text{(C-11)}
$$

From this analysis, the wet-bulb time constant for a step change in vapor concentration (Re=30) is 8 s at 1 ft/s mean flow velocity. The wet-bulb transient response for a step change in temperature is slower, the corresponding time constant is 12 s. The dry-bulb response is much quicker, on the order of one-half second.

An increase in Reynolds number has little effect on the time constants for Re<10. For Re>50 an order of magnitude increase in Re causes a one-half order of magnitude decrease in the time constants.

APPENDIX D
RADIATION EFFECTS

A simple analysis of radiation heat transfer between the probe, the laboratory environment and the cooled plate did not show a significant effect on the accuracy of the wet-bulb temperature measurement. The basic radiation heat transfer equation

$$q_{ij} = \frac{\sigma(T_i^4 - T_j^4)}{\frac{1-\varepsilon_i}{\varepsilon_i A_i} + \frac{1}{A_i F_{ij}} + \frac{1-\varepsilon_j}{\varepsilon_j A_j}} \qquad \text{(D-1)}$$

was employed (Incropera and DeWitt, 1985). An emissivity value of 0.9 was used for the ambient, room, and fluorescent light radiation; and a value of 0.3 was used for the aluminum plate.

Although the net heat transferred from the probe tip by radiation was estimated to be 0.3 mW (0.001 Btuh), the heat transferred by convection and phase change is considerably more troublesome to predict due to the indefinite area available for mass transfer in the urethane foam tip. Assuming a mass-to-radiation transfer surface area factor of 5, the phase change energy loss is 13 mW (0.045 Btuh). Regardless, this effect was counteracted during calibration. Further analysis of the probe is presented in Appendix C.

There is also radiation exchange between the plate and the laboratory surroundings. Radiation heat transfer from the 160 W fluorescent fixture above the cooled-wall channel is negligible due to the small view factor of $F_{ij}=0.007$, calculated as

$$F_{ij} = \frac{1}{L_i}[0.02(L_i+L_j) - 0.03L_j] \tag{D-2}$$

where L_i=the width of the light fixture (0.6 m, 2 ft) and L_j=the vertical distance from the top of the plate to the light fixture (0.9 m, 3 ft). Maximum estimated heat gain from the lights to the cooled plate is 3 W (9 Btuh), assuming a full 160 W of blackbody radiation plus a 32 C (90 F) bulb surface temperature. Heat gain from the Plexiglass wall was estimated to be 17 W (57 Btuh), with an additional 20 W (68 Btuh) through the transparent ($\tau_s=0.9$) wall from the laboratory environment. When the plate is heated to 90 C (195 F), radiation heat loss was estimated to be 74 W (252 Btuh).

APPENDIX E
PROBE-FIELD POTENTIAL

Measurements of the potential difference between the probe tip and the plate were made to test the hypothesis that a weak electric field is maintained due to the concentration gradient of H_2O, a bipolar molecule, and the molecules that comprise dry air. The existence of a potential gradient may provide a means of measuring concentration gradient.

It was initially suggested that a varying potential through the boundary layer would significantly disturb the millivolt thermocouple outputs. This would require the potential to exist across the input terminals of the TC linearization amplifier. Since the input leads are shielded within the earth-grounded probe shank and are joined at the thermocouple junction, it is unlikely that an electric field would induce a significantly (enough to invalidate the results) greater current in one conductor than the other. However, this effect may introduce a small error.

Measurements of the direct current (DC) potential were made using a digital voltmeter (±0.003 mV) connected between the earth-grounded channel-wall plate and the probe shank. The earth-ground to the probe shank was removed for this experiment, leaving the probe assembly and LVDT electrically "floating".

The experimental design consisted of alternating control ant test trials over a period of four days. The control trials were performed with (1) no temperature difference and (2) cooling but no condensation. The test trials were identical to the control trials in every respect, except that the plate was cooled below the dew point of the inlet air. Three trials were performed in alternating traverse directions, through the boundary layers, at each plate temperature each day.

The range of steady-state voltage measurements in the complete set of data is from -0.011 mV to 0.167 mV. Although the results do not confirm the existence of a concentration dependent potential field, they do not conclusively show that a potential field does not exist. The average potential variation across the boundary layer 0.004 mV with no condensation and 0.012 mV with condensation occurring; values which are comparable with the measurement uncertainty but justify further study.

One interesting finding is the high potential as the probe tip is pulled away from the plate, sometimes jumping as high as 75 mV and then exponentially decaying to around 2 mV after a 3 seconds at a distance of 0.6 mm (0.024 in). This effect was not observed for traverses in the opposite direction, toward the plate (the procedure employed when measuring temperature and concentration profiles). Apparently, there is a significant capacitance between the probe and the plate. The magnitude of this effect may depend, among other variables, on the concentration.

What is more interesting, however, is the potential variation between "identical" trials on the same and different test days. Variables such as the experimenters location in the laboratory, whether nearby building exits were open or closed, what other equipment was operating in the laboratory building, and whether the weather was sunny or cloudy seemed to be responsible for most of the measured changes in potential. Possibly changes in the weather and pollutant levels affected the level of ionized molecules in the inlet air. Radio transmissions may be yet another source, even though DC voltage was being measured the probe-meter's capacitive reactance may have caused spurious readings.

It was concluded that the potential differences measured may or may not be a function of concentration, but the effect is weak compared to the effect of other speculated (and unverified) factors. Further work should focus on removing or controlling these spurious factors and quantifying their effect on the potential and capacitance. Once this is accomplished, a more sensitive apparatus could substantiate or refute the existence of a concentration induced potential or capacitance.

APPENDIX F
INSTRUMENTATION AND PROCEDURE

Instrumentation Subsystem

The standard instrumentation subsystem, introduced in Chapter 5, consists of temperature, humidity, dew point, flow, velocity and pressure measurement equipment. A summary of the instrumentation used is given in Table F-1. Temperature measurements were made of the following: (1) coolant at the plate inlet and outlet, and in the tank; (2) the plate surface; (3) the exterior surface of the coolant-side channel insulation; (4) the Plexiglass wall inner and outer surfaces; and (5) the inlet side, outlet side, and ambient air conditions. Humidity and dew point measurements were made of air-side inlet and outlet, and ambient conditions. Coolant flow rate was measured with a turbine meter. Air-side channel inlet-to-outlet pressure differential was measured with an inclined manometer. Barometric pressure was measured with a mercury barometer.

All temperature measurements, except the air-side channel inlet and outlet, were made with type T (copper-Constantan) thermocouples. Type T was selected because it has the lowest ASTM standard error ($\pm 0.8^\circ$ C, $\pm 1.44^\circ$ F). All thermocouples, except the coolant inlet and outlet, were made from the same roll of wire. Shielded wire was used for the coolant inlet and outlet thermocouples, Table F-1. Primary instrumentation used in the experimental system.

MEASUREMENT	INSTRUMENT	UNCERTAINTY
Concentration C(y)	Mini Wet Bulb	15%
Temperature T(y)	Mini Dry Bulb	5%
Probe Position	LVDT	10% @ δ_{gas} 1% @ δ
Isothermal Plate	Infrared Thermometer	0.6 C (1.0 F)
Heat Transfer	Type T Thermocouple	0.2 C (0.3 F)
Air Temp	RTD	0.2%+0.4° C (0.2%+ 0.4° F)
Air Humidity	Film Capacitor	2.1% rh
Air Velocity	Vane Anemometer	1%+0.01 m/s (1%+1 FPM)
Pressure Difference	Incline Manometer	1.25 Pa (0.005" H_2O)

and they were coated with dielectric epoxy. The thermocouples were connected to a 2-pole 20-contact rotary selector switch, and successively read with a 2-channel microprocessor thermocouple thermometer with an accuracy of 0.1%+0.6° C (0.1%+1° F). In addition, the coolant inlet and outlet thermocouples were connected in series. Their differential voltage was amplified (Gain=100) and read with a digital voltmeter. This provided a usable resolution of 1μV. The accuracy of the calibration slope was 0.9 μV/° F (0.5 μV/° F), contributing a temperature reading error of ±0.03° C (±0.05° F).

The temperature, humidity, dew point and velocity at the inlet and outlet of the channel were measured with two RTDs, a thin film capacitance sensor, and a vane anemometer. The capacitance of the humidity sensor varies according to the number of water molecules absorbed by the active polymer it is made from.

The four probes were connected to a hygrothermoanemometer which stores temperature, humidity, dew point, and velocity data for download to a PC. The accuracy of the system, reported as 0.2%+0.4° C (0.2%+ 0.4° F), 2.1% rh, 1%+0.01 m/s (1%+1 fpm) by the manufacturer, was verified using an NBS-150 mercury-in-glass thermometer (±0.1° C) and a dew point hygrometer (±0.5° F). The outlet flow boundary layers were thoroughly mixed with the bulk flow in an adiabatic mixing chamber to obtain mean psychometric conditions. The chamber contains a series of baffles, passages, and vanes.

The turbine liquid flow meter used to measure coolant flow rate was calibrated to a standard with an uncertainty of ±0.25% in the range 0.06 to 0.32 ℓ/s (1 to 5 gpm). Measurement of the frequency output of the meter (±0.05 Hz) contributed an insignificant error.

Data Collection Procedure

The evening before a test day, the desired temperature set point for the coolant was entered into the process controller. With stable coolant temperature, the centrifugal blower (and the motor cooling fan) was switched on and the air flow relief door set to provide the desired air-side channel inlet velocity. The apparatus was left undisturbed for about 1 hour to achieve steady state conditions. Coolant temperature and air exit conditions were measured after a 30 minute interval, and again after 1 hour to determine if the desired conditions had stabilized.

When a steady state condition had been reached, the data in Table F-2 was collected in the order listed and transferred to a spreadsheet.

Table F-2. List of data taken for each trial.

#	MEASUREMENT	DEVICE
1	barometric pressure	barometer
2	air inlet velocity (3 x-locations)	HTA
3	air inlet temperature	HTA
4	air inlet humidity	HTA
5	air inlet dew point	HTA
6	air mean outlet temperature	mixer + HTA
7	air mean outlet humidity	mixer + HTA
8	air mean outlet dew point	mixer + HTA
9	coolant TC voltage differential	DVM
10	coolant TC shunted voltage zero point	DVM
11	coolant inlet temperature	TC thermom
12	coolant outlet temperature	TC thermom
13	coolant temperature differential	TC thermom
14	plate inlet surface temperature	TC thermom
15	plate outlet surface temperature	TC thermom
16	plexiglass inside outlet temperature	TC thermom
17	plexiglass outside outlet temperature	TC thermom
18	air ambient temperature	TC thermom
19	insulation back temperature	TC thermom
20	insulation side temperature	TC thermom
21	insulation bottom temperature	TC thermom
22	plate back temperature (3 locations)	TC thermom
23	air differential pressure	manometer
24	coolant turbine flow meter frequency	DMM

Next, final preparations for a probe traverse were made: the wet-bulb tip and cotton jacket were checked for wetness, and condensation on the plate was wiped to a film. Starting at the Plexiglass wall (y=1) the probe was traversed across the channel width until it contacted the wall. The data collected during the probe traverse, listed in Table F-3, was transferred to a second spreadsheet.

Table F-3. List of data taken during each probe traverse.

#	MEASUREMENT	DEVICE
1	LVDT-A and LVDT-B input voltage	DVM
2	LVDT-A and LVDT-B output voltage	computer
3	dry-bulb thermocouple voltage	computer
4	wet-bulb thermocouple voltage	computer

From the analyzed probe data, the specific humidity and dry-bulb temperature at the wall and outside the boundary layer, and the mean specific humidity and mean dry-bulb temperature were transferred into the first spreadsheet. This concluded one trial of data collection. Trials were made at a series of 12 logarithmical spaced velocities between 0.3 and 12 m/s (60 to 2400 fpm), at plate temperatures of 2.8 and around 11 C (37 and 52 F); the higher temperature being slightly less than the inlet dew point temperature. A total of 120 cooled-plate trials were completed.

Data from the probe traverses were taken at logarithmical spaced points to provide fine resolution in the gas film and avoid collecting unessential data outside the boundary layer. Typically, probe data from about 30 y-positions and 2 z-positions was taken.

REFERENCE LIST

Abdel-Wahed, R.M.; Hifni, M.A. and Sherif, S.A. "Heat and mass transfer from a laminar humid air stream to a plate at subfreezing temperature," International Journal of Refrigeration, V.7, n.1, pp.49-55, 1984.

Anderson, Dale A.; Tannehill, John C. and Pletcher, Richard H. Computational Fluid Mechanics and Heat Transfer. Hemisphere Pub. Corp., New York, 1984.

Asano, Koichi; Nakano, Yoshimi and Inaba, Masashi. "Condensation of vapors in the presence of noncondensable gas on a vertical flat plate," Pac. Chem. Eng. Congr., [Proc.], V.2, n.1, pp. 74-81. 1977.

Asano, Koichi; Nakano, Yoshimi and Inaba, Masashi. "Forced convection film condensation of vapors in the presence of noncondensable gas on a small vertical flat plate," J. Chem. Eng. Jpn. V.12, n.3, pp.196-202. 1979.

ASHRAE. ASHRAE Handbook. Four volume set: Fundamentals, Systems, Equipment, and Applications. American Society of Heating, Refrigerating, and Air-Conditioning Engineers, Inc., Atlanta, Georgia, 1985.

Atkins, P.W. Physical Chemistry, Third Edition. Freeman and Company, New York, 1986.

Baer, E. and McKelvey, J.M. "Heat transfer in film condensation," AIChE Journal, V.4, n.2, pp.218-222. 1958.

Blasius, Von H. Grenzschichten in Flüssigkeiten mit kleiner Reibung, Dissertation Göttingen 1907, sowie Zeitschrift f. Mathematik und Physik, V.55, n.1, 1908.

Bracewell, R.N. The Fourier Transform and Its Applications, Second Edition. McGraw-Hill, 1978.

Brouwers, H.J.H. "Film condensation on non-isothermal vertical plates," International Journal of Heat and Mass Transfer, V.32, n.4, pp.655-663. Pergamon Press Ltd., 1989.

Brown, G.L. and Rebollo M.R. "A small fast-response probe to measure composition of a binary gas mixture," AIAA Journal, V.10, n.5, pp.649-652, May, 1972.

Chaoyang, W. and Chuanjing, T. "The effect of non-condensable gas on forced convection condensation along a horizontal plate in a porous medium," International Journal of Heat and Mass Transfer, V.32, pp.1847-1852. Pergamon Press Ltd., 1989.

Chapman, Sydney and Cowling, T.G. The Mathematical Theory of Non-Uniform Gases, Third Edition. Cambridge University Press, 1970.

Coney, J.E.R.; Kazeminejad, H.; and Sheppard, C.G.W. "Dehumidification of air on a vertical rectangular fin: a numerical study," Proceedings of the Institution of Mechanical Engineers, V.203, n.c3, pp.165-175. 1989a.

Coney, J.E.R.; Kazeminejad, H.; and Sheppard, C.G.W. "Dehumidification of turbulent air flow over a thick fin: an experimental study," Proceedings of the Institution of Mechanical Engineers, V.203, n.c3, p.177-188. 1989b.

Davis, J.E. and Venkatesh, S. "The solution of conjugated multiphase heat and mass transfer problems," Chemical Engineering Science, V.34, pp.775-787. Pergamon Press Ltd., 1979.

Denny, V.E. and Jusionis, V.J. "Effects of forced flow and variable properties on binary film condensation," International Journal of Heat and Mass Transfer, V.15, pp.2142-2153. Pergamon Press Ltd., 1972.

Denny, V.E.; Mills, A.F.; and Jusionis, V.J. "Laminar film condensation from a steam-air mixture undergoing forced flow down a vertical surface," Journal of Heat Transfer, V.93, pp.297-304. ASME, August 1971.

Drew, Thomas B. and Hoopes, John W. Jr. Advances in Chemical Engineering, V.1. Academic Press, New York, 1956.

Eckels, P.W. and Rabas, T.J. "Dehumidification: on the correlation of wet and dry transport processes in plate finned-tube heat exchangers," Journal of Heat Transfer, V.109, August. ASME, 1987.

Eckert, E.R.G. and Drake, Robert M. Jr. Analysis of Heat and Mass Transfer. Hemisphere Pub. Corp., 1972.

El-Wakil, M.M. Powerplant Technology. McGraw Hill, 1984.

Finnicum, S.S. and Westwater, J.W. "Dropwise vs filmwise condensation of steam on chromium," International Journal of Heat and Mass Transfer, V.32, pp.1541-1549. Pergamon Press Ltd., 1989.

Fujii, T and Koyama, S. "Laminar forced convection condensation of a ternary vapor mixture on a flat plate," Fund. of Phase Change: Boiling and Condensation HTD, V.38, pp.81-87. Edited by Avedsian, C.T. and Rudy, T.M. Presented at Winter Mtg. ASME, New Orleans, Louisiana, Dec 9-14, 1984.

Gusev, V.A. "Further examination of condensation of vapour from vapour/gas mixtures," Teploenergetijka (Thermal Engineering), V.35, n.5, pp.46-47. U.D.C. 536.423.4, 1988.

Hampson, H. Proceedings of the General Discussion on Heat Transfer, V.84, pp.58-61. IME, London and ASME, New York, 1951.

Harriot, P. "Reply to Professor McKelvey's Note," AIChE Journal V.6, n.4, p.708, 1960.

HijiKata, Kunio and Mori, Yasuo. "Forced convective heat transfer of a gas with condensing vapor around a flat plate," Heat Transfer, Japenese Research V.2 n.1, pp. 81-101. Scripta Pub. Corp., Silver Spring, MD, 1973.

Hines, Anthony L. and Maddox, Robert N. Mass Transfer Fundamentals and Applications. Prentice-Hall, Englewood Cliffs, New Jersey, 1985.

Holden, K.M.; Wanniarachchi, A.S.; Marto, P.J.; Boone, D.H.; and Rose, J.W. "Evaluation of organic coatings for the promotion of dropwise condensation of steam," Two Phase Heat Exchanger Symposium HTD V.44, pp.89-97. Presented at the 23rd National Heat Transfer Conference [Proc.] Aug 4 - Aug 7 1985. Edited by Pearson, Joseph T. and Kitto, John B. Jr. ASME Heat Transfer Committee (K-10), New York, 1985.

Honda, H. and Nozu, S. "A prediction method for heat transfer during film condendsation on low integral-fin tubes," Two Phase Heat Exchanger Symposium HTD V.44, pp.107-114. Presented at the 23rd National Heat Transfer Conference [Proc.] Aug 4 - Aug 7 1985. Edited by Pearson, Joseph T. and Kitto, John B. Jr. ASME Heat Transfer Committee (K-10), New York, 1985.

Howarth, L. "On the solution of the laminar boundary layer equation," Proceedings of the Royal Society of London, Series A -- Mathematics, V.164, p.547, 1938.

Huhtiniemi, I.; Barry, J.J.; and Corradini, M.L. "Condensation in the presence of a noncondensable gas: the effect of surface orientation," AIChE Symposium Series, V.85, n.269, pp.205-210. Heat Transfer--Philadelphia, 1989.

Incropera, Frank P. and DeWitt, David P. Introduction to Heat Transfer. John Wiley and Sons, 1985.

Irvine, T.F. and Hartnett, J.P. Advances in Heat Transfer, V.9, pp.181-272. Academic Press, New York, 1973.

Jackson, Janice E. Boundary Layer Measurements of Condensation in Humid Air over a Flat Plate, M.S. Report, University of Florida Mechanical Engineering Department, (Advisor: E.C. Hansen, Ph.D.), 1992.

Joos, F.M. "Thin liquid films on arbitrary surfaces with condensation or evaporation," Two Phase Heat Exchanger Symposium HTD V.44, pp.123-132. Presented at the 23rd National Heat Transfer Conference [Proc.] Aug 4 - Aug 7 1985. Edited by Pearson, Joseph T. and Kitto, John B. Jr. ASME Heat Transfer Committee (K-10), New York, 1985.

Kakac, S.; Bergles, A.E. and Fernandes, E.O., Editors. Two-Phase Flow Heat Exchangers -- Thermal-Hydraulic Fundamentals and Design, proceedings of the NATO Advanced Study Institute, Portugal, July 6-17. NATO ASI Series E: Applied Sciences - V.143. Kulwer Academic Publishers, Dordrecht, the Netherlands, Boston, London, 1987.

Kays, W.M. and Crawford, M.E. Convective Heat and Mass Transfer, Second Edition. McGraw-Hill, 1980.

Kazeminejad, H. Dehumidification of Turbulent Air Flow over a Thick Fin, Ph.D thesis, University of Leeds, United Kingdom, Department of Mechanical Engineering, 1987.

Keenan, Joseph H. Thermodynamics. The MIT Press, Cambridge MA, 1970.

Kobayashi, Yasunori and Matsumoto, Tsuyoshi. "Two-dimensional condensing vapor flow on parallel flat plates in an enclosure," Journal of Thermophysics and Heat Transfer V.1, n.2, pp.122-8. American Institute of Aeronautics and Astronautics, New York, NY, 1986.

Kobayashi, Yasunori and Matsumoto, Tsuyoshi. "Vapor condensation in the presence of a non-condensable gas in a gravity assisted thermosyphon," Nippon Kikai Gakkai Ronbunshu B Hen, V.54, n.504, pp.1970-1976. 1987.

Koh, J.C.Y. "Film condensation in a forced-convection boundary-layer flow," International Journal of Heat and Mass Transfer, V.5, pp.941-954. Pergamon Press Ltd., 1962.

Kotake, S. "Film condensation of binary mixture flow in a vertical channel," International Journal of Heat and Mass Transfer, V.21, pp.875-884. Pergamon Press Ltd., 1978.

Kotake, S. "Effects of a small amount of noncondensable gas on film condensation of multicomponent mixtures," International Journal of Heat and Mass Transfer, V.28, pp.407-414. Pergamon Press Ltd., 1985.

Kotake, S. and Oswatitsch K. "Parameters of binary-mixture film condensation," International Journal of Heat and Mass Transfer, V.23, pp.1405-1416. Pergamon Press Ltd., 1980.

Lebedev, P.D.; Baklastov, A.M.; and Sergazin, Zh.F. "Aerodynamics, heat and mass transfer in vapour condensation from humid air on a flat plate in a longitudinal flow in asymmetrically cooled slot," International Journal of Heat and Mass Transfer, V.12, pp.833-842. Pergamon Press Ltd., 1969.

Le Fevre, E.J. and Rose, J.W. "An experimental study of heat transfer by dropwise condensation," International Journal of Heat and Mass Transfer, V.8, pp.1117-1133. Pergamon Press Ltd., 1965.

LeGay-Desesquelles, F. and Prunet-Foch, B. "Dynamic behaviour of a boundary layer with condensation along a flat plate: comparison with suction," International Journal of Heat and Mass Transfer V.28, n.12, pp.2363-2370. Pergamon Press, Ltd., 1985.

LeGay-Desesquelles, F. and Prunet-Foch, B. "Heat and mass transfer with condensation in laminar and turbulent boundary layers along a flat plate," International Journal of Heat and Mass Transfer V.29, n.1, pp.95-105. Pergamon Press, Ltd., 1986.

Mansour, A.R. "Two-dimensional heat or mass transfer in laminer flow between parallel plates: closed-form solution," Journal of Heat Transfer, V.111, May. ASME, 1989.

McAdams, William H. Heat Transmission, Third Edition. McGraw-Hill, 1954.

McQuiston, F.C. "Finned tube heat exchangers: state of the art for the air side," ASHRAE Transactions, V.87, pt1, pp.1077-1085. ASHRAE, 1981.

Mikhailov, M.D. and Ozisik, M.N. Unified Analysis and Solutions of Heat and Mass Diffusion. Wiley, 1984.

Minkowycz, W.J. and Sparrow, E.M. "The effect of superheating on condensation heat transfer in a forced convection boundary layer flow," International Journal of Heat and Mass Transfer, V.12, pp.147-154. Pergamon Press Ltd., 1969.

Moy, Han-chuan. On Laminar Film Condensation of Vapors on a Vertical Flat Plate. Ph.D. Thesis, University of Iowa, February 1, 1969.

Nagendra, K.R. and Tirunarayanan, M.A. "Laminar film condensation from nonisothermal vertical flat plates," Chemical Engineering Science, V.25, n.6-k. Pergamon Press, Ltd. 1970.

Nolte, G. and Mayinger, F. "Condensation out of steam-air-mixtures in a horizontal annular flow channel," Experimental Heat Transfer, pp.1077-1085. Elsevier Publishing Company, 1988.

Nusselt, W. "Die oberflachen kondensation des wasserdampfes," Zeitschrift des Vereines Deutsher Ingenieure, V.60, pp.541-569. 1916.

Othmer, D.F. "The condensation of steam," Ind. Eng. Chem., V.21, n.6, pp.576-583. June, 1929.

Peterson, P.F. and Tien, C.L. "Miniature wet-bulb technique for measuring gas concentrations in condensing or evaporating systems," Experimental Heat Transfer, V.1, n.1, pp.1-15. Hemisphere Publishing Corp., 1987.

Prandtl, L. "Über flüssigkeitsbewegung bei sehr kleiner reibung," Proc. 3rd Intern. Math. Congr., pp.484-491. Heidelburg, 1904.

Prasad, Manohar. "A generalised solution for condensation over a vertical flat plate," Indian Journal of Technology V.17, June, pp.212-215. Council of Scientific and Industrial Research, New Delhi, 1979.

Raffellini, G. and Tarabusi. "Heat and mass transfer in dehumidifying extended surface coils: fin efficiency," Multiphase Transport: Fundamentals, Reactor Safety, Applications, V.2., pp.765-785. Hemisphere Publishing Corp., Washington, D.C., 1980.

Rose, J.W. "Condensation of a vapour in the presence of a non-condensing gas," International Journal of Heat and Mass Transfer, V.12, pp.233-237. Pergamon Press Ltd., 1969.

Rose, J.W. "Boundary layer flow with transpiration on an isothermal flat plate," International Journal of Heat and Mass Transfer, V.22, pp.1243-1244. Pergamon Press Ltd., 1979.

Rose, J.W. "Approximate equations for forced-convection condensation in the presence of a non-condensing gas on a flat plate and horizontal tube," International Journal of Heat and Mass Transfer, V.23, pp.539-546. Pergamon Press Ltd., 1980.

Rowe, P.N. "Correlating data," Chemtech, January, 1974, pp.9-14. 1974.

Sarma, P.K.; Chary, S.P.; and Rao, V.D. "Condensation on a vertical plate fin of variable thickness," International Journal of Heat and Mass Transfer, V.31, n.9, pp.1941-1944. Pergamon Press Ltd., 1988.

Savin, I.K. and Bologa, M.K. "Combined effect of an electric field on condensation of a vapor-gas mixture," Elektronnaya Obrabotka Materialov, n.6, pp.58-60. Allerton Press, Inc., 1988.

Schlichting, Hermann. Boundary-Layer Theory. Translated by Kestin, J. Seventh Edition, McGraw-Hill, (German 1951) 1955.

Schröppel, J. "Impact of wall temperature variation on the film condensation of binary gas-vapour mixtures," International Journal of Heat and Mass Transfer, V.24, pp.165-170. Pergamon Press Ltd., 1981.

Sherif, S.A.; Abdel-Wahed, R.M. and Hifini, M.A. "A mathematical model for the heat and mass transfer on a flat plate under frosting conditions," ASME Proceedings of the 1988 National Heat Transfer Conference, HTD-96, V.3., Edited by Jacobs, H.R., pp.301-306. Houston, Texas, July 24-27, 1988.

Siddique, M.; Golay, M.W.; and Kazimi, M.S. "The effect of hydrogen on forced convection steam condensation," AIChE Symposium Series, V.85, n.269, pp.211-216. Heat Transfer--Philadelphia, 1989.

Skelland, A.H.P. Diffusional Mass Transfer. Krieger Publishing; Malabar, Florida; (reprint) 1985.

Slater, L.J. Confluent Hypergeometric Functions. Cambridge University Press, 1960.

Sneddon, I.N. The Use of Integral Transforms. McGraw-Hill, 1972.

Sparrow, E.M. and Eckert, E.R.G. "Effects of superheated vapor and noncondensable gases on laminar film condensation," AIChE Journal, V.7, n.3, pp.473-477. 1961.

Sparrow, E.M. and Lin, S.H. "Condensation heat transfer in the presence of a noncondensable gas," Journal of Heat Transfer, V.86, pp.430-436. ASME, 1964.

Sparrow, E.M.; Minkowycz, W.J.; and Saddy, M. "Forced convection condensation in the presence of noncondensables and interfacial resistance," International Journal of Heat and Mass Transfer, V.10, pp.1829-1845. Pergamon Press Ltd., 1967.

Sundararaman, T.G. and Venkatram, T. "Fundamental studies on dropwise condensation on a vertical chrome-plated copper surface by dehumidification process," Pac. Chem. Eng. Congr. [Proc.], V.2, n.1, pp.82-87. 1977.

Taitel, Y. and Tamir, A. "Condensation in the presence of a noncondensable gas in direct contact," International Journal of Heat and Mass Transfer, V.12, pp.1157-1169. Pergamon Press Ltd., 1969.

Tanner, D.W.; Potter, C.J.; Pope, D.; and West, D. "Heat Transfer in dropwise condensation--part I the effects of heat flux, steam velocity, and non-condensable gas concentration," International Journal of Heat and Mass Transfer, V.8, pp.419-426. Pergamon Press Ltd., 1965.

Tietjens, O. Strömungslehre Physikalische Grundlagen vom technischen Standpunkt. Springer-Verlag, 1970.

Tu, C.J. and Wang, C.Y. "Noncondensable gas effect on condensation in a separate type two-phase closed thermosyphon," Warme- und Stoffubertragung, V.23, n.3, pp.153-158. Springer-Verlag, 1988.

Turaga, M.; Lin, S.; and Fazio, P.P. "Performance of direct expansion plate finned tube coils for air cooling and dehumidification," International Journal of Refrigeration, V.11, n.2, pp.78-86. Butterworths, International Institute of Refrigeration, March 1988.

Usmanov, A.G.; Bol'shov, V.P.; Mischenko, A.P.; Fatkullen, G.Sh.; and Sergeenko, E.S. "Optical investigation of heat and mass transfer in vapor condensation from vapor-gas mixtures," Journal of Engineering Physics, V.53, n.5, pp.1369-1373. Plenum Publishing Corp., May 1988.

Van Wylen, Gordon J. and Sonntag, Richard E. Fundamentals of Classical Thermodynamics. John Wiley and Sons, 1986.

Wang, C. and Tu, C. "Effects of noncondensable gas on laminar film condensation in a vertical tube," International Journal of Heat and Mass Transfer, V.31, pp.2339-2345. Pergamon Press Ltd., 1988.

Webb, R.L. and Murawski, C.G. "Row effect for R-11 condensation on enhanced tubes," Transactions of the ASME, Journal of Heat Transfer, V.112, August. ASME, 1990.

Welty, James R.; Wicks, Charles E.; and Wilson, Robert E. Fundamentals of Momentum, Heat, and Mass Transfer, Second Edition. John Wiley and Sons, New York, 1976.

West, M.K. Sorption Behavior of Hygroscopic Materials and its Effect on Building Moisture and Air Quality, Masters Thesis, University of Florida, Gainesville, Department of Mechanical Engineering, 1988.

West, M.K. and Hansen, E.C. "Determination of material hygroscopic properties which effect indoor air quality," ASHRAE paper n.890073, IAQ89: The Human Equation: Health and Comfort. ASHRAE, Atlanta, Georgia, pp.60-63, 1989.

West, M.K. and Hansen, E.C. "Effect of hygroscopic materials on indoor relative humidity and air quality," ASHRAE paper n.890074, IAQ89: The Human Equation: Health and Comfort. ASHRAE, Atlanta, Georgia, pp.56-59, 1989.

Whalley, P.B. Boiling, Condensation, and Gas-Liquid Flow. Clarendon Press, Oxford, 1987.

Yamali, S. and Merta, H. "Conduction heat transfer through condensation drops with variable interphase coefficients," Two Phase Heat Exchanger Symposium HTD V.44, pp.143-9. Presented at the 23rd National Heat Transfer Conference [Proc.] Aug 4 - Aug 7 1985. Edited by Pearson, Joseph T. and Kitto, John B. Jr. ASME Heat Transfer Committee (K-10), New York, 1985.

Yau, K.K.; Cooper, J.R. and Rose J.W. "Effecs of drainage strips and fin spacing on heat transfer and condensate retention for horizontal finned and plain condenser tubes," Two Phase Heat Exchanger Symposium HTD V.44, pp.151-6. Presented at the 23rd National Heat Transfer Conference [Proc.] Aug 4 - Aug 7 1985. Edited by Pearson, Joseph T. and Kitto, John B. Jr. ASME Heat Transfer Committee (K-10), New York, 1985.

BIOGRAPHICAL SKETCH

Many years ago, Michael Kenneth West was born early on a muggy summer morning in Washington, D.C. After an adequate, yet inspiring, thirteen years (K-12) of scholastic instruction in the Maryland public school system, he began his study of mechanical engineering at the University of Maryland. Before completing the Bachelor of Science curriculum at UM in 1986, he experienced an enlightening one-year internship as a research technician for ORI, Inc. Mike enrolled in graduate school at the University of Florida in 1986, major: mechanical engineering. He performed his thesis work on the effect of hygroscopic materials on residential cooling load under the direction of Dr. Elmer Hansen and Dr. Skip Ingley, and received the M.S. degree in 1988. He continued working with Dr. Hansen towards a doctorate in mechanical engineering, which he received in 1992.

While attending UF, he was a student member of ASME and ASHRAE. He has been offered a nomination for Sigma Xi membership. The Florida Solar Energy Center and the Florida Energy Extension Service have indicated their interest in employing him as an assistant research scientist. Mike is currently in a supine position on an untenanted beach, *Somewhere in the Caribbean*, rehabilitating his brain from synaptic overutilization.

I certify that I have read this study and that in my opinion it conforms to acceptable standards of scholarly presentation and is fully adequate, in scope and quality, as a dissertation for the degree of Doctor of Philosophy.

Elmer C. Hansen

Elmer C. Hansen, Chair
Assistant Professor of
Mechanical Engineering

I certify that I have read this study and that in my opinion it conforms to acceptable standards of scholarly presentation and is fully adequate, in scope and quality, as a dissertation for the degree of Doctor of Philosophy.

Chung K. Hsieh
Professor of Mechanical Engineering

I certify that I have read this study and that in my opinion it conforms to acceptable standards of scholarly presentation and is fully adequate, in scope and quality, as a dissertation for the degree of Doctor of Philosophy.

Bruce H. Edwards
Professor of Mathematics

I certify that I have read this study and that in my opinion it conforms to acceptable standards of scholarly presentation and is fully adequate, in scope and quality, as a dissertation for the degree of Doctor of Philosophy.

Herbert A. Ingley
Associate Professor of
Mechanical Engineering

I certify that I have read this study and that in my opinion it conforms to acceptable standards of scholarly presentation and is fully adequate, in scope and quality, as a dissertation for the degree of Doctor of Philosophy.

Paul Oppenheim

Paul Oppenheim
Assistant Professor of
Building Construction

This dissertation was submitted to the Graduate Faculty of the College of Engineering and to the Graduate School and was accepted as partial fulfillment of the requirements for the degree of Doctor of Philosophy.

May 1992

Winfred M. Phillips
Dean, College of Engineering

Madelyn M. Lockhart
Dean, Graduate School